MAREES TERRESTRES

BULLETIN D'INFORMATIONS

1 2 3

10 OCTOBRE 1995

Association Internationale de Géodésie

Commission Permanente des Marées Terrestres

Editeur Prof. Paul MELCHIOR
Observatoire Royal de Belgique
Avenue Circulaire 3
1180 Bruxelles

BIM 123

10 octobre 1995

p.

HARTMAN, T. and WENZEL H-G. 9278
Catalogue HW95 of the Tide Generating Potential.

VAN CAMP, M. 9302
Noise induced by the refrigerating device of a superconducting gravimeter in the seismological station of Membach (Belgium).

PERTSEV, B.P., IVANONA, M.V. (Traduction) 9315
Estimation de la précision de calcul des corrections de marées.

PERTSEV, B.P., KOUZNETSOV, M.V., IVANOVA, M.V., 9319
KOVALEVA, O.V. and KOUZNETSOVA, L.V. (Traduction)
Observations de marées terrestres et hypothèse de l'effet d'écran de l'attraction.

TIMOFEEV V.Yu, GRIDNEV, D.G., SARYCHEVA, Y.K., 9324
ANISIMOVA, L.V. and PANIN, S.F.
Observed tidal gravity changes at the compression region and at the extension-shift region Garm-Baikal.

TIMOFEEV, V. You, SARITCHEVA, You K. (Traduction) 9336
Recherches clinométriques à Niefteiougansk.

TIMOFEYEV, V. You, SARITCHEVA, You K., ANISIMOVA, L.V. 9344
PANINE, S.F., KHOMOUTOV, S. You. (Traduction)
Effet dynamique du noyau liquide dans les observations de marées terrestres dans les stations de Sibérie (Novosibirsk, Talaïa, Irkoutsk).

SEMIBALAMUT, V.M., FOMIN, Yu.N., TIMOFEEV, V. Yu, 9355
RYBUSHKIN, A. Yu, GRIBANOVA, E.I., KUZNETSOV, S. Yu
POPOV, M.E., SARYCHEVA, Y.K.
Tidal parameters from the results of laser deformographic measurements in the South-West part of the Baikal rift, Talaya station.

MELCHIOR, P. 9365
About "Data Rescue" An historical tidal gravity series of R. Tomaschek.

WENZEL, H-G. 9367
Re-analysis of Tomaschek's gravity tide observations made in 1954 at Baltasound, Shetlands Islands.

LATYNINA, L.A. 9374
The relation between tidal deformation and the velocities of recent tectonic movements.

Catalogue HW95 of the Tide Generating Potential

Torsten Hartmann,
Institut für Theoretische Astrophysik, Universität Tübingen, Auf der Morgenstelle 10, D-72076 Tübingen, Germany. e-mail: hartmann@tat.physik.uni-tuebingen.de

and

Hans-Georg Wenzel,
Geodätisches Institut, Universität Karlsruhe, Englerstraße 7, D-76128 Karlsruhe, Germany. e-mail: wenzel@gik.bau-verm.uni-karlsruhe.de

Abstract

This paper gives a short description of the HW95 harmonic development of the tide generating potential with 12 935 tidal waves containing 19 300 adjusted coefficients (see also Hartmann and Wenzel 1995). The HW95 tidal potential catalogue has been computed using the DE200 numerical ephemerides of Jet Propulsion Laboratory, Pasadena, of the solar system bodies between 1850 and 2150. The expansion is carried out to degree 6 for the Moon, to degree 3 for the Sun and to degree 2 for the planets Mercury, Venus, Mars, Jupiter, Saturn, and includes tides generated by the Moon and the Sun due to the Earth's flattening. The computation has been carried out by an iterative procedure combining spectral analysis and least squares adjustment. The HW95 tidal potential catalogue has been validated using different gravity tide benchmark series (Merriam 1992, Wenzel 1995). The error of gravity tides computed at mid-latitude stations from HW95 is estimated to 1.4 (12.3) pm/s^2 rms (at maximum) in time domain and 0.002 (0.11) pm/s^2 rms (at maximum) in frequency domain (1 pm/s^2 = 0.1 ngal) by comparison with the benchmark gravity tide series of Wenzel (1995) between years 1850 and 2150.

The HW95 tidal potential catalogue is distributed together with the necessary programs and benchmark series to public domain by INTERNET (see Appendix D):

adress:	gik.bau-verm.uni-karlsruhe.de = 129.13.100.201
login:	ftp
password:	ftp
directory:	cd pub, cd hw95
description file:	hw95.txt (see Appendix D)

1 Introduction

High precision gravimeters, such as cryogenic gravimeters and LaCoste-Romberg gravimeters with electrostatic feedback, can nowadays achieve a precision of about 500 pm/s^2 rms in time domain (1 pm/s^2 = 10^{-12} m/s^2 = 0.1 ngal) and of a few pm/s^2 rms in frequency domain for frequencies above 1 cpd (e.g. Richter et al. 1995). For the analysis of gravity records obtained with such instruments, the errors of the tidal potential catalogue should contribute only marginally to the residuals. The currently used tidal potential catalogues (e.g. Tamura 1987, Xi 1989) are accurate to about 70 pm/s^2 rms in time domain and to about 10 pm/s^2 at maximum in frequency domain. These tidal potential catalogues are thus not suitable for the analysis of precise gravimeter records.

In order to generate a tidal potential catalogue with a standard deviation of 1 pm/s^2 in time domain, the amplitude threshold of the tidal potential catalogue has to be below $5 \cdot 10^{-8}$ m^2/s^2 (see e.g. Fig. 8). Fortunately, the number of waves is only slightly above 10 000 at this amplitude threshold (Fig. 8). The tidal potential catalogue presented here has been computed with the aim to generate gravity tides with an rms error of about 1 pm/s^2 in time domain; this seems to be sufficiently accurate for the analysis of precise gravimeter records. The amplitude threshold of the tidal potential catalogue has been chosen to 10^{-8} m^2/s^2 equivalent to about 0.003 pm/s^2 at degree 2.

2 Definition of the tidal potential

The tidal potential $V_{(t)}$ due to a specific body at the surface of the Earth is given by (e.g. Ilk 1983)

$$V_{(t)} = GM_b \sum_{\ell=2}^{\ell=\ell_{max}} \sum_{m=0}^{m=\ell} \frac{r^\ell}{r_b^{\ell+1}(t)} \frac{1}{2\ell+1} \overline{P}_{\ell m}(\cos\theta) \overline{P}_{\ell m}(\cos\theta_b(t)) \cos[m(\lambda - \Lambda_b(t))] \quad (1)$$

$$+ GM_\oplus \frac{r_\oplus^2 r}{r_b^4(t)} J_{2\oplus} \left[\sqrt{\frac{3}{7}} \overline{P}_{10}(\cos\theta) \overline{P}_{30}(\cos\theta_b(t)) + \sqrt{\frac{2}{7}} \overline{P}_{11}(\cos\theta) \overline{P}_{31}(\cos\theta_b(t)) \cos(\lambda - \Lambda_b(t)) \right]$$

The second line in (1) accounts for the Earth's flattening effect (e.g. Wilhelm 1982, Dahlen 1993). Here, r, θ, λ denote the geocentric spherical coordinates of the station on (or near) the Earth and r_b, θ_b, Λ_b are those of the center of mass of the specific planet, whose mass is denoted by M_b. G is the gravitational constant.

The fully normalized Legendre functions of degree ℓ and order m used for the computation of the HW95 tidal potential catalogue are defined by (e.g. Heiskanen and Moritz 1967)

$$\overline{P}_{\ell m}(x) = (1-x^2)^{m/2} \frac{d^m}{dx^m} \left[\frac{1}{2^\ell \ell!} \frac{d^\ell}{dx^\ell} (x^2-1)^\ell \right] \sqrt{(2\ell+1) \frac{(\ell-m)!}{(\ell+m)!} (2-\delta_{m,0})} \quad (2)$$

with

$$\delta_{m,0} = \left\{ \begin{array}{ll} 1 & \text{for m} = 0 \\ 0 & \text{for m} \neq 0 \end{array} \right\}.$$

Recurrence relations for the fully normalized Legendre functions and their derivatives which are numerically stable up to very high degrees are given e.g. in Wenzel (1985). Closed expressions for the fully normalized Legendre functions and their derivatives are given to degree and order 6 in Appendix B.

The maximum tidal potential and maximum gravity tide due to a specific celestial body at a specific degree can be estimated from

$$V_{\ell,\max} \sim GM_b \cdot \frac{r^\ell}{r_{\min}^{\ell+1}} \quad (3)$$

$$g_{\ell,\max} \sim (\partial V_\ell / \partial r)_{\max} = GM_b \cdot \ell \cdot \frac{r^{\ell-1}}{r_{\min}^{\ell+1}} \quad (4)$$

with $r_{\min}$ = minimum geocentric distance to the celestial body and are given in Tab. 1. For our amplitude threshold of about 0.01 pm/s^2 in tidal gravity, we have to include the tidal potential for the Moon to degree 6, for the Sun to degree 3, and for the planets Mercury, Venus, Mars, Jupiter and Saturn to degree 2. The effect of the Earth's flattening on the tidal potential due to the Moon (e.g. Wilhelm 1982, Dahlen 1993) and due to the Sun has to be included into the solution as well. The asteroids (e.g. Ceres) and the satellites of the other planets (e.g. Deimos as satellite of Mars or Ganymede as satellite of Jupiter) do not generate significant tidal accelerations at the Earth's surface.

3 Computation of the HW95 tidal potential catalogue

Our catalogue HW95 of the Earth tide generating potential has been computed by using an expansion of the form

$$V_{(t)} = \sum_{\ell=1}^{\ell=\ell_{max}} \sum_{m=0}^{m=\ell} \left(\frac{r}{a}\right)^\ell \overline{P}_{\ell m}(\cos\theta) \sum_i \left[C_i^{\ell m}(t) \cos(\alpha_i(t)) + S_i^{\ell m}(t) \sin(\alpha_i(t)) \right] \quad (5)$$

where a is the semi-major axis of the Earth, t is the time from J2000 in Julian centuries. It should be mentioned that our tidal potential coefficients are not normalized by a so-called Doodson-constant because it is unnecessary and there are problems in defining this constant (e.g. Ducarme 1989). We also have not used the normalization by so-called geodetic coefficients (e.g. Doodson 1921) because it is unnecessary. Additionally, there are problems with partly wrong geodetic coefficients (e.g. Tamura 1987) and with different definitions of these geodetic coefficients at higher degrees (e.g. Büllesfeld 1985). The definition of our tidal potential catalogue by (5) is much easier and simpler than the definition which has been used by e.g. Doodson (1921).

Table 1: The maximum tidal potential and tidal gravity due to solar system bodies ($r \sim a$)

body	ℓ	$GM[\mathrm{m}^2/\mathrm{s}^2]$	$r_{\min}[\mathrm{m}]$	$V_{\ell,\max}[\mathrm{m}^2/\mathrm{s}^2]$	$g_{\ell,\max}[\mathrm{pm}/\mathrm{s}^2]$	included
Moon	2	$4.903 \cdot 10^{12}$	$3.564 \cdot 10^{8}$	4.41	1 382 000.00	yes
	3			$7.89 \cdot 10^{-2}$	37 090.00	yes
	4			$1.41 \cdot 10^{-3}$	884.90	yes
	5			$2.53 \cdot 10^{-5}$	19.80	yes
	6			$4.52 \cdot 10^{-7}$	0.42	yes
	7			$8.09 \cdot 10^{-9}$	< 0.01	no
Sun	2	$1.327 \cdot 10^{20}$	$1.50 \cdot 10^{11}$	1.60	501 600.00	yes
	3			$6.79 \cdot 10^{-5}$	31.99	yes
	4			$2.89 \cdot 10^{-9}$	< 0.01	no
Mercury	2	$2.20 \cdot 10^{13}$	$9.17 \cdot 10^{10}$	$1.16 \cdot 10^{-6}$	0.36	yes
Venus	2	$3.25 \cdot 10^{14}$	$4.13 \cdot 10^{10}$	$1.88 \cdot 10^{-4}$	58.85	yes
Mars	2	$4.28 \cdot 10^{13}$	$7.73 \cdot 10^{10}$	$3.77 \cdot 10^{-6}$	1.18	yes
Jupiter	2	$1.27 \cdot 10^{17}$	$6.28 \cdot 10^{11}$	$2.09 \cdot 10^{-5}$	6.54	yes
Saturn	2	$3.79 \cdot 10^{16}$	$1.27 \cdot 10^{12}$	$7.53 \cdot 10^{-7}$	0.24	yes
Uranus	2	$5.80 \cdot 10^{15}$	$2.72 \cdot 10^{12}$	$1.17 \cdot 10^{-8}$	< 0.01	no
Neptune	2	$6.87 \cdot 10^{15}$	$4.35 \cdot 10^{12}$	$3.40 \cdot 10^{-9}$	< 0.01	no
Pluto	2	$1.02 \cdot 10^{12}$	$5.55 \cdot 10^{12}$	$2.43 \cdot 10^{-13}$	< 0.01	no
Deimos	2	$1.33 \cdot 10^{6}$	$7.73 \cdot 10^{10}$	$1.18 \cdot 10^{-13}$	< 0.01	no
Ganymede	2	$9.96 \cdot 10^{12}$	$6.28 \cdot 10^{11}$	$1.64 \cdot 10^{-9}$	< 0.01	no
Ceres	2	$6.87 \cdot 10^{10}$	$2.32 \cdot 10^{11}$	$2.24 \cdot 10^{-10}$	< 0.01	no
Moon and $J_{2\oplus}$	1	–	–	$5.12 \cdot 10^{-4}$	80.30	yes
Sun and $J_{2\oplus}$	1	–	–	$4.42 \cdot 10^{-7}$	0.07	yes

The time dependent tidal potential coefficients are given by

$$C_i^{\ell m}(t) = \mathrm{C0}_i^{\ell m} + t \cdot \mathrm{C1}_i^{\ell m} \quad (6)$$

$$S_i^{\ell m}(t) = \mathrm{S0}_i^{\ell m} + t \cdot \mathrm{S1}_i^{\ell m} \quad (7)$$

where the potential coefficients $\mathrm{C0}_i^{\ell m}$ and $\mathrm{S0}_i^{\ell m}$ have the dimension $\mathrm{m}^2/\mathrm{s}^2$ and the linear drift coefficients $\mathrm{C1}_i^{\ell m}$ and $\mathrm{S1}_i^{\ell m}$ have the dimension $\mathrm{m}^2/\mathrm{s}^2/\mathrm{J.cy}$. The arguments $\alpha_i(t)$ are computed from

$$\alpha_i(t) = m \cdot \lambda + \sum_{j=1}^{j=11} k_{ij} \cdot arg_j(t) \qquad \text{with } k_{i1} = m. \quad (8)$$

The integer coefficients k_{ij} are given in our catalogue, while the eleven astronomical arguments $arg_j(t)$ (τ = mean local lunar time, s = mean lunar longitude, h = mean solar longitude, p = mean longitude of lunar perigee, N' = negative mean longitude of the lunar ascending node, p_s = mean longitude of solar perigee, L_{Mer} = mean longitude of Mercury, L_{Ven} = mean longitude of Venus, L_{Mar} = mean longitude of Mars, L_{Jup} = mean longitude of Jupiter, L_{Sat} = mean longitude of Saturn) can be computed from polynomials in time, given

in Appendix A. The table containing numerical values of the fundamental arguments at specific epochs is also given in Appendix A.

The numerical standard ephemerides DE200 (Standish and Williams 1981) containing polynomials for the celestial coordinates of all solar system bodies between years 1599 and 2169 have been used to compute the celestial geocentric coordinates for the time interval 1850 to 2150. The numerical ephemerides DE102 (Newhall et al. 1983) which have been used in (and had sufficient accuracy for) the computation of our catalogue of the tidal potential due to the planets (Hartmann and Wenzel 1994a,b) has been found to be not sufficiently accurate for the computation of the luni-solar tidal potential, mainly because of a different constant used for the secular deceleration of the lunar longitude due to tidal friction (see below).

The conversion to terrestial geocentric coordinates has been done using the relation (e.g. Mueller 1969, p. 85)

$$\vec{r}_{\text{terr.}} = \mathcal{S} \cdot \mathcal{N} \cdot \mathcal{P} \cdot \vec{r}_{\text{cel.}} \tag{9}$$

where $\mathcal{S}$ denotes the Earth's rotation matrix, $\mathcal{P}$ the precession matrix and $\mathcal{N}$ the nutation matrix.
The precession formulas of Simon et al. (1994) have been used (including corrections for modern masses, units are arcseconds and Julian centuries)

$$\zeta(t) = 2\,306.090\,99 + 0.302\,228\,t + 0.018\,018\,3\,t^2 - 5.830 \cdot 10^{-6}\,t^3 - 2.85 \cdot 10^{-7}\,t^4 - 2 \cdot 10^{-10}\,t^5 \tag{10}$$

$$z(t) = 2\,306.090\,99 + 1.095\,280\,t + 0.018\,266\,7\,t^2 - 2.821 \cdot 10^{-5}\,t^3 - 3.01 \cdot 10^{-7}\,t^4 - 1 \cdot 10^{-10}\,t^5 \tag{11}$$

$$\theta(t) = 2\,004.201\,98 - 0.426\,568\,t - 0.041\,823\,8\,t^2 - 7.310 \cdot 10^{-6}\,t^3 - 1.27 \cdot 10^{-7}\,t^4 + 4 \cdot 10^{-10}\,t^5 \tag{12}$$

These expressions are consistent with the nutation theory ZMOA 1990 (Herring 1991). The mean obliquity has also been taken from Simon et el. (1994) (units are arcseconds and Julian centuries)

$$\varepsilon = 84\,381.412 - 46.809\,56\,t - 1.52 \cdot 10^{-4}\,t^2 + 1.9989 \cdot 10^{-3}\,t^3 - 5.1 \cdot 10^{-7}\,t^4 - 2.5 \cdot 10^{-8}\,t^5. \tag{13}$$

The IAU 1980 Nutation theory (Seidelmann 1982) was used with the Delaunay arguments replaced by those of Simon et al. (1994), see Appendix A for their numerical values.

The model Earth we have used in our computation rotates according to the theory of Aoki et al. (1982), eqn.(14), by using the expression for Greenwich Mean Sidereal Time (units are seconds and Julian centuries)

$$\text{GMST} = 67\,310.54841 + (3\,155\,760\,000 + 8\,640\,184.812\,866)\,t + 0.093\,104\,t^2 - 6.2 \cdot 10^{-6}\,t^3 \tag{14}$$

and adding the equation of equinoxes to obtain the Greenwich Apparent Siderial Time

$$\text{GAST} = \text{GMST} + \Delta\Psi \cdot \cos\varepsilon. \tag{15}$$

The time base for our catalogue is TDB (dynamic barycentric time). No correction for the polar motion and variation of the Earth's rotation has been applied (because both are not known for the time span 1850 – 2150 which has been used for the numerical computations); this has to be done afterwards in the application programs.

We believe that we have included all effects significant at our amplitude threshold into the computation of the tidal potential catalogue. The IERS 1992 standards (McCarthy 1992, see Appendix A) used in the computations and the ephemerides of the celestial bodies are in general sufficiently accurate. The accuracy of our computations is however limited by the accuracy of the secular deceleration of the lunar longitude due to tidal friction, for which the different sets of numerical ephemerides (e.g. Standish and Williams 1981, Newhall et al. 1983) use significantly different parameters ($-26.3''/\text{cy}^2$ for DE102, $-23.9''/\text{cy}^2$ for DE200, $-25.8''/\text{cy}^2$ for DE245).

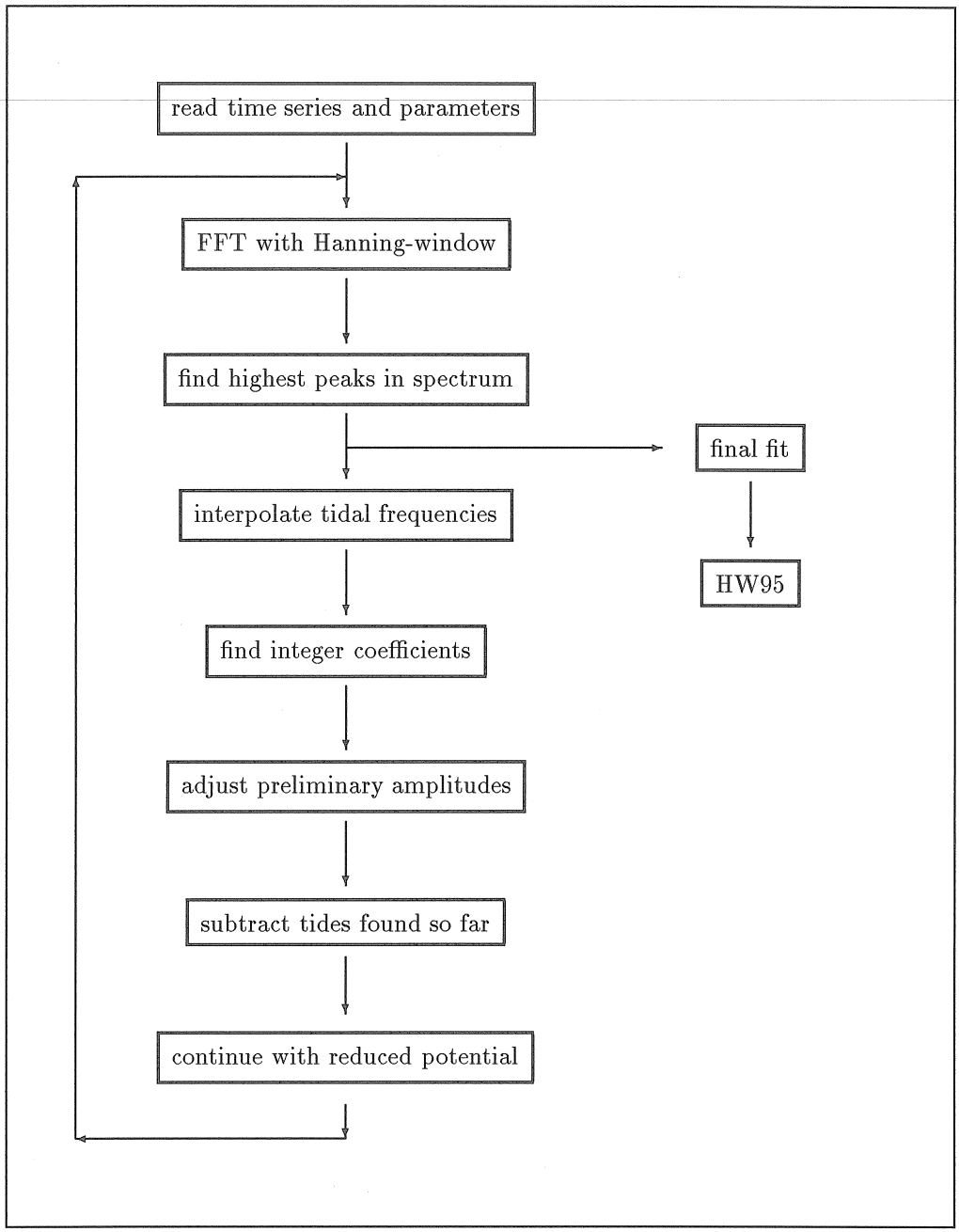

Figure 1: Schematic diagram for the computation of the HW95 tidal potential catalogue

A number of different time series of the tidal potential related to a specific body and a specific degree and order has been computed over the time span 1850 – 2150 (see Tab. 2), where the number of samples has been chosen between 2^{17} and 2^{21}. It should be mentioned that this is the maximum time span available from the DE200 numerical ephemerides which is free of errors and symmetric to J2000.

The analysis was made using an iterative procedure (see Fig. 1). A similar technique has already been used by Cartwright et al. (1971, 1973) and by Tamura (1987). First, we computed a Fast Fourier Transform (FFT) of the tidal series and interpolated the equidistant grid of frequencies to obtain a first approximation for the tidal frequency as the frequency of the highest peak in the spectrum. This frequency was replaced by integer combination of the fundamental arguments mentioned in the previous section. Preliminary potential coefficients were determined by a least squares fit. Then, the tides computed using the adjusted potential coefficients were subtracted and the next iteration was started using the reduced time series until the amplitudes were below a threshold chosen to be $1 \cdot 10^{-8}$ m^2/s^2 corresponding to about 0.003 pm/s^2 at degree 2 for gravity (for the

main parts $\ell = 2$ a slightly higher threshold had to be chosen). A final least squares adjustment determined the final potential coefficients and residuals of the time series. It has to be noted that the numerical effort to compute the least squares solutions was rather high and that a number of special methods (including the development of closed expressions for the elements of the normal equation matrices) had to be used to reduce the computational burden and to give sufficient numerical accuracy for the final solution. Most of the programs used for the computation of the HW95 catalogue have been written in two different languages (C and Fortran 77) and have been executed under two different operation systems (UNIX and MS-DOS) on different platforms in order to protect against programming errors.

Table 2: Time series used for the analysis of the tidal potential

Start: June 23rd 1850, 04:00 TDB, JD = 2 396 931.666
End: July 11th 2149, 20:00 TDB, JD = 2 506 158.333

order m	time interval [hours]	number of samples	time span [years]	file length [Mbyte]
0	20.0	131 072 = 2^{17}	299.046	1.31
1	5.0	524 288 = 2^{19}	299.046	5.24
2	2.5	1 048 576 = 2^{20}	299.046	10.48
3	2.5	1 048 576 = 2^{20}	299.046	10.48
4	1.25	2 097 152 = 2^{21}	299.046	20.97
5	1.25	2 097 152 = 2^{21}	299.046	20.97
6	1.25	2 097 152 = 2^{21}	299.046	20.97

The smallest frequency difference between adjacent tidal waves in our catalogue is

$$2 \cdot \partial p_s / \partial t \;=\; 3.923 \cdot 10^{-6}\ ^0/\text{ hour} \quad \text{at } t = 0$$

corresponding to a period of 10 468^a. One might wonder that we were able to separate waves with such a small frequency difference from data covering about 300^a time span only. Whereas this is impossible for a standard spectral analysis method, the least squares adjustment technique is able to do so provided the noise (residuals after adjustment) is sufficiently small (e.g. Munk and Hasselmann 1964). In order to demonstrate this capability of the least squares adjustment technique, we have used a non-iterative adjustment of a simulated time series

$$y_{(t)} \;=\; (a + b \cdot t) \cos(\omega_1 t) + c \cdot \cos(\omega_2 t) + r_{(t)} \tag{16}$$

(524 288 samples with a sampling interval of 5.0^h covering 299.046^a) with a = 10 000 000 000, b = 10 000 000, c = 1 000, ω_1 = 14.492 052 120 18 ^{0} / hour, ω_2 = 14.492 056 043 20 ^{0} / hour, and $r_{(t)}$ = normally distributed pseudo random variable with variable standard deviation (computed with routines taken from Press et al. 1992). The adjusted unknowns given in Tab. 3 show only very small deviations from the input parameters, depending on the simulated noise.

Table 3: Adjusted unknowns from tests using 524 288 simulated samples with 5^h interval in a non-iterative least squares adjustment

simulated stdv.	a	b	c
10.	10 000 000 000.	10 000 000.	1 000.
100.	9 999 999 999.	10 000 000.	1 001.
1 000.	9 999 999 989.	9 999 998.	1 010.
10 000.	9 999 999 894.	9 999 979.	1 096.

Tab. 4 gives the statistics of the computed tidal potential catalogue named HW95. The 45 waves of our catalogue exceeding an amplitude threshold of 10^{-2} m^2/s^2 are listed in Appendix C. The catalogue ist available to public domain and distributed via INTERNET (see Appendix C and D).

Table 4: Statistics of the HW95 tidal potential catalogue

source	ℓ	m	no. of waves	no. of coeff.	rms of fit [pm/s^2]	source	ℓ	m	no. of waves	no. of coeff.	rms of fit [pm/s^2]
Moon	2	0	1568	2502	0.243	Moon	2	1	1915	3074	0.563
Moon	2	2	1353	2256	0.775	Moon	3	0	643	817	0.089
Moon	3	1	1065	1340	0.133	Moon	3	2	926	1177	0.135
Moon	3	3	696	917	0.144	Moon	4	0	256	283	0.029
Moon	4	1	419	458	0.043	Moon	4	2	363	403	0.047
Moon	4	3	364	399	0.037	Moon	4	4	226	254	0.049
Moon	5	0	38	39	0.018	Moon	5	1	59	59	0.026
Moon	5	2	69	71	0.023	Moon	5	3	62	62	0.022
Moon	5	4	66	68	0.020	Moon	5	5	53	55	0.016
Moon	6	0	1	1	0.009	Moon	6	1	2	2	0.011
Moon	6	2	2	2	0.009	Moon	6	3	2	2	0.010
Moon	6	4	2	2	0.010	Moon	6	5	3	3	0.010
Moon	6	6	2	2	0.010	Sun	2	0	227	410	0.052
Sun	2	1	370	674	0.064	Sun	2	2	308	575	0.092
Sun	3	0	7	9	0.002	Sun	3	1	13	16	0.001
Sun	3	2	12	14	0.001	Sun	3	3	8	11	0.003
$J_{2\oplus}$ by Moon	1	0	141	153	0.004	$J_{2\oplus}$ by Moon	1	1	206	219	0.005
$J_{2\oplus}$ by Sun	1	0	2	2	0.000	$J_{2\oplus}$ by Sun	1	1	3	3	0.000
Mercury	2	0	12	24	0.003	Mercury	2	1	35	70	0.002
Mercury	2	2	27	54	0.003	Venus	2	0	173	346	0.011
Venus	2	1	407	814	0.010	Venus	2	2	281	562	0.016
Mars	2	0	68	136	0.006	Mars	2	1	195	390	0.004
Mars	2	2	133	266	0.008	Jupiter	2	0	26	52	0.004
Jupiter	2	1	56	112	0.004	Jupiter	2	2	45	90	0.010
Saturn	2	0	5	10	0.002	Saturn	2	1	12	24	0.001
Saturn	2	2	8	16	0.002						
total sum			12935	19300		total sum			12935	19300	

(rms of fit is rms of residuals from adjustment of potential coefficients, converted to gravity)

4 Formulas for the tidal acceleration

The tidal acceleration $\vec{f}_S$ due to part V_{lm} of the tidal potential in a spherical coordinate system is given by

$$f_{S.x} = -\frac{1}{r}\frac{\partial}{\partial\theta}V_{lm} = -\frac{1}{r}\frac{1}{\overline{P}_{lm}}\left(\frac{\partial}{\partial\theta}\overline{P}_{lm}\right)V_{lm} \tag{17a}$$

$$f_{S.y} = \frac{1}{r\cos\theta}\frac{\partial}{\partial\lambda}V_{lm} \tag{17b}$$

$$f_{S.z} = \frac{\partial}{\partial r}V_{lm} = \frac{l}{r}V_{lm} \tag{17c}$$

while its components $\vec{f}_E$ in an ellipsoidal coordinate system are given by (e.g. Wenzel 1976)

$$f_{E.x} = \cos\alpha\, f_{S.x} - \sin\alpha\, f_{S.z} \tag{18a}$$

$$f_{E.y} = f_{S.y} \tag{18b}$$

$$f_{E.z} = \sin\alpha\, f_{S.x} + \cos\alpha\, f_{S.z}\,. \tag{18c}$$

α is the angular difference between the ellipsoidal latitude and the geocentric latitude. $-f_{E.z}$ is the gravity tide, while $f_{E.x}$ and $f_{E.y}$ are the tidal accelerations in north-direction and east-direction, respectively. The tidal

potential, tidal gravity and horizontal tidal accelerations computed at station BFO (Black Forest Observatory Schiltach $\phi = 48.3306^0$ N, $\lambda = 8.3300^0$ E, h = 589 m) from the HW95 tidal potential catalogue are given in Tab. 5 at 50^a interval between 1850 and 2150.

Table 5: Tidal potential and tidal accelerations for a rigid Earth model at station BFO ($\phi = 48.3306^0$ N, $\lambda = 8.3300^0$ E, h = 589 m) computed at 50^a interval from HW95 tidal potential catalogue

date 0^h TDB	Julian date	$V(t)$ [m^2/s^2]	$f_{E.x}(t)$ [pm/s^2]	$f_{E.y}(t)$ [pm/s^2]	$g(t) = -f_{E.z}(t)$ [pm/s^2]
1850.01.01	2 396 758.500	2.827 197 786	-1 006 974.821	616 594.735	-884 394.293
1900.01.01	2 415 020.500	3.779 619 606	-957 074.888	-490 573.676	-1 180 140.484
1950.01.01	2 433 282.500	1.909 706 596	-472 249.278	-811 992.934	-596 649.060
2000.01.01	2 451 544.500	0.174 017 413	-360 419.889	-533 182.699	-56 545.781
2050.01.01	2 469 807.500	-0.578 027 858	-274 536.738	-237 591.604	183 778.341
2100.01.01	2 488 069.500	0.973 633 635	-655 711.503	674 947.785	-299 234.790
2150.01.01	2 506 331.500	3.185 479 672	-838 999.820	235 443.789	-995 200.014

5 Validation of the HW95 tidal potential catalogue

The new tidal potential catalogue HW95 has been validated by comparison with existing tidal potential catalogues (Doodson 1921, Cartwright et al. 1971, 1973, Büllesfeld 1985, Tamura 1987 and Xi 1989) and by comparison with benchmark gravity tide series (Merriam 1992, Wenzel 1995). The Tamura (1993) tidal potential catalogue cannot directly be compared with other catalogues because it does not use the integer combination of astronomical arguments for all waves.
To compare the previous catalogues with our catalogue, we had to transform the previous catalogues into our normalization and format, and we had to merge those waves of our cataloge with identical degree and order but referring to a different celestial body. The statistics of the differences of the coefficients of the catalogues (transformed into gravity variation) is given in Tab. 6; the rms differences are generally in the order of a few pm/s^2. The maximum difference with 185 pm/s^2 is produced by a wave with frequency 28.984 108 16^0 per hour ($2 \cdot \partial p_s/\partial t$ larger than M_2) which does not exist in most of the previous catalogues. By a similar difference for the C0-coefficient of wave M_2 with opposite sign, the effect of these two discrepancies almost cancels in time domain for the time span 1850 – 2150. This example shows that direct comparisons of tidal potential catalogues (in frequency domain) do not make much sense, and that a better validation of tidal potential catalogues has to be carried out by comparison with gravity tide benchmark series in time domain.

Table 6: Comparison of tidal potential catalogue HW95 with previous catalogues (all differences given in pm/s^2).

catalogue	no. of waves	ΔC0		ΔS0		ΔC1		ΔS1	
		rms	max.	rms	max.	rms	max.	rms	max.
Doodson (1921)[1)]	378	9.473	542.644	5.520	219.633	3.210	88.617	3.717	87.297
Cartwright et al. (1971, 1973)	505	4.629	185.009	3.356	70.970	1.774	30.546	1.437	18.157
Büllesfeld (1985)[1)]	656	3.951	205.341	2.425	65.126	3.210	88.617	3.717	87.297
Tamura (1987)	1200	3.090	185.009	1.239	48.561	1.206	32.577	0.571	10.721
Xi (1989)[1)]	2934	3.064	185.009	1.474	65.195	3.210	88.617	3.717	87.297

[1)] no drift coefficients given in these catalogues

As a final check we computed from our catalogue the total tidal gravity at station BFO at hourly interval between years 1850 and 2150. The effect due to the Earth's flattening has not been included in the computations because it is also not included in the benchmark series used for the comparisons.

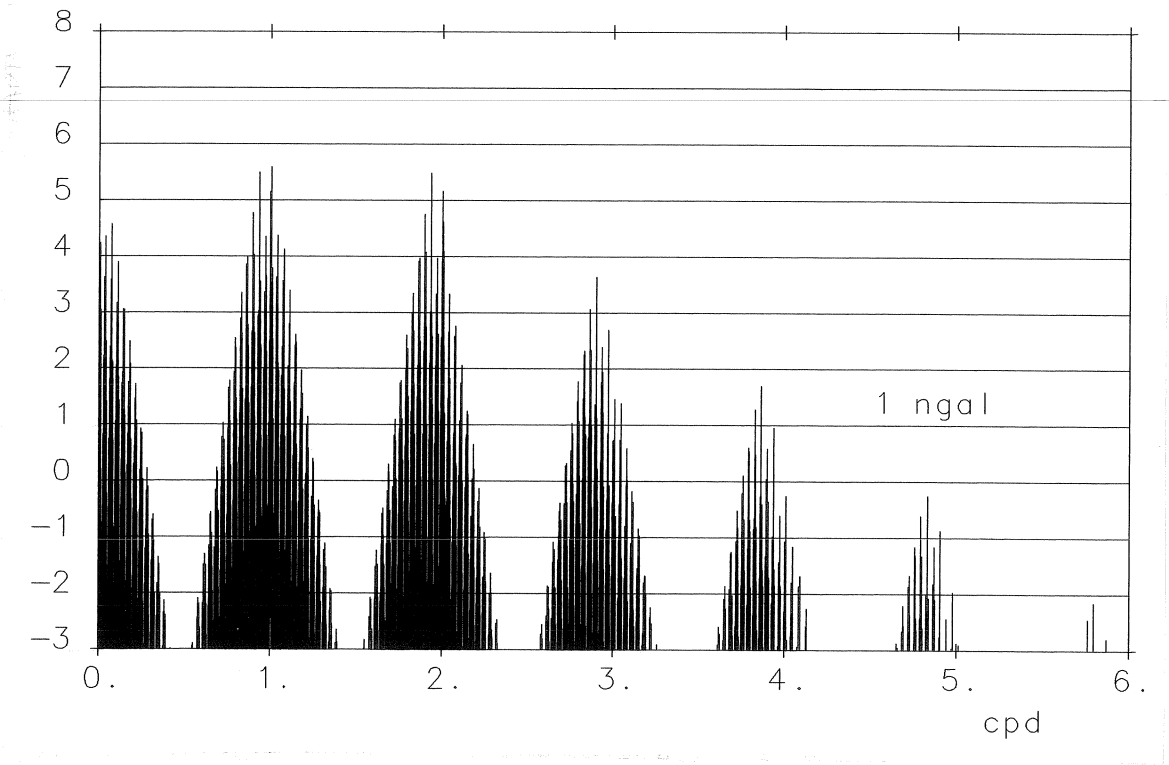

Figure 2: Logarithmic Fourier amplitude spectrum of gravity tides in pm/s^2 at station BFO ($\phi = 48.3306^0$ N, $\lambda = 8.3300^0$ E, h = 589 m)

This series has been compared with the benchmark gravity tide series computed by program GTIDE (Merriam 1992), which is independent from our computations, and to the benchmark gravity tide series of Wenzel (1995). Merriam (1992) claims that his program (based on Newcomb's ephemerides for Sun and on Brown's ephemerides for Moon) is accurate to about 10 pm/s^2, whereas Wenzel (1995) estimates the accuracy of the benchmark gravity tide series computed from the DE200 numerical ephemerides using simple formulas (tidal acceleration as the difference of topocentric and geocentric gravitation) to about 0.01 pm/s^2. A Fourier amplitude spectrum of the benchmark series of Wenzel (1995) is given in Fig. 2, showing e.g. the order 5 gravity tides due to the Moon reaching the 1 pm/s^2 = 0.1 ngal amplitude level and the order 6 gravity tides due to the Moon reaching the 0.01 pm/s^2 = 0.001 ngal level. A comparison of the benchmark gravity tide series of Merriam (1992) and Wenzel (1995) over the time span 1970–2029 at 524 288 hourly samples gave 12.381 pm/s^2 rms difference (-45.527 pm/s^2 at minimum, 43.722 pm/s^2 at maximum) in time domain and 0.041 pm/s^2 rms difference (11.779 pm/s^2 at maximum) in frequency domain. These discrepancies are due to truncations and errors of the ephemeris series used by the GTIDE program.

The result of comparisons for different benchmark gravity tide series and different time spans are given in Tab. 7. There can clearly be seen that gravity tides computed from the HW95 catalogue show much larger differences to the benchmark series of Merriam (1992) than to the benchmark series of Wenzel (1995). The differences between gravity tides computed from the HW95 catalogue and from GTIDE are shown in Fig. 3 in time domain and in Fig. 4 in frequency domain. They are very similar to the differences between the benchmark gravity tide series by Merriam (1992) and Wenzel (1995) not shown here. The differences between gravity tides computed from the HW95 catalogue and from the benchmark gravity series by Wenzel (1995) are shown in Fig. 5 in time domain and in Fig. 6 in frequency domain. A histogram of the differences in time domain (Fig. 7) shows an almost perfect normal distribution. These differences can be attributed to errors and omissions of the HW95 catalogue. The comparison over 300^a time span suggests an accuracy of our catalogue of 1.4 pm/s^2 rms in time domain and of 0.002 pm/s^2 rms in frequency domain.

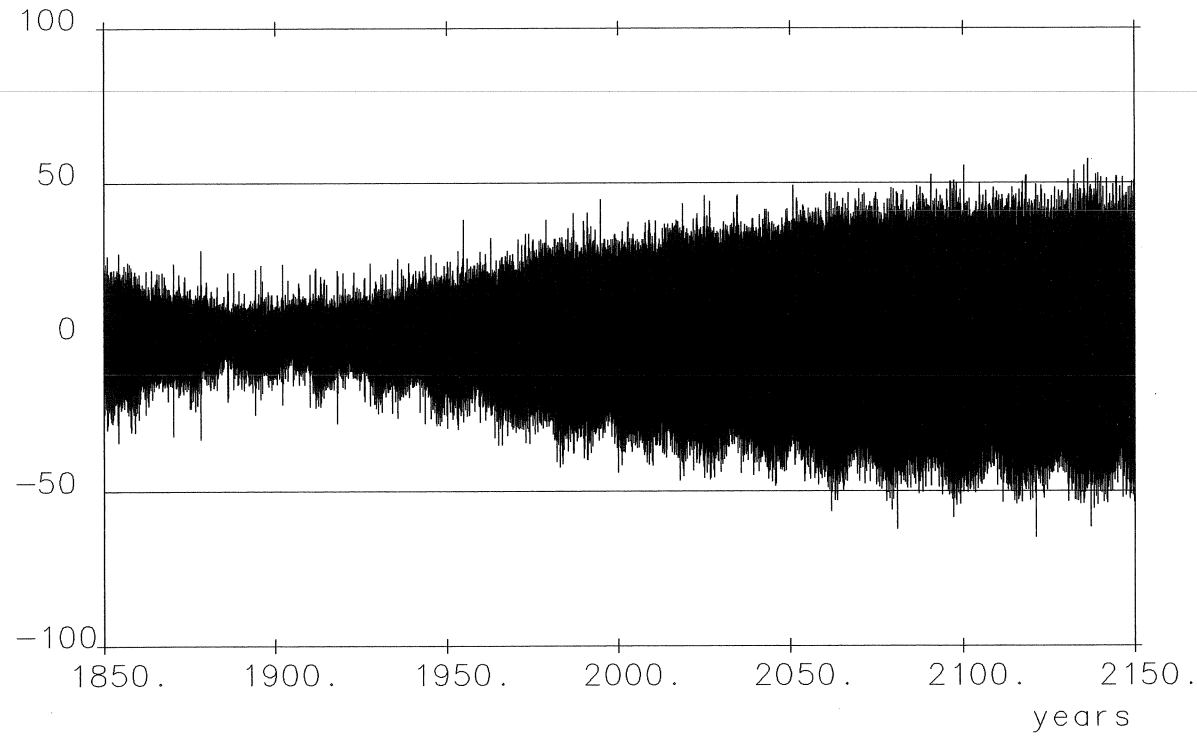

Figure 3: Differences in pm/s^2 between gravity tides computed at station BFO ($\phi = 48.3306^0$ N, $\lambda = 8.3300^0$ E, h = 589 m) from HW95 tidal potential catalogue and the benchmark gravity tide series of Merriam (1992)

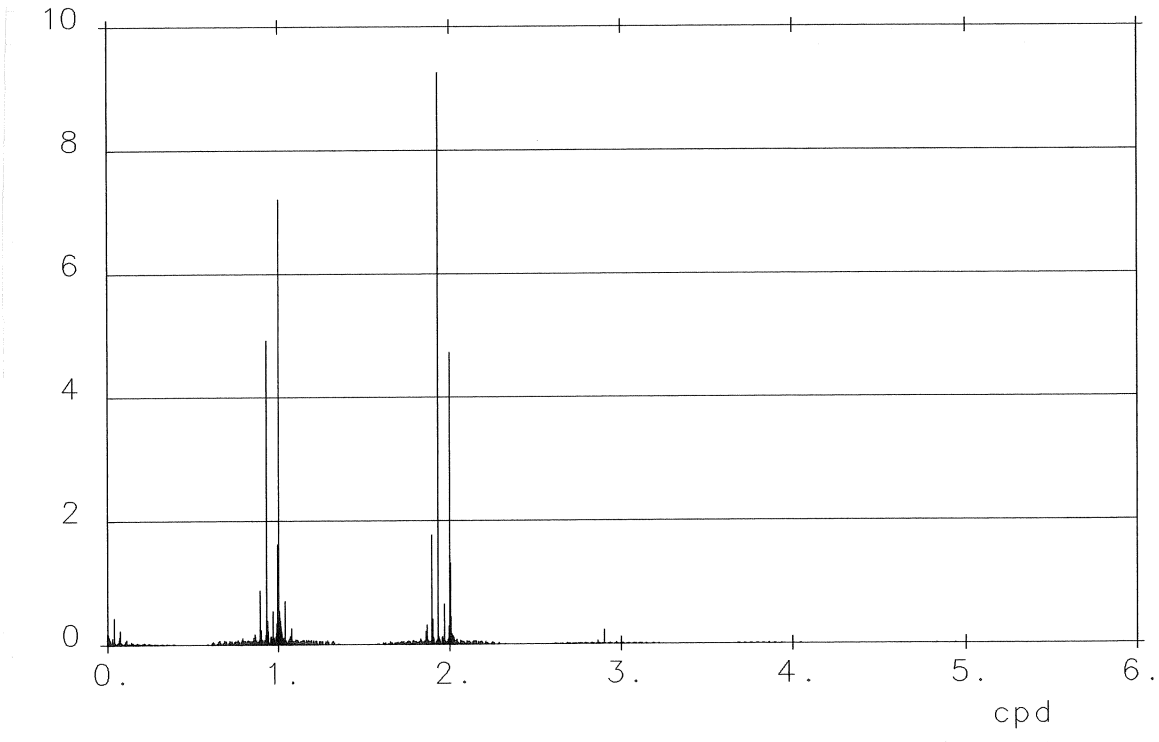

Figure 4: Fourier amplitude spectrum in pm/s^2 of differences between gravity tides computed at station BFO ($\phi = 48.3306^0$ N, $\lambda = 8.3300^0$ E, h = 589 m) from HW95 tidal potential catalogue and the benchmark gravity tide series of Merriam (1992)

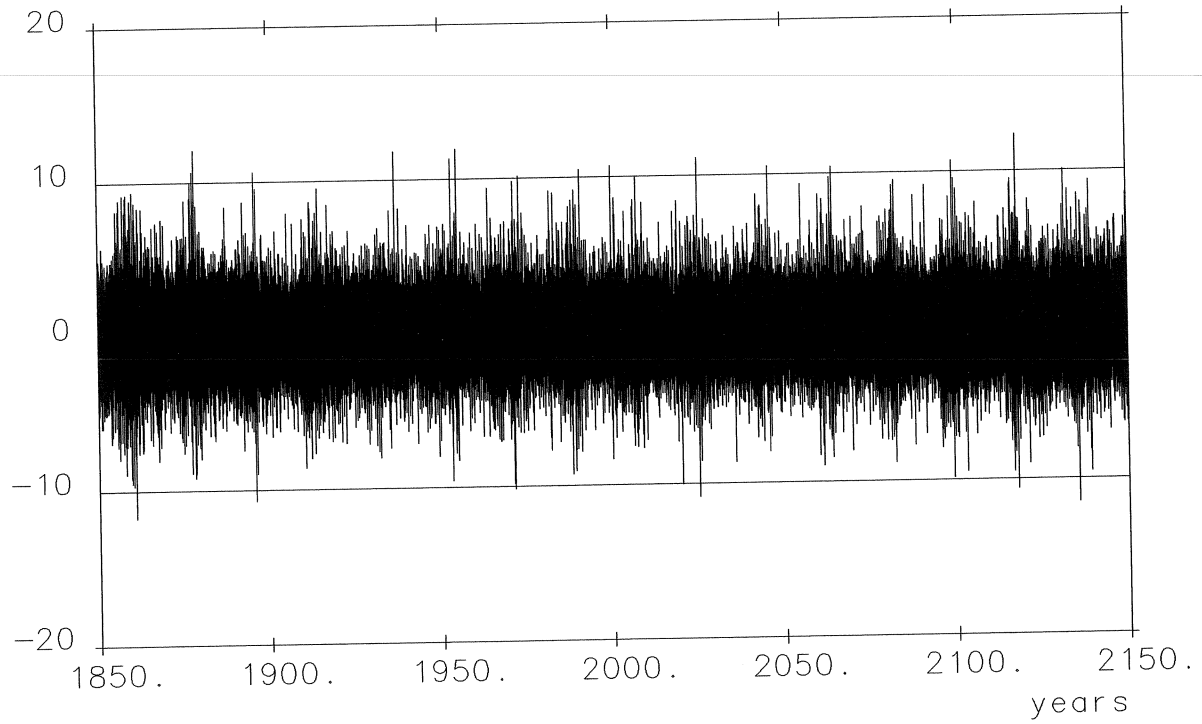

Figure 5: Differences in pm/s^2 between gravity tides computed at station BFO (ϕ = 48.3306^0 N, λ = 8.3300^0 E, h = 589 m) from HW95 tidal potential catalogue and the benchmark gravity tide series of Wenzel (1995)

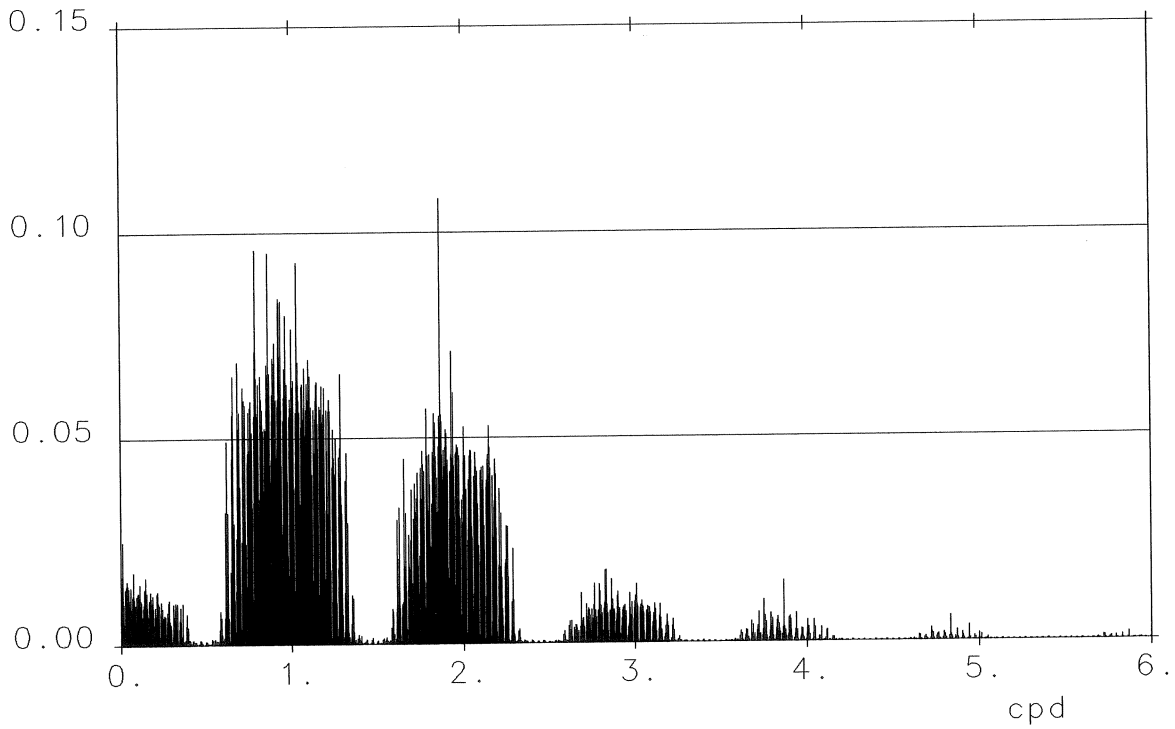

Figure 6: Fourier amplitude spectrum in pm/s^2 of differences between gravity tides computed at station BFO (ϕ = 48.3306^0 N, λ = 8.3300^0 E, h = 589 m) from HW95 tidal potential catalogue and the benchmark gravity tide series of Wenzel (1995)

Table 7: Comparison of gravity tides computed at station BFO (ϕ = 48.3306^0 N, λ = 8.3300^0 E, h = 589 m) from tidal potential catalogue HW95 and taken from different benchmark series.

benchmark series	time span	samples	time domain [pm/s^2]			freq. domain [pm/s^2]	
			rms	min.	max.	rms	max.
Merriam (1992)	1850–2150	2 629 752	12.668	−64.774	57.503	− − −	− − −
Merriam (1992)	1881–2120	2 097 152	12.467	−62.287	55.496	0.021	9.261
Wenzel (1995)	1850–1909	524 288	1.453	−11.749	12.059	0.005	0.207
Wenzel (1995)	1910–1969	524 288	1.314	−9.561	11.924	0.004	0.162
Wenzel (1995)	1970–2029	524 288	1.317	−10.863	11.128	0.004	0.160
Wenzel (1995)	2030–2089	524 288	1.303	−8.947	10.516	0.004	0.159
Wenzel (1995)	2090–2149	524 288	1.433	−11.514	12.340	0.005	0.338
Wenzel (1995)	1881–2120	2 097 152	1.326	−10.863	12.340	0.002	0.108
Wenzel (1995)	1850–2150	2 629 752	1.366	−11.749	12.340	− − −	− − −

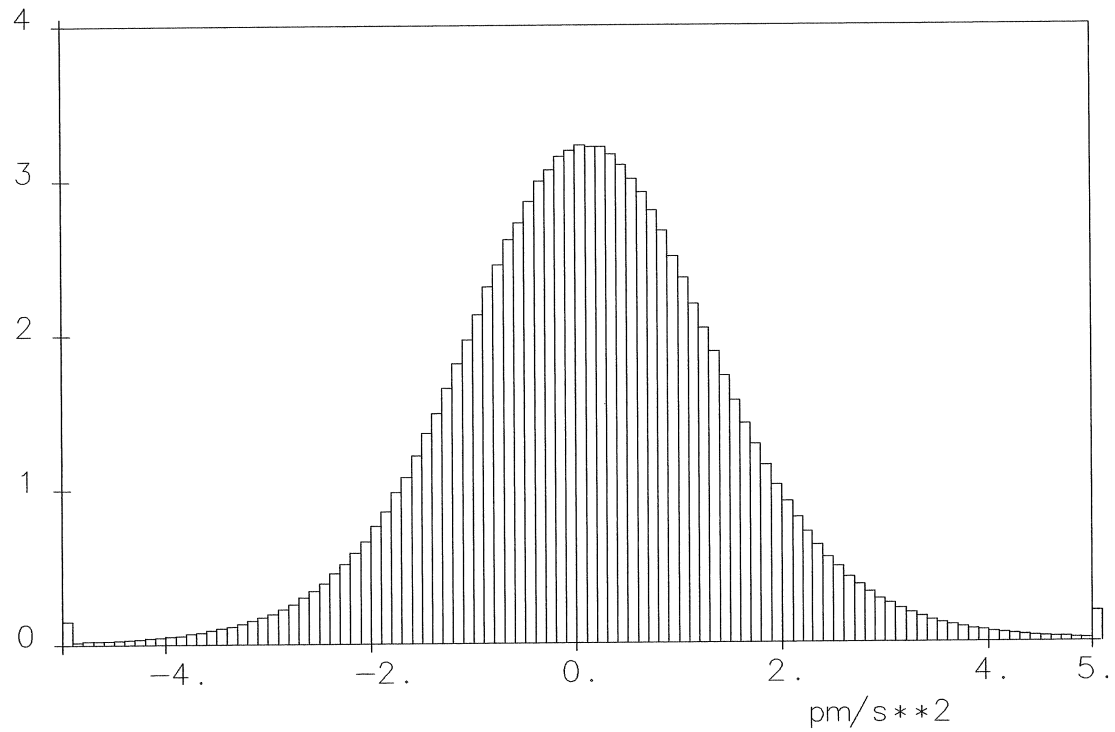

Figure 7: Histogram in % of differences (1850–2150, 2 629 752 hourly samples) between gravity tides computed at station BFO (ϕ = 48.3306^0 N, λ = 8.3300^0 E, h = 589 m) from HW95 tidal potential catalogue and the benchmark gravity tide series of Wenzel (1995)

Comparisons of gravity tides computed from different tidal potential catalogues with the benchmark gravity tide series of Merriam (1992, see Tab. 8) and Wenzel (1995, see Tab. 9) show that the accuracy of the HW95 tidal potential catalogue is superior by a factor of 10 to the benchmark gravity tide series of Merriam (1992), by a factor of 50 to the catalogues of Tamura (1987) and Xi (1989) and by a factor of 25 to the currently best catalogue of Tamura (1993). The comparison with a tidal potential catalogue containing approximately 7700 waves which was recently made available by Roosbeek (1995) was unfortunately impossible because of incomplete description and missing software for that catalogue.

It should be noted that the formulas used to compute the astronomical arguments have an important role in such computations. We have used for Tab. 8 and 9 the formulas derived from Simon et al. (1994) (Appendix A) for the Doodson (1921), Cartwright et al. (1971, 1973), Büllesfeld (1985) and for the HW95 catalogue, and the formulas given by Tamura (1987) for the Tamura (1987, 1993) and the Xi (1989) tidal potential catalogues. The formulas given by Xi (1987) produce much larger errors for the Xi (1989) catalogue.

Table 8: Comparison of gravity tides (1970–2029, 524 288 hourly samples) computed at station BFO (ϕ = 48.3306^0 N, λ = 8.3300^0 E, h = 589 m) from different tidal potential catalogues and from program GTIDE of Merriam (1992).

catalogue	waves	time domain [pm/s^2]			freq. dom. [pm/s^2]	
		rms	min.	max.	rms	max.
Doodson (1921)	378	1 019.464	−4 535.876	4 554.334	3.433	1 030.273
Cartwright et al. (1971, 1973)	505	376.442	−2 221.622	2 530.509	1.266	153.401
Büllesfeld (1985)	656	240.356	−1 316.290	1 501.160	0.802	60.116
Tamura (1987)[1)]	1 200	68.350	−512.823	528.597	0.229	12.111
Xi (1989)[1)]	2 934	84.653	−496.061	546.135	0.279	49.192
Tamura (1993)[1)]	2 114	32.460	−232.042	269.676	0.108	12.773
Hartmann and Wenzel (1995)	12 935	12.425	−46.425	45.859	0.042	11.768
benchmark series Wenzel (1995)	–	12.381	−45.527	43.722	0.041	11.779

[1)] Tamura (1987) astronomical arguments used

Table 9: Comparison of gravity tides (1970–2029, 524 288 hourly samples) computed at station BFO (ϕ = 48.3306^0 N, λ = 8.3300^0 E, h = 589 m) from different tidal potential catalogues with benchmark gravity tide series of Wenzel (1995).

catalogue	waves	time domain [pm/s^2]			freq. dom. [pm/s^2]	
		rms	min.	max.	rms	max.
Doodson (1921)	378	1 018.863	−4 538.043	4 520.695	3.431	1 030.269
Cartwright et al. (1971, 1973)	505	373.835	−2 235.637	2 518.319	1.257	145.666
Büllesfeld (1985)	656	239.280	−1 302.376	1 467.521	0.799	55.180
Tamura (1987)[1)]	1 200	67.144	−531.447	507.583	0.225	12.211
Xi (1989)[1)]	2 934	79.371	−499.843	535.262	0.259	38.506
Tamura (1993)[1)]	2 114	29.901	−243.946	248.661	0.100	6.677
Hartmann and Wenzel (1995)	12 935	1.317	−10.863	11.128	0.004	0.160

[1)] Tamura (1987) astronomical arguments used

The programs HWTIDF.FOR and HWTIDC.C supplied within the HW95 package (see Appendix D) allow the use of tidal potential catalogues given in the HW-normalization and format (see Appendix C) with a user defined amplitude threshold in order to minimize the computational effort; the number of waves and the obtained accuracy naturally depends on the chosen amplitude threshold (see Tab. 10 and Fig. 8).

The number of used waves can roughly be predicted from the input amplitude threshold by

$$\log(\text{no. of waves}) = 0.8 - 0.448 \cdot \log(\text{threshold}[\text{m/s}^2]) \tag{19}$$

and the accuracy of gravity tides computed at mid-latitude stations can roughly be predicted from the input amplitude threshold by

$$\log(\text{accuracy}[\text{pm/s}^2]) = 5.7 + 0.767 \cdot \log(\text{threshold}[\text{m/s}^2]). \tag{20}$$

Using this option, the HW95 tidal potential catalogue is able to achieve nearly the same performance with respect to computation time and accuracy as all previous tidal potential catalogues.

Table 10: Comparison of gravity tides (1970–2029, 524 288 hourly samples) computed at station BFO (ϕ = 48.3306^0 N, λ = 8.3300^0 E, h = 589 m) from catalogue HW95 using different amplitude thresholds with benchmark gravity tide series of Wenzel (1995).

threshold	no. of	time domain [pm/s^2]		
[m^2/s^2]	waves	rms	min.	max.
$1.00 \cdot 10^{-1}$	11	88 403.330	−321 492.678	297 866.988
$3.16 \cdot 10^{-2}$	28	27 319.455	−108 174.675	109 525.103
$1.00 \cdot 10^{-2}$	45	14 449.139	−62 286.861	67 322.802
$3.16 \cdot 10^{-3}$	85	6 020.159	−32 560.229	28 931.931
$1.00 \cdot 10^{-3}$	158	2 249.690	−14 587.415	11 931.120
$3.16 \cdot 10^{-4}$	268	978.419	−6 780.051	5 934.767
$1.00 \cdot 10^{-4}$	441	436.992	−3 049.676	2 943.019
$3.16 \cdot 10^{-5}$	768	173.071	−1 331.572	1 242.490
$1.00 \cdot 10^{-5}$	1 273	68.262	−520.909	484.510
$3.16 \cdot 10^{-6}$	2 052	29.229	−217.114	229.504
$1.00 \cdot 10^{-6}$	3 359	11.528	−99.736	85.920
$3.16 \cdot 10^{-7}$	5 363	4.706	−38.247	35.942
$1.00 \cdot 10^{-7}$	8 074	1.999	−19.407	17.684
$3.16 \cdot 10^{-8}$	10 670	1.391	−12.350	12.287
$1.00 \cdot 10^{-8}$	12 234	1.321	−10.875	11.307

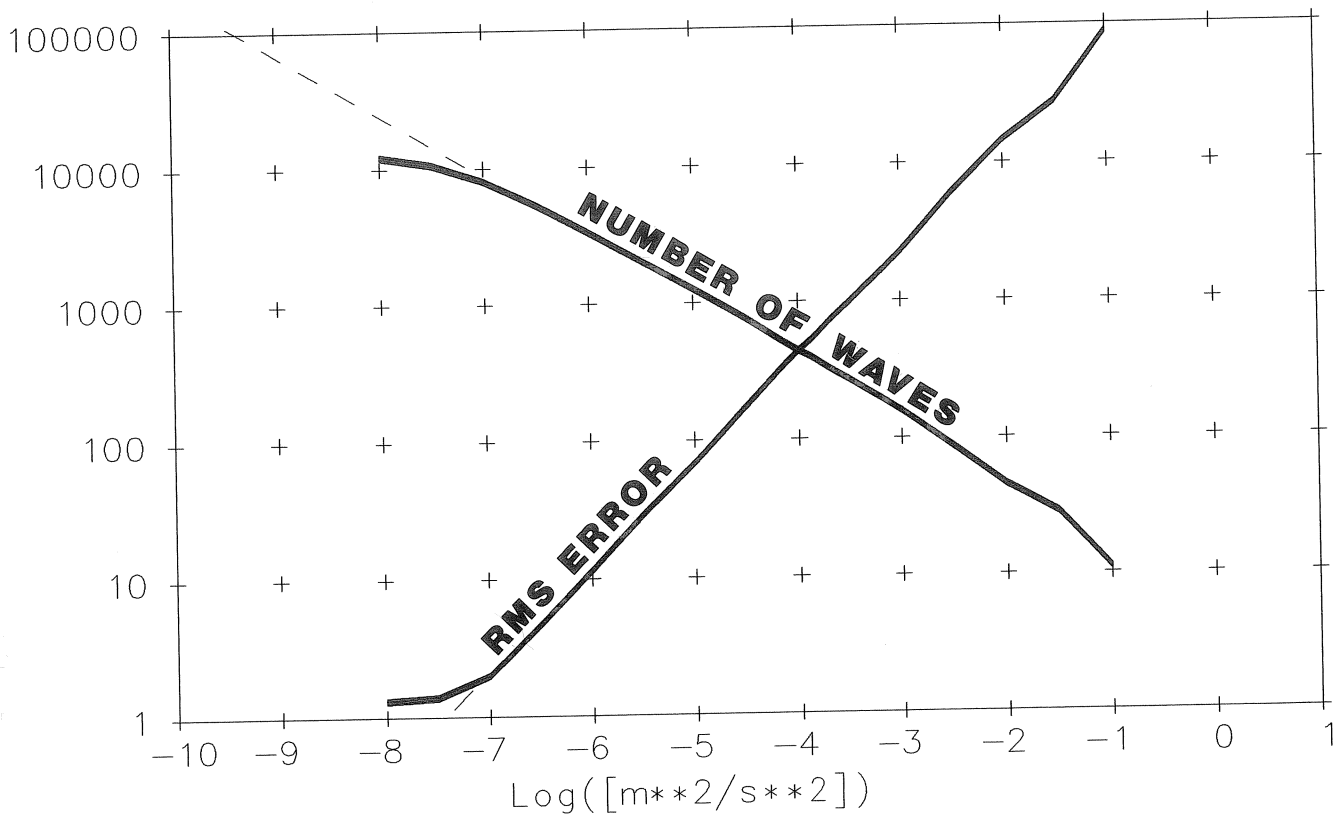

Figure 8: Number of waves and rms error (rms difference to gravity tide benchmark series of Wenzel 1995) of computed tides at mid-latitude stations (ϕ = 48.3^0) as a function of amplitude threshold for the HW95 tidal potential catalogue

6 Conclusions

A catalogue with 12 935 tidal waves containing 19 300 adjusted coefficients of the tide generating potential due to the Moon, the Sun and the planets Mercury, Venus, Mars, Jupiter and Saturn has been computed. The comparison of gravity tides computed from our catalogue and from different benchmark series over 300^a time span suggests an accuracy of our catalogue of 1.4 pm/s^2 rms and 0.002 pm/s^2 rms in time and frequency domain, respectively. This accuracy is superior by a factor of 50 to the catalogues of Tamura (1987) and Xi (1989), by a factor of 25 to the currently best catalogue of Tamura (1993) and higher than currently needed for the analysis of precise gravimeter records.

Acknowledgements

Data and programs used in this investigation have been supplied by E.M. Standish (Jet Propulsion Laboratory, Pasadena/USA) and Y. Tamura (National Astronomical Observatory, Mizusawa/Japan). Fruitful discussions with J. Schastok (Universität Tübingen), L. Timmen (Universität Hannover), W. Zick (Universität Karlsuhe) and W. Zürn (Black Forest Observatory, Schiltach) helped to carry out this investigation. Torsten Hartmann is supported by the Sonderforschungsbereich 228 (Special Collaborative Program) of the Deutsche Forschungsgemeinschaft. The manuscript has been read by Ch. Wenzel and H.A. Miller. All this is gratefully acknowledged.

References

Aoki, S., Guinot, B., Kaplan, G.H., Kinoshita, H., McCarthy, D.D. and Seidelmann, P.K. (1982): *The new definition of Universal Time*, Astronomy and Astrophysics, **105**, 359–361.

Büllesfeld, F.-J. (1985): *Ein Beitrag zur harmonischen Darstellung des gezeitenerzeugenden Potentials*, Deutsche Geodätische Kommission, Reihe C, **314**, München.

Cartwright, D.E. and Tayler, R.J. (1971): *New computations of the tide generating potential*, The Geophysical Journal of the Royal Astronomical Society, **23**, no. 1, Oxford.

Cartwright, D.E. and Edden, C.A. (1973): *Corrected tables of tidal harmonics*, The Geophysical Journal of the Royal Astronomical Society, **33**, no. 3, Oxford.

Dahlen, F.A. (1993): *Effect of the Earth's ellipticity on the lunar potential*, Geophysical Journal International, **113**, 250–251.

Doodson, A.T. (1921): *The harmonic development of the tide generating potential*, Proceedings of the Royal Society (London), Series A 100, 306–328. Reprint in International Hydrographic Revue, **31**, no. 1, Monaco 1954.

Ducarme, B. (1989): *Tidal potential developments for precise tidal evaluation*, Bulletin d'Informations Marées Terrestres, **104**, 7338–7360.

Hartmann, T. and Wenzel, H.-G. (1994a): *Catalogue of the Earth tide generating potential due to the planets,* Bulletin d'Information Marees Terrestres, **118**, 8847–8880.

Hartmann, T. und Wenzel, H.-G. (1994b): *The harmonic development of the Earth tide generating potential due to the direct effect of the planets,* Geophysical Research Letters, **21**, 1991–1993.

Hartmann, T. and Wenzel, H.-G. (1995): *The HW95 tidal potential catalogue,* submitted to Geophysical Research Letters for publication.

Heiskanen, W.A. and Moritz, H. (1967): *Physical geodesy*, W.H.Freeman and Co., San Francisco.

Herring, T. (1991): *The ZMOA-1990 nutation series*, in: Hughes J.A., Smith C.A., Kaplan G.H. (eds.) Proceedings 127th IAU Colloqium, USNO, Washington D.C., p. 157.

Ilk, K.H. (1983): *Ein Beitrag zur Dynamik ausgedehnter Körper - Gravitationswechselwirkung,* Deutsche Geodätische Kommission, Reihe C, **288**, München 1983.

McCarthy, D. (1992): *IERS Standards 1992*, IERS Technical note no. 13, Central Bureau of International Earth Rotation Service, Observatoire de Paris.

Merriam, J. (1992): *An ephemeris for gravity tide predictions at the 1 ngal level*, Geophysical Journal International, **108**, 415–422, 1992.

Mueller, I. (1969): *Spherical and practical astronomy as applied to Geodesy*, Frederick Ungar Publishing Co., New York.

Munk, W. and Hasselmann, K. (1964): *Super-resolution of tides*, Studies on Oceanography, 339-344, 1964.

Newhall, X.X., Standish, E.M. and Williams, J.G. (1983): *DE102: A numerically integrated ephemeris of the Moon and planets spanning forty-four centuries*, Astronomy and Astrophysics, **125**, 150–167.

Press, W.H., Teukolsky, S.A., Vetterling, W.T. and Flannery, B.P. (1992): *Numerical recipes in Fortran/C: The art of scientific computing*, 2nd edition, Cambridge University Press.

Richter, B., Wenzel, H.-G., Zürn, W. and Klopping, F. (1995): *From Chandler Wobble to free oscillations: Comparison of cryogenic gravimeters and other instruments in a wide period range*, Physics of the Earth and Planetary Interior, in print.

Roosbeek, F. (1995): *personal communication by e-mail.*

Seidelmann, P.K. (1982): *1980 IAU Nutation: The final report of the IAU working group on Nutation, Celestial Mechanics*, **27**, 79–106.

Simon, J.L., Bretagnon, P., Chapront, J., Chapront-Touze, M., Francou, G. and Laskar, J. (1994): *Numerical expressions for precession formulae and mean elements for the Moon and the planets*, Astron. Astrophys., **282**, 663–683.

Standish, E.M. and Williams, J.G. (1981): *Planetary and lunar ephemerides DE200–LE200*, (magnetic tape).

Tamura, Y. (1987): *A harmonic development of the tide-generating potential*, Bulletin d'Informations Marées Terrestres, **99**, 6813–6855.

Tamura, Y. (1993): *Additional terms to the tidal harmonic tables*, Proceedings 12th International Symposium on Earth Tides, Beijing 1993, 345–350, Science Press, Beijing/New York.

Wenzel, H.-G. (1976): *Zur Genauigkeit von gravimetrischen Erdgezeitenbeobachtungen*, Wissenschaftliche Arbeiten der Lehrstühle für Geodäsie, Photogrammetrie und Kartographie an der Technischen Universität Hannover, **67**.

Wenzel, H.-G. (1985): *Hochauflösende Kugelfunktionsmodelle für das Gravitationspotential der Erde*, Wissenschaftliche Arbeiten der Fachrichtung Vermessungswesen der Universität Hannover, **137**.

Wenzel, H.-G. (1995): *Benchmark gravity tide series for the validation of tidal potential catalogues*, in preparation for Bulletin d'Informations Marées Terrestres.

Wilhelm, H. (1982): *Earth's flattening effect on the tidal forcing field*, Journal of Geophysics, **1983**, no. 52, 131–135.

Xi, Q.W. (1987): *A new complete development of the tide-generating potential for the epoch J2000.0*, Bulletin d'Informations Marées Terrestres, **99**, 6766–6812.

Xi, Q.W. (1989): *The precision of the development of the tidal generating potential and some explanatory notes*, Bulletin d'Informations Marées Terrestres, **105**, 7396–7404.

Appendix A: Numerical reference values

Table 11: IERS 1992 numerical constants used for the HW95 catalogue

Item	Numerical value	Comment
f	1 / 298.256 421 984 6	flattening of the Earth's ellipsoid
a	6 378 136.3 m	semi-major axis of the Earth's ellipsoid
$J_{2\oplus}$	$1.082\,636\,2 \cdot 10^{-3}$	2nd degree zonal harmonic coeff. of the Earth's gravity field
GM	$3.986\,004\,418 \cdot 10^{14}$ m^3/s^2	geocentric gravitational constant
M/Ea	0.012 300 034	ratio of mass of Moon to that of the Earth
S/Me	6 023 600	ratio of mass of Sun to that of the Mercury
S/Ve	408 523.71	ratio of mass of Sun to that of the Venus
S/Ea	332 946.045	ratio of mass of Sun to that of the Earth
S/Ma	3 098 708.	ratio of mass of Sun to that of the Mars
S/Ju	1 047.348 6	ratio of mass of Sun to that of the Jupiter
S/Sa	3 497.90	ratio of mass of Sun to that of the Saturn

Table 12: Fundamental frequencies in °/hour after Simon et al. (1994) at J2000

j	argument	symbol	frequency [°/hour]
1.	mean local lunar time	τ	14.492 052 120 18
2.	mean lunar longitude	s	0.549 016 519 73
3.	mean solar longitude	h	0.041 068 639 91
4.	mean longitude of lunar perigee	p	0.004 641 813 41
5.	negative mean longitude of lunar ascending node	N'	0.002 206 406 87
6.	mean longitude of solar perigee	p_s	0.000 001 961 51
7.	mean longitude of Mercury	L_{Mer}	0.170 515 710 90
8.	mean longitude of Venus	L_{Ven}	0.066 757 030 52
9.	mean longitude of Mars	L_{Mar}	0.021 836 295 20
10.	mean longitude of Jupiter	L_{Jup}	0.003 463 726 64
11.	mean longitude of Saturn	L_{Sat}	0.001 395 746 14

Table 13: Polynomial coefficients for astronomical arguments after Simon et al. (1994), units are: ° and °/1000 yrs

j	Constant	t	t^2	t^3	t^4
1.	242.149 804 529 99	127 037 328.885 530 56	0.176 961 11	−0.001 831 40	0.000 088 24
2.	218.316 645 629 99	4 812 678.811 957 50	−0.146 638 89	0.001 851 40	−0.000 153 55
3.	280.466 450 160 02	360 007.697 488 06	0.030 322 22	0.000 020 00	−0.000 065 32
4.	83.353 243 119 98	40 690.136 352 50	−1.032 172 22	−0.012 491 68	0.000 526 55
5.	234.955 444 990 00	19 341.362 619 72	−0.207 561 11	−0.002 139 42	0.000 165 01
6.	282.937 340 980 01	17.194 576 67	0.045 688 89	−0.000 017 76	−0.000 033 23
7.	252.250 905 519 99	1 494 740.721 722 33	0.030 349 84	0.000 018 11	−0.000 065 32
8.	181.979 800 850 00	585 192.129 533 30	0.031 013 95	0.000 014 90	−0.000 065 32
9.	355.432 999 580 02	191 416.963 702 97	0.031 051 87	0.000 015 64	−0.000 065 32
10.	34.351 518 740 03	30 363.027 748 48	0.022 329 72	0.000 037 01	−0.000 052 14
11.	50.077 444 300 00	12 235.110 686 22	0.051 907 83	−0.000 029 85	−0.000 097 40

Table 14: Astronomical arguments in ° at 0^h TDB computed at $\lambda = 8.3300^0$ E for specific epochs

argument	1850.01.01	1950.01.01	2050.01.01	2150.01.01
local lunar time	150.630 213 535 74	215.705 970 634 44	268.594 523 232 20	333.677 358 572 37
lunar longitude	129.667 942 898 35	64.375 680 925 41	12.256 877 138 22	306.958 749 697 54
solar longitude	280.298 156 434 10	280.081 651 559 86	280.851 400 370 43	280.636 108 269 91
lunar perigee	99.921 013 163 12	208.843 846 629 19	317.857 478 756 28	66.739 027 555 30
lunar node longit.	213.799 343 145 76	347.886 795 369 57	122.023 056 806 93	256.102 207 092 22
solar perigee	280.359 229 561 74	282.077 726 370 91	283.797 184 033 12	285.517 508 289 35
longitude Mercury	325.235 706 985 14	35.214 895 275 68	109.287 067 512 71	179.267 469 681 80
longitude Venus	244.763 237 292 03	82.373 401 717 46	281.586 355 051 46	119.197 759 918 50
longitude Mars	83.413 213 775 18	144.584 892 058 84	206.281 262 359 70	267.454 182 601 92
longitude Jupiter	159.980 988 156 21	316.200 187 135 32	112.502 961 992 64	268.723 054 071 59
longitude Saturn	14.845 507 210 23	158.322 039 761 85	301.833 108 376 06	85.311 717 058 19

Table 15: Delaunay arguments after Simon et al. (1994), units are: ° and °/1000 yrs

	Constant	t	t^2	t^3	t^4
l	134.963 402 51	1 717 915 923.217 8	31.879 2	0.051 635	−0.000 244 70
l'	357.529 109 18	129 596 581.048 1	−0.553 2	0.000 136	−0.000 011 49
F	93.272 090 62	1 739 527 262.847 8	−12.751 2	−0.001 037	0.000 004 17
D	297.850 195 47	1 602 961 601.209 0	−6.370 6	0.006 593	−0.000 031 69
Ω	125.044 555 01	−6 962 890.543 1	7.472 2	0.007 702	−0.000 059 39

Appendix B: Fully normalized Legendre functions and their derivatives

ℓ	m	$\overline{P}_{\ell m}(\cos\theta)$	$\partial/\partial\theta\ \overline{P}_{\ell m}(\cos\theta)$
1	0	$\sqrt{3}\ \cos\theta$	$-\sqrt{3}\ \sin\theta$
1	1	$\sqrt{3}\ \sin\theta$	$\sqrt{3}\ \cos\theta$
2	0	$\sqrt{\frac{5}{4}}\ (3\cos^2\theta - 1)$	$-\sqrt{45}\ \sin\theta\cos\theta$
2	1	$\sqrt{15}\ \sin\theta\cos\theta$	$\sqrt{15}\ (1 - 2\sin^2\theta)$
2	2	$\sqrt{\frac{15}{4}}\ \sin^2\theta$	$\sqrt{15}\ \sin\theta\cos\theta$
3	0	$\sqrt{\frac{7}{4}}\ \cos\theta\ (5\cos^2\theta - 3)$	$\sqrt{\frac{63}{4}}\ \sin\theta\ (1 - 5\cos^2\theta)$
3	1	$\sqrt{\frac{21}{8}}\ \sin\theta\ (5\cos^2\theta - 1)$	$\sqrt{\frac{21}{8}}\ \cos\theta\ (4 - 15\sin^2\theta)$
3	2	$\sqrt{\frac{105}{4}}\ \sin^2\theta\cos\theta$	$\sqrt{\frac{105}{4}}\ \sin\theta\ (3\cos^2\theta - 1)$
3	3	$\sqrt{\frac{35}{8}}\ \sin^3\theta$	$\sqrt{\frac{315}{8}}\ \sin^2\theta\cos\theta$
4	0	$\sqrt{\frac{9}{64}}\ (3 - 30\cos^2\theta + 35\cos^4\theta)$	$\sqrt{\frac{225}{4}}\ (3 - 7\cos^2\theta)\sin\theta\cos\theta$
4	1	$\sqrt{\frac{45}{8}}\ \sin\theta\cos\theta\ (7\cos^2\theta - 3)$	$\sqrt{\frac{45}{8}}\ (3 - 27\cos^2\theta + 28\cos^4\theta)$
4	2	$\sqrt{\frac{45}{16}}\ \sin^2\theta\ (7\cos^2\theta - 1)$	$\sqrt{45}\ (7\cos^2\theta - 4)\sin\theta\cos\theta$
4	3	$\sqrt{\frac{315}{8}}\ \sin^3\theta\cos\theta$	$\sqrt{\frac{315}{8}}\ \sin^2\theta\ (4\cos^2\theta - 1)$
4	4	$\sqrt{\frac{315}{64}}\ \sin^4\theta$	$\sqrt{\frac{315}{4}}\ \sin^3\theta\cos\theta$
5	0	$\sqrt{\frac{11}{64}}\ \cos\theta\ (15 - 70\cos^2\theta + 63\cos^4\theta)$	$\sqrt{\frac{2475}{64}}\ \sin\theta\ (-1 + 14\cos^2\theta - 21\cos^4\theta)$
5	1	$\sqrt{\frac{165}{64}}\ \sin\theta\ (1 - 14\cos^2\theta + 21\cos^4\theta)$	$\sqrt{\frac{165}{64}}\ \cos\theta\ (29 - 126\cos^2\theta + 105\cos^4\theta)$
5	2	$\sqrt{\frac{1155}{16}}\ \sin^2\theta\cos\theta\ (3\cos^2\theta - 1)$	$\sqrt{\frac{1155}{16}}\ \sin\theta\ (1 - 12\cos^2\theta + 15\cos^4\theta)$
5	3	$\sqrt{\frac{385}{128}}\ \sin^3\theta\ (9\cos^2\theta - 1)$	$\sqrt{\frac{3465}{128}}\ \sin^2\theta\cos\theta\ (15\cos^2\theta - 7)$
5	4	$\sqrt{\frac{3465}{64}}\ \sin^4\theta\cos\theta$	$\sqrt{\frac{3465}{64}}\ \sin\theta\ (-1 + 6\cos^2\theta - 5\cos^4\theta)$
5	5	$\sqrt{\frac{693}{128}}\ \sin^5\theta$	$\sqrt{\frac{17325}{128}}\ \cos\theta\sin^4\theta$
6	0	$\sqrt{\frac{13}{256}}\ (-5 + 105\cos^2\theta - 315\cos^4\theta + 231\cos^6\theta)$	$\sqrt{\frac{5733}{64}}\ \sin\theta\cos\theta\ (-5 + 30\cos^2\theta - 33\cos^4\theta)$
6	1	$\sqrt{\frac{273}{64}}\ \sin\theta\cos\theta\ (5 - 30\cos^2\theta + 33\cos^4\theta)$	$\sqrt{\frac{273}{64}}\ (-5 + 100\cos^2\theta - 285\cos^4\theta + 198\cos^6\theta)$
6	2	$\sqrt{\frac{1365}{512}}\ \sin^2\theta\ (1 - 18\cos^2\theta + 33\cos^4\theta)$	$\sqrt{\frac{1365}{128}}\ \sin\theta\cos\theta\ (19 - 102\cos^2\theta + 99\cos^4\theta)$
6	3	$\sqrt{\frac{1365}{128}}\ \sin^3\theta\cos\theta\ (-3 + 11\cos^2\theta)$	$\sqrt{\frac{12285}{128}}\ \sin^2\theta\ (1 - 15\cos^2\theta + 22\cos^4\theta)$
6	4	$\sqrt{\frac{819}{256}}\ \sin^4\theta\ (11\cos^2\theta - 1)$	$\sqrt{\frac{819}{64}}\ \cos\theta\sin\theta\ (-13 + 46\cos^2\theta - 33\cos^4\theta)$
6	5	$\sqrt{\frac{9009}{128}}\ \sin^5\theta\cos\theta$	$\sqrt{\frac{9009}{128}}\ \sin^4\theta\ (6\cos^2\theta - 1)$
6	6	$\sqrt{\frac{3003}{512}}\ \sin^6\theta$	$\sqrt{\frac{27027}{128}}\ \sin^5\theta\cos\theta$

Numerical values for the fully normalized Legendre functions and their derivatives at $\theta = 30^0$ and 147.86^0 are given below for the validation of computer programs.

ℓ	m	$\overline{P}_{\ell m}(\cos 30^0)$	$\partial/\partial\theta\ \overline{P}_{\ell m}(\cos 30^0)$	$\overline{P}_{\ell m}(\cos 147.86^0)$	$\partial/\partial\theta\ \overline{P}_{\ell m}(\cos 147.86^0)$
0	0	+1.000 000 000 000 00	+0.000 000 000 000 00	+1.000 000 000 000 00	+0.000 000 000 000 00
1	0	+1.500 000 000 000 00	−0.866 025 403 784 44	−1.466 615 283 592 39	−0.921 433 453 882 16
1	1	+0.866 025 403 784 44	+1.500 000 000 000 00	+0.921 433 453 882 16	−1.466 615 283 592 39
2	0	+1.397 542 485 937 37	−2.904 737 509 655 56	+1.286 812 835 799 50	+3.021 796 295 718 90
2	1	+1.677 050 983 124 84	+1.936 491 673 103 71	−1.744 634 904 769 52	+1.680 772 499 846 23
2	2	+0.484 122 918 275 93	+1.677 050 983 124 84	+0.548 052 711 590 30	−1.744 634 904 769 52
3	0	+0.859 232 942 804 22	−5.456 862 079 070 72	−0.655 211 418 187 53	−5.457 491 697 511 43
3	1	+2.227 754 615 077 70	+0.350 780 380 010 05	+2.228 011 655 729 77	+0.336 385 482 397 35
3	2	+1.109 264 959 331 18	+3.202 172 114 362 37	−1.227 798 023 592 12	+3.137 100 125 708 62
3	3	+0.261 456 258 291 90	+1.358 566 569 955 26	+0.314 919 152 596 77	−1.503 739 332 499 18
4	0	+0.070 312 500 000 00	−7.307 089 344 431 20	−0.193 931 838 280 90	+6.820 820 630 710 94
4	1	+2.310 704 539 474 92	−3.557 562 367 689 43	−2.156 932 870 451 28	−4.659 651 656 651 40
4	2	+1.781 866 669 570 14	+3.630 921 887 069 45	+1.907 484 340 658 50	−3.078 931 141 322 16
4	3	+0.679 283 284 977 63	+3.137 475 099 502 78	−0.799 974 065 904 00	+3.317 275 746 315 42
4	4	+0.138 658 119 916 40	+0.960 651 634 308 71	+0.177 696 422 280 90	−1.131 334 173 548 18
5	0	−0.740 510 028 655 29	−7.190 338 900 965 81	+0.983 858 389 680 44	−5.814 801 647 513 63
5	1	+1.856 537 521 135 19	−8.951 583 330 127 18	+1.501 375 329 487 98	+10.010 623 984 673 76
5	2	+2.299 384 789 493 97	+1.858 570 598 058 83	−2.343 439 007 470 49	+0.484 582 106 224 10
5	3	+1.246 531 442 526 43	+4.787 471 538 090 58	+1.423 840 883 777 68	−4.681 617 690 346 57
5	4	+0.398 265 128 155 46	+2.529 323 268 443 37	−0.499 034 539 740 47	+2.863 657 895 362 77
5	5	+0.072 712 931 519 48	+0.629 712 458 795 06	+0.099 146 725 388 07	−0.789 042 888 336 85
6	0	−1.348 560 682 131 55	−4.354 422 432 477 01	−1.466 139 355 488 27	+1.938 620 456 907 68
6	1	+0.950 212 876 411 41	−14.005 579 790 168 96	−0.423 041 666 074 73	−14.110 730 639 900 35
6	2	+2.474 703 117 829 05	−2.562 949 164 497 77	+2.337 567 050 841 44	+4.765 706 566 686 09
6	3	+1.855 928 705 325 97	+5.204 530 268 423 98	−2.034 493 925 544 87	+4.310 691 363 063 77
6	4	+0.810 475 688 703 85	+4.550 199 885 746 13	+0.986 634 474 858 22	−4.861 807 755 448 23
6	5	+0.227 046 055 898 41	+1.835 191 420 879 45	−0.302 695 266 919 92	+2.218 775 450 582 08
6	6	+0.037 841 009 316 40	+0.393 255 304 474 17	+0.054 898 790 516 10	−0.524 283 581 515 93

Appendix C: The HW-Format for tidal potential catalogues

For the representation of our tidal potential catalogue, the following "HW-Format" was introduced. Most other catalogues (Doodson 1921, Cartwright et al. 1971, 1973, Büllesfeld 1985, Tamura 1987, Xi 1989) have been transformed into that format. Each data line consists of

```
FORTRAN-77:
  I6,1X,A2,I2,11A3,F12.8,2F11.0,2F9.0

ANSI-C:
  "%6i %2s%2i%3i%3i%3i%3i%3i%3i%3i%3i%3i%12.8f%#12.0f%#12.0f%#10.0f%#10.0f\n"
```

where the entries denote

Col.	1... 6:	sequence number (1...12935; 999999 = end of file)
Col.	7:	blank
Col.	8... 9:	body generating the potential. MO = Moon, SU = Sun, ME = Mercury, VE= Venus, MA = Mars, JU= Jupiter, SA = Saturn, FM = quadrupole moment of the Earth on Moon, FS = quadrupole moment of the Earth on Sun.
Col.	10... 11:	l = degree of the spherical harmonic development.
Col.	12... 14:	m = order of the spherical harmonic development, equal k1 = integer argument number for the mean local Moontime
Col.	15... 17:	k2 = integer argument number for the mean longitude of the Moon
Col.	18... 20:	k3 = integer argument number for the mean longitude of the Sun
Col.	21... 23:	k4 = integer argument number for the mean longitude of the lunar perigee
Col.	24... 26:	k5 = integer argument number for the negative mean longitude of the lunar ascending node
Col.	27... 29:	k6 = integer argument number for the mean longitude of the solar perigee
Col.	30... 32:	k7 = integer argument number for the mean longitude of Mercury
Col.	33... 35:	k8 = integer argument number for the mean longitude of Venus
Col.	36... 38:	k9 = integer argument number for the mean longitude of Mars
Col.	39... 41:	k10= integer argument number for the mean longitude of Jupiter
Col.	42... 44:	k11= integer argument number for the mean longitude of Saturn
Col.	45... 56:	fr= frequency of the tidal wave at J2000 in degree per hour.
Col.	57... 68:	C0 = COS-coefficient of the tidal potential in $10^{-10}\mathrm{m}^2/\mathrm{s}^2$. The C0 coefficient has to be multiplied with the COS of the argument.
Col.	69... 80:	S0 = SIN-coefficient of the tidal potential in $10^{-10}\mathrm{m}^2/\mathrm{s}^2$. The S0 coefficient has to be multiplied with the SIN of the argument.
Col.	81... 90:	C1 = $t\cdot$ COS-coefficent of the tidal potential in $10^{-10}\mathrm{m}^2/\mathrm{s}^2$ per Julian century. The C1 coefficient has to be multiplied with the time difference between the epoch and J2000 (in Julian centuries) and with the COS of the argument.
Col.	91...100:	S1 = $t\cdot$ SIN-coefficent of the tidal potential in $10^{-10}\mathrm{m}^2/\mathrm{s}^2$ per Julian century. The S1 coefficient has to be multiplied with the time difference between the epoch and J2000 (in Julian centuries) and with the SIN of the argument.
Col.	101:	blank
Col.	102...105:	nam= Darwin name of the tidal wave (for very few main tidal waves available only).

Listing of those 45 waves with amplitudes exceeding $1 \cdot 10^{-2}$ m^2/s^2:

number	l	m	k 2	k 3	k 4	k 5	k 6	k 7	k 8	k 9	k 10	k 11	frequency (deg/hour)	C0	S0	C1	S1	nam
1	MO	2	0	0	0	0	0	0	0	0	0	0	0.00000000	-5944286666.	0.	-1935360.	0.	M0
3	SU	2	0	0	0	0	0	0	0	0	0	0	0.00000000	-2751200919.	0.	-890704.	0.	S0
23	MO	2	0	0	0	1	0	0	0	0	0	0	0.00220641	771788513.	0.	-325040.	0.	
194	SU	2	0	0	1	0	0	-1	0	0	0	0	0.04106668	-137899524.	0.	306581.	0.	SA
358	SU	2	0	0	2	0	0	0	0	0	0	0	0.08213728	-855082729.	0.	885919.	0.	SSA
799	MO	2	0	1	-2	1	0	0	0	0	0	0	0.47152105	-185961196.	0.	-64233.	0.	MSM
946	MO	2	0	1	0	-1	0	0	0	0	0	0	0.54437471	-972501389.	0.	-322767.	0.	MM
984	MO	3	0	1	0	0	0	0	0	0	0	0	0.54901652	0.	-103721679.	0.	22110.	
1325	MO	2	0	2	-2	0	0	0	0	0	0	0	1.01589576	-161326507.	0.	-56860.	0.	MSF
1512	MO	2	0	2	0	0	0	0	0	0	0	0	1.09803304	-1841041825.	0.	1939970.	0.	MF
1529	MO	2	0	2	0	0	1	0	0	0	0	0	1.10023945	-763323862.	0.	324410.	0.	
1989	MO	2	0	3	0	-1	0	0	0	0	0	0	1.64240775	-352500762.	0.	370294.	0.	MTM
2001	MO	2	0	3	0	-1	1	0	0	0	0	0	1.64461415	-146096331.	0.	62177.	0.	
3876	MO	2	1	-3	0	2	0	0	0	0	0	0	12.85428619	0.	129857156.	0.	-66007.	2Q1
3979	MO	2	1	-3	2	0	0	0	0	0	0	0	12.92713984	0.	156593207.	0.	-60053.	SIG1
4251	MO	2	1	-2	0	1	-1	0	0	0	0	0	13.39645449	0.	185063773.	0.	44599.	
4263	MO	2	1	-2	0	1	0	0	0	0	0	0	13.39866089	0.	981305656.	0.	-510204.	Q1
4388	MO	2	1	-2	2	-1	0	0	0	0	0	0	13.47151455	0.	186260860.	0.	-76093.	RO1
4664	MO	2	1	-1	0	0	-1	0	0	0	0	0	13.94082919	0.	966886565.	0.	220455.	
4681	MO	2	1	-1	0	0	0	0	0	0	0	0	13.94303560	0.	5125256711.	0.	-2762670.	O1
5059	MO	2	1	0	0	-1	0	0	0	0	0	0	14.48741031	0.	-144896357.	0.	63561.	
5110	MO	2	1	0	0	1	0	0	0	0	0	0	14.49669393	0.	-402872065.	0.	161257.	M1
5525	SU	2	1	1	-3	0	0	1	0	0	0	0	14.91786468	0.	139201619.	0.	-415011.	PI1
5653	SU	2	1	1	-2	0	0	0	0	0	0	0	14.95893136	0.	2380313224.	0.	-1207214.	P1
5946	MO	2	1	1	0	0	-1	0	0	0	0	0	15.03886223	0.	142689589.	0.	-141064.	
5958	MO	2	1	1	0	0	0	0	0	0	0	0	15.04106864	0.	-4925288540.	0.	1908945.	K1
5961	SU	2	1	1	0	0	0	0	0	0	0	0	15.04106864	0.	-2279779400.	0.	875007.	K1
5978	MO	2	1	1	0	0	1	0	0	0	0	0	15.04327505	0.	-977663900.	0.	-226210.	
6244	SU	2	1	1	2	0	0	0	0	0	0	0	15.12320592	0.	-102392652.	0.	159986.	FI1
6738	MO	2	1	2	0	-1	0	0	0	0	0	0	15.58544335	0.	-403016900.	0.	187668.	J1
7106	MO	2	1	3	0	0	0	0	0	0	0	0	16.13910168	0.	-220445439.	0.	349751.	OO1
7112	MO	2	1	3	0	0	1	0	0	0	0	0	16.14130809	0.	-141251705.	0.	150453.	
8628	MO	2	2	-2	0	2	0	0	0	0	0	0	27.89535483	313070026.	0.	8483.	0.	2N2
8720	MO	2	2	-2	2	0	0	0	0	0	0	0	27.96820848	377850712.	0.	2561.	0.	MI2
8976	MO	2	2	-1	0	1	0	0	0	0	0	0	28.43972953	2365821950.	0.	40182.	0.	N2
9082	MO	2	2	-1	2	-1	0	0	0	0	0	0	28.51258319	449404707.	0.	-2587.	0.	NI2
9323	MO	2	2	0	0	0	-1	0	0	0	0	0	28.98189783	-461038339.	0.	258211.	0.	
9337	MO	2	2	0	0	0	0	0	0	0	0	0	28.98410424	12356348081.	0.	130692.	0.	M2
9622	MO	2	2	1	0	-1	0	0	0	0	0	0	29.52847895	-349288916.	0.	-1547.	0.	L2
9947	SU	2	2	2	-3	0	0	1	0	0	0	0	29.95893332	335581352.	0.	-823253.	0.	T2
10068	SU	2	2	2	-2	0	0	0	0	0	0	0	30.00000000	5738394275.	0.	138617.	0.	S2
10303	MO	2	2	2	0	0	0	0	0	0	0	0	30.08213728	1067392061.	0.	-1036988.	0.	K2
10306	SU	2	2	2	0	0	0	0	0	0	0	0	30.08213728	494523165.	0.	-563232.	0.	K2
10318	MO	2	2	2	0	0	1	0	0	0	0	0	30.08434369	465420663.	0.	-184316.	0.	
12022	MO	3	3	0	0	0	0	0	0	0	0	0	43.47615636	-149687399.	0.	993.	0.	M3

Appendix D: Distribution of the HW95 tidal potential catalogue

The HW95 tidal potential catalogue is distributed together with programs in Fortran and C and benchmark gravity tide series to public domain by INTERNET:

adress:	gik.bau-verm.uni-karlsruhe.de = 129.13.100.201
login:	ftp
password:	ftp
directory:	cd pub, cd hw95
description file:	hw95.txt

The contents of the directory `/pub/hw95` is described in file `hw95.txt`, which is given in the following:

```
File: hw95.txt
Status: August 3rd 1995
Contents: Description of files stored in directory hw95

These files are available since July 25th 1995 to anybody on INTERNET/FTP
------------------------------------------------------------------------

adress:    gik.bau-verm.uni-karlsruhe.de = 129.13.100.201
login:     ftp
password:  ftp
directory: cd pub, cd hw95

files:              bytes: contents:

#01 hw95.txt          9.246 contents of the directory hw95
#02 hw95a.tex        29.156 Latex description of the Hartmann and Wenzel (1995) tidal potential cata-
                            logue, needs files here.sty and eqnarray.sty
#03 here.sty            329 Latex style file needed by hw95a.tex
#04 eqnarray.sty      5.729 Latex style file needed by hw95a.tex
#05 doodsehw.dat     46.046 Doodson (1921) tidal potential catalogue
#06 cted73hw.dat     61.186 CTED73 tidal potential catalogue
#07 buellehw.dat     75.609 Buellesfeld (1985) tidal potential catalogue
#08 tamurahw.dat    133.886 Tamura (1987) tidal potential catalogue
#09 xi1989hw.dat    319.599 Xi (1989) tidal potential catalogue
#10 hw95.dat       1.397.665 Hartmann and Wenzel (1995) tidal potential catalogue
#11 hw95.zip         237.886 Hartmann and Wenzel (1995) tidal potential catalogue in compressed form
#12 bfde200a.dat 4.668.460 gravity tide benchmark series 1987-1993
#13 bfde200a.zip 1.781.451 benchmark series bfde200a in compressed form
#14 bfde200b.dat 4.666.636 gravity tide benchmark series 2017-2023
#15 bfde200b.zip 1.786.671 benchmark series bfde200b in compressed form
#16 bfde200c.dat 4.666.636 gravity tide benchmark series 1901-1907
#17 bfde200c.zip 1.782.234 benchmark series bfde200c in compressed form
#18 bfde200d.dat 4.666.636 gravity tide benchmark series 2093-2100
#19 bfde200d.zip 1.789.171 benchmark series bfde200d in compressed form
#20 bfde200s.dat    670.252 gravity tide benchmark series 1987
#21 hwtidf.doc        5.076 documentation of program HWTIDF
#22 hwtidf.for       89.164 Fortran 77 source code of HWTIDF
#23 hwtidf.exe      259.609 executable file under MS-DOS of HWTIDF
#24 hwtidf.ini        3.229 control parameter file for program HWTIDF
#25 hwtidc.doc       10.474 documentation of program HWTIDC
#26 hwtidc.c         48.450 C source code file of program HWTIDC
#27 hwtidc.inp        1.062 control parameter file for program HWTIDC

Please note that the non-ascii files (as e.g. the files with extension .zip and .exe) must be trans-
ferred in the binary mode (using option binary within ftp). The compressed files (with extension
.zip) must be decompressed with program PKUNZIP version 2.x (by Pkware Inc., 9025 N. Deerwood Drive,
Brown Deer, WI 53223 USA) before they can be used, by executing

                    pkunzip filename.zip filename.dat
```

Short description of the files available to public domain in directory hw95:

no:	file:	description:
#01	hw95.txt	this file, gives a description of the contents of hw95 directory
#02	hw95a.tex	Latex file describing the computation and use of the Hartmann and Wenzel (1995) tidal potential catalogue.
#03	here.sty	Latex style file, needed by file hw95a.tex
#04	eqnarray.sty	Latex style file, needed by file hw95a.tex
#05	doodsehw.dat	Doodson (1921) tidal potential catalogue in Hartmann and Wenzel (1995) normalization and format, with 378 waves. Status June 28th 1995, 46.036 bytes under MS-DOS.
#06	cted73hw.dat	Cartwright and Tayler (1971) and Cartwright and Edden (1973) tidal potential catalogue in Hartmann and Wenzel (1995) normalization and format, with 505 waves. Status June 28th 1995, 61.186 bytes under MS-DOS.
#07	buellehw.dat	Buellesfeld (1985) tidal potential catalogue in Hartmann and Wenzel (1995) normalization and format, with 656 waves. Status June 28th 1995, 75.609 bytes under MS-DOS.
#08	tamurahw.dat	Tamura (1987) tidal potential catalogue in Hartmann and Wenzel (1995) normalization tion and format, with 1200 waves. Status June 28th 1995, 133.886 bytes under MS-DOS.
#09	xi1989hw.dat	Xi (1989) tidal potential catalogue in Hartmann and Wenzel (1995) normalization and format, with 2934 waves. Status June 28th 1995, 319.599 bytes under MS-DOS.
#10	hw95.dat	Hartmann and Wenzel (1995) tidal potential catalog with 12935 tidal waves, 19300 adjusted parameters. Status July 25th 1995, 1.399.648 bytes under MS-DOS.
#11	hw95.zip	Hartmann and Wenzel (1995) tidal potential catalog with 12935 tidal waves, 19300 adjusted parameters, compressed under MS-DOS with program PKZIP. Status July 25th 1995, 237.964 bytes under MS-DOS.
#12	bfde200a.dat	benchmark gravity tide series 1987-1993, hourly gravity tides computed for station BFO Schiltach from DE200 numerical ephemeris using a rigid earth model. Status May 27th 1995, 4.668.460 bytes under MS-DOS.
#13	bfde200a.zip	file bfde200a.dat compressed with program PKZIP. Status July 25th 1995, 1.781.451 bytes under MS-DOS.
#14	bfde200b.dat	benchmark gravity tide series 2017-2023, hourly gravity tides computed for station BFO Schiltach from DE200 numerical ephemeris using a rigid earth model. Status May 27th 1995, 4.666.636 bytes under MS-DOS.
#15	bfde200b.zip	file bfde200b.dat compressed with program PKZIP. Status July 25th 1995, 1.786.671 bytes under MS-DOS.
#16	bfde200c.dat	benchmark gravity tide series 1901-1907, hourly gravity tides computed for station BFO Schiltach from DE200 numerical ephemeris using a rigid earth model. Status May 27th 1995, 4.666.636 bytes under MS-DOS.
#17	bfde200c.zip	file bfde200c.dat compressed with program PKZIP. Status July 25th 1995, 1.782.234 bytes under MS-DOS.
#18	bfde200d.dat	benchmark gravity tide series 2093-2100, hourly gravity tides computed for station BFO Schiltach from DE200 numerical ephemeris using a rigid earth model. Status May 27th 1995, 4.666.636 bytes under MS-DOS.
#19	bfde200d.zip	file bfde200d.dat compressed with program PKZIP. Status July 25th, 1995, 1.789.171 bytes under MS-DOS.
#20	bfde200s.dat	benchmark gravity tide series 1987, hourly gravity tides computed for station BFO Schiltach from DE200 numerical ephemeris using a rigid earth model. Status July 25th 1995, 670.252 bytes under MS-DOS.
#21	hwtidf.doc	documentation of program HWTIDF. Status June 28th, 1995, 5.076 bytes under MS-DOS.
#22	hwtidf.for	Fortran 77 source code of HWTIDF. Status June 28th, 1995, 89.164 bytes under MS-DOS.
#23	hwtidf.exe	executable file under MS-DOS of HWTIDF 1.00. This file has been created by compilation of file hwtidf.for using the Lahey F77L3 compiler. Status June 28th, 1995, 259.609 bytes under MS-DOS.
#24	hwtidf.ini	control parameter file for HWTIDF. Status June 28th, 1995, 3.229 bytes under MS-DOS.
#25	hwtidc.doc	documentation of program HWTIDC. Status June 28th, 1995, 10.474 bytes under MS-DOS.
#26	hwtidc.c	C source code file of HWTIDC. Status June 28th, 1995, 48.450 bytes under MS-DOS.
#27	hwtidc.inp	control parameter file for program HWTIDC. Status June 28th, 1995, 1.062 bytes under MS-DOS.

Noise induced by the refrigerating device of a superconducting gravimeter in the seismological station of Membach (Belgium)

M. Van Camp
Observatoire Royal de Belgique, Avenue Circulaire, 3, B-1180 Bruxelles

Abstract

A spectral analysis of the noise produced by the superconducting gravimeter refrigerating system at the seismic station Membach is presented. We give an overview of the different shock absorbers possibilities beneath both the compressor and the "coldhead", (the expander module of the refrigerating system). When the compressor is at 100 m from the sismometers but still in the same galery, it is possible to have a rise of the noise level lower than 5 dB below 40 Hz and for the 40 to 47.5 Hz interval a rise less than 11 dB and 16 dB for the vertical and horizontal components, respectively. The coldhead effect seems to be weak.

1 Introduction

In August 1995 the Royal Observatory of Belgium installed a new superconducting gravimeter (GWR T021) at the Fundamental Geophysical Station of Membach, in the east of Belgium (50.6090° N, 6.0060° E at 250 m elevation). This instrument is the second one in Belgium, the first one (GWR T003) working in Brussels since 1981, the coordinates of which are 50.7986° N, 4.3581° E at 98 m elevation (cf. Figure 1).

For obtaining longer periods of undisturbed gravity data, it is necessary to save the liquid helium contained in the superconducting gravimeter, so GWR Instruments added a "coldhead" (GWR, 1989), a cryogenic refrigerating device made to minimize thermal leaks. This coldhead, actually an expander module, uses gaseous helium as a refrigerant. Power to operate the expander module is drawn from and controlled by a compressor module which also supplies the required gaseous helium in a closed circuit. Both the compressor and the coldhead are sources of vibrations.

Our aim is to see if these are not a too large source of perturbations for the Membach seismic station which is at the extremity of a 150 m long tunnel excavated in schists

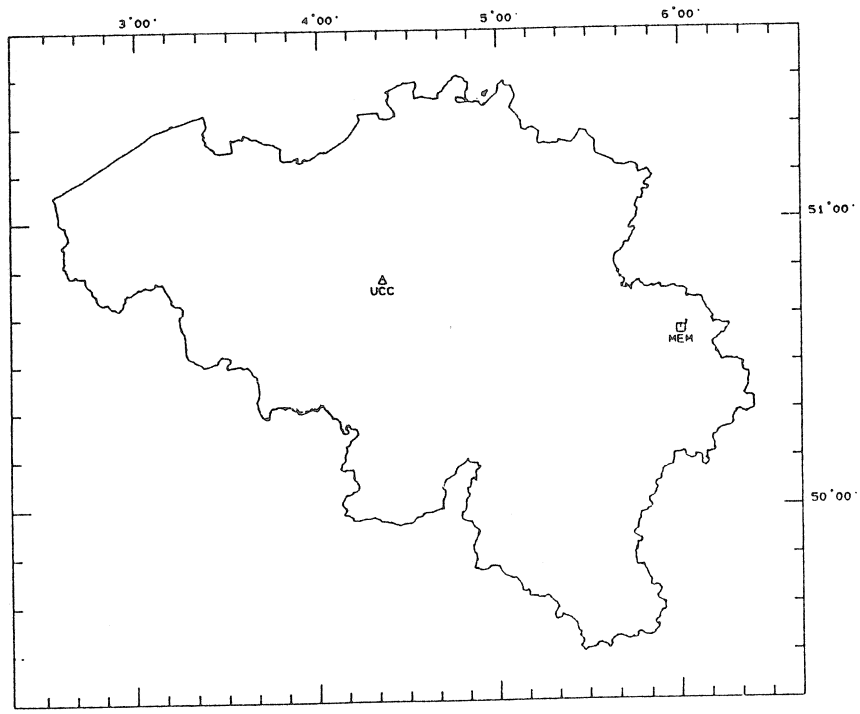

Figure 1: Location of the stations of Uccle (ucc) and Membach (mem) in Belgium

and is remarkably weakly disturbed by the industrial noise. Before installing the new superconducting gravimeter we made different tests in the station, placing the compressor at different distances from the sismometers and using different vibrations absorbers under both compressor and coldhead.

The results of these tests recorded by a three-component sismometer are presented here. A comparison with the data collected during a similar experience at the station of Bad Homburg (Germany) is also given.

2 Description of the measurements in Membach

The used data consist in three-component short period (T_0 = 1s) velocity recordings of L4 – 3D seismometers, sampled at 250 data/s and having a resolution of 15 bits. The corner frequency of the antialiasing filter is at 50 Hz. A restitution filter is used to obtain a flat velocity response between 0.2 Hz and 50 Hz. We calculated the spectra for the different tests with a Parzen window of 16384 points corresponding to 65.392 seconds.

In order to allow an easy comparison between the different spectra we averaged the different spectral amplitudes on 2.5 Hz intervals. Then we took for each test and each interval the logarithm of the ratio of the averaged amplitude and an averaged reference amplitude, taken when the compressor is off. These data are plotted on Figures 2 & 3 for

the vertical component and on Figures 8 & 9 for one of the horizontal components. The first series of points at the left of these figures represents the ratios (in dB) of the averaged amplitudes of the different spectra between 0 and 2.5 Hz, the second one is taken between 2.5 Hz and 5 Hz, and so on until 50 Hz. For each component we took two figures for more lisibility.

We give now a description of the different tests and the symbols used on Figures 2 & 3 and Figures 8 & 9.

1. A reference level, allowing comparisons with the noise increment due to the refrigerating device, is obtained with a recording of the Membach natural noise, when no compressor is present. Unfortunately we do not have a good recording for the date of the test, on september 12^{th}, 1994; so we took an average of the noise taken on the 1^{st}, 10^{th} and 13^{th} of June 1994.

2. The compressor is turned on and is placed on lead shock absorbers near the entrance of the galery, i. e. at a distance of 100 m from the sismometers. Then, we made 2 different tests with the coldhead placed at 15 m from the sismometers :

   (a) the coldhead support frame is directly on the floor without any vibration insulation (+ on Fig. 2 & 8);

   (b) the coldhead support frame is on lead shock absorbers and ballasted by additional mass (• on Fig. 2 & 8).

   A third test was made when the support frame was on shock absorbers, ballasted and surrounded by a phonic insulation, but unfortunately the recording is too noisy. As we shall see it later, it will not prevent us from drawing conclusions.

3. Two other tests were made with the compressor still at 100 m from the sismometers, without lead shock absorber but on a trailer whose tires are good shock absorbers. Then again 2 tests were made with the coldhead, still at 15 m from the sismometer :

   (a) the coldhead support frame is on lead shock absorbers, ballasted and surrounded by a phonic insulation (△ on Fig. 2 & 8);

   (b) the coldhead support frame is without shock absorbers but ballasted and phonic insulated (⋆ on Fig. 2, 3, 8 & 9).

   All these 4 tests are plotted on Figure 2 for the vertical component and on Figure 8 for the horizontal one. The last one (⋆) is also on Figure 3 & 9 to facilitate comparisons.

4. Finally we disconnected the coldhead from the compressor and placed this one directly on the floor, without any vibration insulation. Then 3 tests occured :

(a) one with the compressor at 100 m from the sismometers (□ on Fig. 3 & 9);

(b) one with the compressor at 60 m (○ on Fig. 3 & 9);

(c) one with the compressor at 12 m (◇ on Fig. 3 & 9).

3 Analysis

3.1 Vertical component

First we compare on Figure 2 the noise level produced on the vertical component when the compressor is on the trailer (△ and ⋆) with the level when lead shock absorbers are placed under the compressor (+ and ●). We see that this last one is no more higher than 4 dB. When no shock absorbers are placed under the compressor (Figure 3), the noise level is of course worse, especially when the compressor is at 12 m from the sismometers : then the difference reaches 9 dB between ◇ and ⋆ for the 45 – 47.5 Hz interval.

The high values (between 11 and 23 db) of the 45 to 47.5 Hz averages are due to the 47.2 Hz peak, as it is shown on Figure 4. This comes from the compressor, as it disappears when the compressor is off (Figure 5) and rises to 23 dB when compressor approaches the sismometers (○ and ◇ on Fig. 3). The same effect appears in Bad Homburg too (Figures 6 & 7). We should expect rather only a 50 Hz peak and we asked the compressor manufacturer about this phenomenon but no convincing answer was given. We think that there is a power regulating electronic device inside the compressor which forces it to produce the observed 47.2 Hz peak. Note that the 50 Hz peak doesn't rise when the compressor is on, except when the compressor is closer to the sismometers (○ and ◇ on Fig. 3). On Figure 2 some averages between 47.5 and 50 Hz are even slightly smaller (min. – 2 dB for ●) than the natural noise, probably due to a natural fluctuation. This indicates that for a minimum distance of 100 m the compressor doesn't produce noise around 50 Hz.

The noise on respectively the 45 – 47.5 Hz and the 47.5 – 50 Hz interval is higher of respectively 3 dB and 6 dB when the compressor is at 60 m (○ on Fig. 3) than when it is at 12 m (◇ on Fig. 3). We suspect a resonance effect in the galery depending on the noise source position.

The effect of the coldhead insulation doesn't appear to be significant here : an exemple is the test N° 3, where the noise level when the coldhead is not on shock absorbers (⋆ on Fig. 2) is a little lower than when it is (△ on Fig. 2), which is illogical. However, the difference is small (max. 2 dB) and certainly due more to a fluctuation of the environmental noise than to the head insulation.

3.2 Horizontal component

Concerning the horizontal component, we only show the east-west one, as no more information appears on the north-south one. We see that below 40 Hz the effect is not much

place :	Membach	Membach	Bad Homburg	Bad Homburg
frequency interval :	45-47.5 Hz	47.5-50 Hz	45-47.5 Hz	47.5-50 Hz
natural noise (compressor off)	5.77	23.78	137.81	349.5
no shock absorbers below compressor				
3 m pillar 1			3168.4	363.82
7 m pillar 2			357.50	395.17
12 m	61.35 (◇)	35.00 (◇)		
60 m	82.95 (○)	74.95 (○)	120.49	111.59
100 m	16.11 (□)	24.79 (□)		
compressor on trailer				
100 m	21.78 (⋆)	20.94 (⋆)		

Table 1: averages (in μm/s/ Hz) on the $45 - 47.5$ Hz and $47.5 - 50$ Hz intervals of the spectral amplitudes. These are calculated after restitution of the data of the vertical component of a L4-3D sismometer (Membach) and a LE-3D sismometer (Bad Homburg). The used symbols are the same as those plotted on Figures 2, 3, 8 & 9.

different than for the vertical component. However, over 40 Hz the noise is higher, between 16 and 31 dB for the $45 - 47.5$ Hz interval (in place of 11 and 23 dB for the vertical component). For the horizontal component the compressor on trailer ($\star$ on Fig. 8 & 9) is the best way to absorb shocks as it does for the vertical component.

For all the tests the noise level on the $0 - 2.5$ Hz interval stays between 3.5 and 6 dB for both vertical and horizontal components. Perhaps this is due to the industrial and microsismic noise level, maybe higher on September 12^{th} than on the 1^{st}, 10^{th} and 13^{th} of June.

3.3 Comparison with Bad Homburg

All the values shown on Figures 2, 3, 8 & 9 are relative ones; so to allow comparisons with other stations we plot on table 1 the real values calculated for some tests made in Membach and Bad Homburg. We show only the vertical component results as in Bad Homburg tests were made with just a vertical sismometer. In Bad Homburg two tests were made with the sismometer on well anchored pillars ("pillar 1" and "pillar 2"), discoupled from the floor on which stays the compressor. The high values on these pillars are certainly due to the acoustic noise. At 60 m in Bad Homburg the sismometer is outside the compressor building; then the noise level is even lower than in the building. This is because the sismometer is on a different ground than the compressor and because the natural noise covers the remaining effects. Note on Figure 10 that the Bad Homburg natural noise is higher (up to 33 dB) than in Membach.

4 Conclusions

The best results, with a noise level of less than 5 dB below 40 Hz and for the 40 to 50 Hz interval less than 11 dB and 16 dB for respectively the vertical and horizontal components are obtained with the compressor on the trailer. Of course the distance to the compressor is important too, so when we installed the gravimeter we placed the compressor at $\sim$ 150 m from the sismometers in a shelter outside the galery. This has also the advantage of decoupling the compressor from the rocky floor of the galery. Doing so we hope that no more acoustical effects will occur, if they did (Oncescu *etal*, 1994), and that the decoupling from the rock combined with good shock absorbers, will preserve the site quality. Then perhaps shall we be able to study the effect of the coldhead.

A study with the compressor outside the galery, 150 m far from the coldhead will be done after the installation of the gravimeter. However, we think that the 47.2 Hz effect could not disappear completely. Concerning the industrial and microsismic noise below 2.5 Hz, other tests should be done, taken the noise reference level the same day than for the tests made with the refrigerating device on.

Acknowledgements

This study has greatly benefited from comments and numerous discussions with Dr B. Ducarme. We are very grateful to P. Defraigne who gave her spectral analysis program, to Dr T. Camelbeeck for his sismometers data and to Dr Schwahn (IFAG Frankfurt) who gave the opportunity to make measurements at the Bad Homburg station. I thank also Dr R. Warburton and Dr O. Francis who made the tests in Membach with Dr B. Ducarme, and B. Bukasa for having made the tests at Bad Homburg.

This work was supported by the Royal Observatory of Belgium and by the "Fonds pour la Formation à la Recherche dans l'Industrie et l'Agriculture".

References

Bloomfield, P., *Fourier Analysis of Time Series: an Introduction*, John Wiley & Sons, New-York, 1976.

GWR Instruments. Operating Manual, 1989.

Oncescu, M.L., Camelbeeck, T. and Martin, H., Source parameters for the Roermond aftershocks of 1992 April 13-May 2 and site spectra for P and S waves at the Belgian seismic network. *Geophys. J. Int.*, **116**, 673-682, 1994.

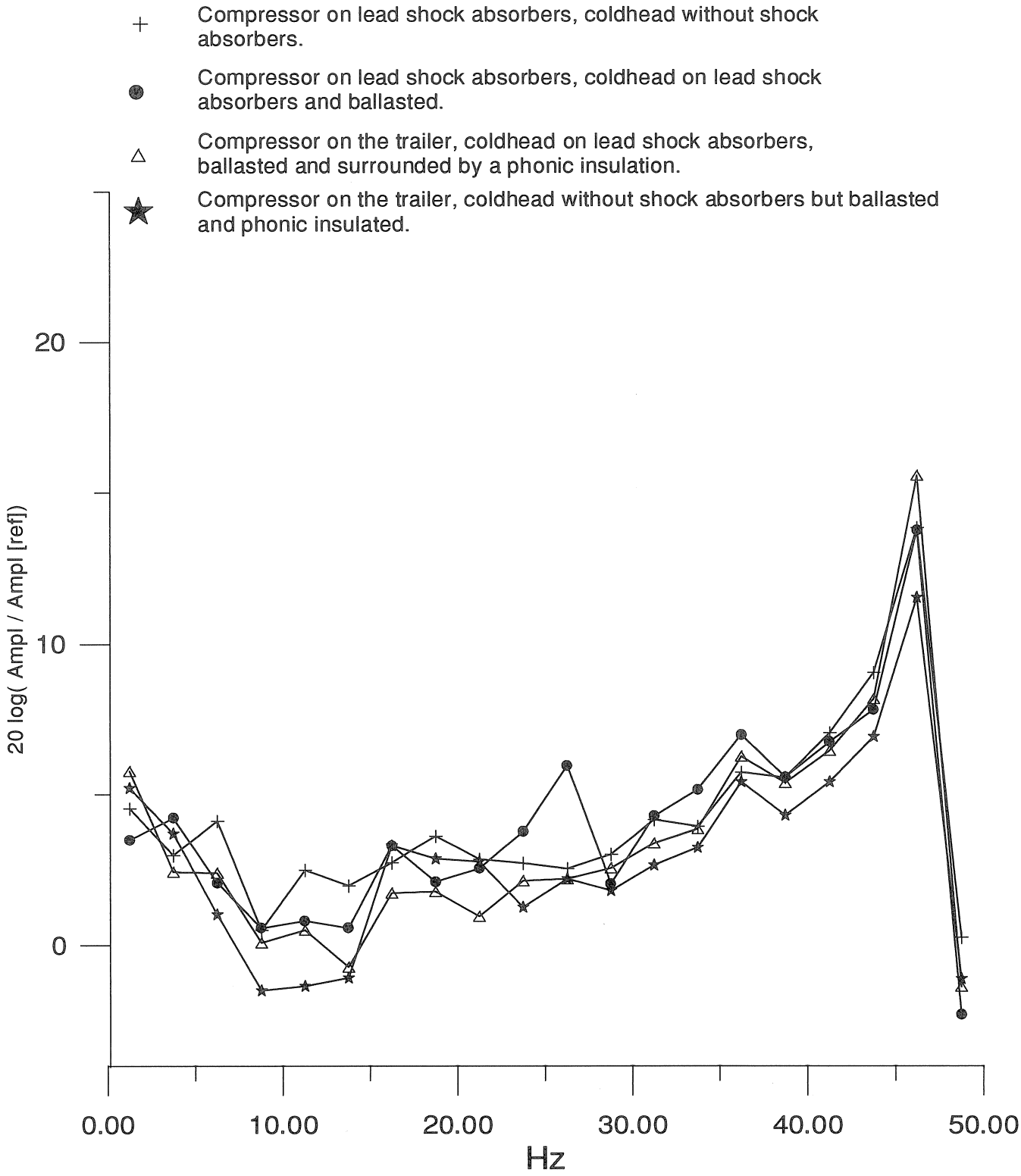

Fig.2 : Membach : vertical component : comparison (in dB) of a reference spectrum with the spectra calculated for different shock absorbers placed beneath both the compressor and the coldhead. The compressor is at 100 m from the seismometers and the coldhead at 15 m. The reference spectrum is calculated when no compressor is present.
Each point is an average of the amplitude on a 2.5 Hz interval.

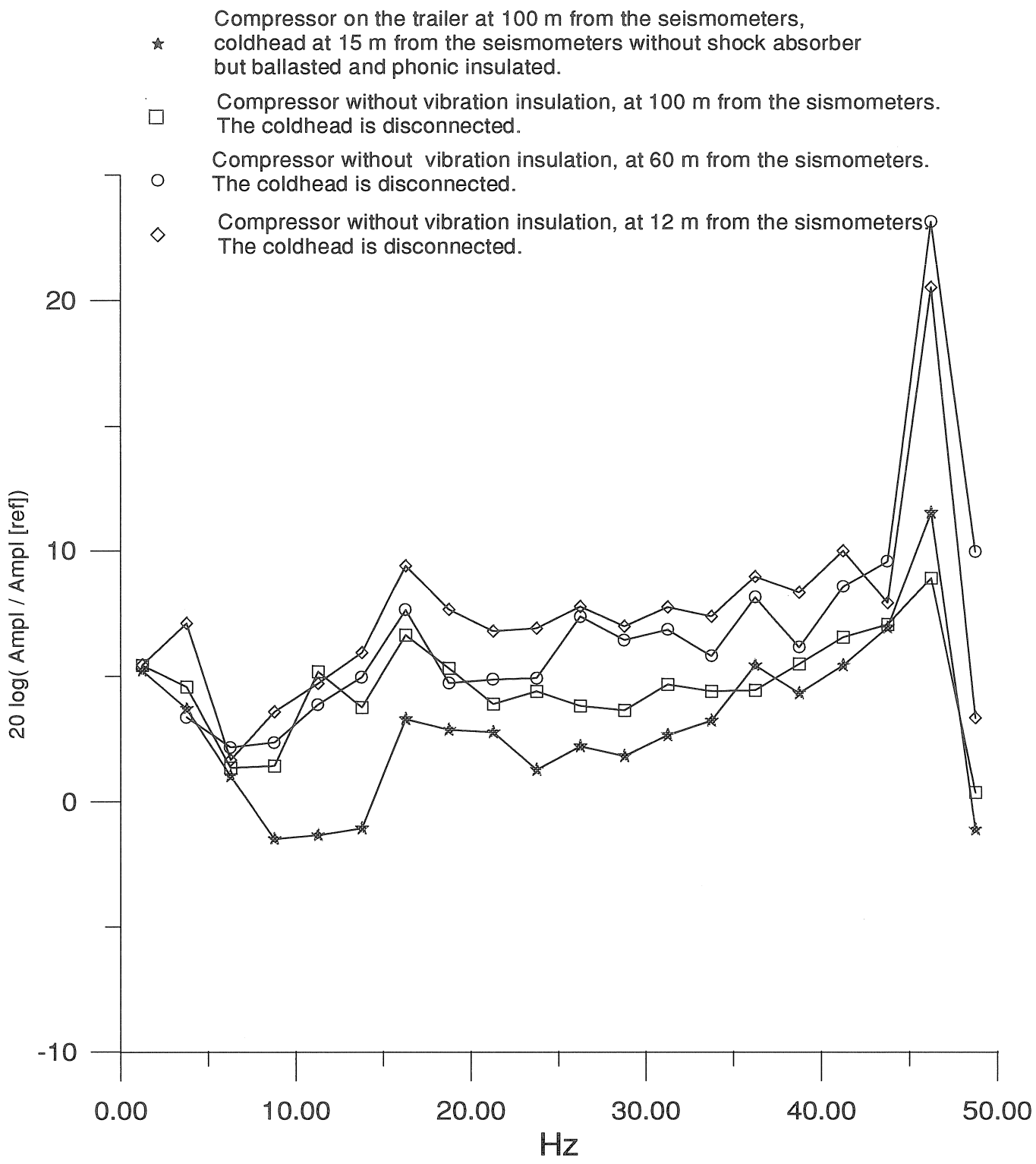

Fig.3 : Membach : vertical component : comparison (in dB) of a reference spectrum with the spectra calculated for different distances of the compressor to the sismometer. There is no shock absorber below the compressor. The reference spectrum is calculated when no compressor is present. The comparison when the compressor is on the trailer is also shown as it has the best noise level.
Each point is an average of the amplitude on a 2.5 Hz interval.

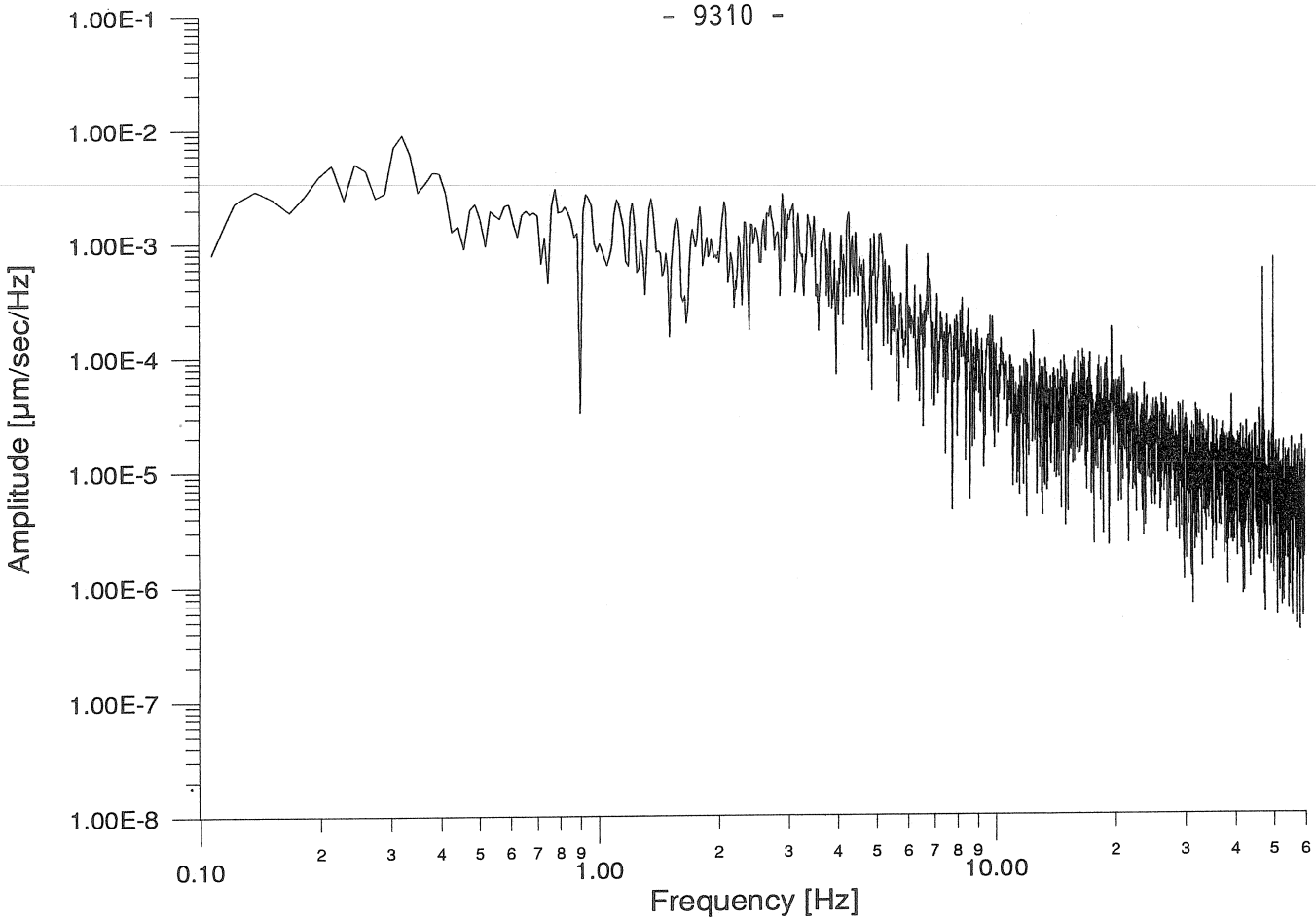

fig. 4: Membach, exemple of spectrum (vertical component) taken when the refrigerating device is on. In this exemple the compressor is on the trailer, at 100 m from the sismometers, there is no shock absorber below the ballasted and phonic insulated coldhead. Note the 47.2 Hz peak.

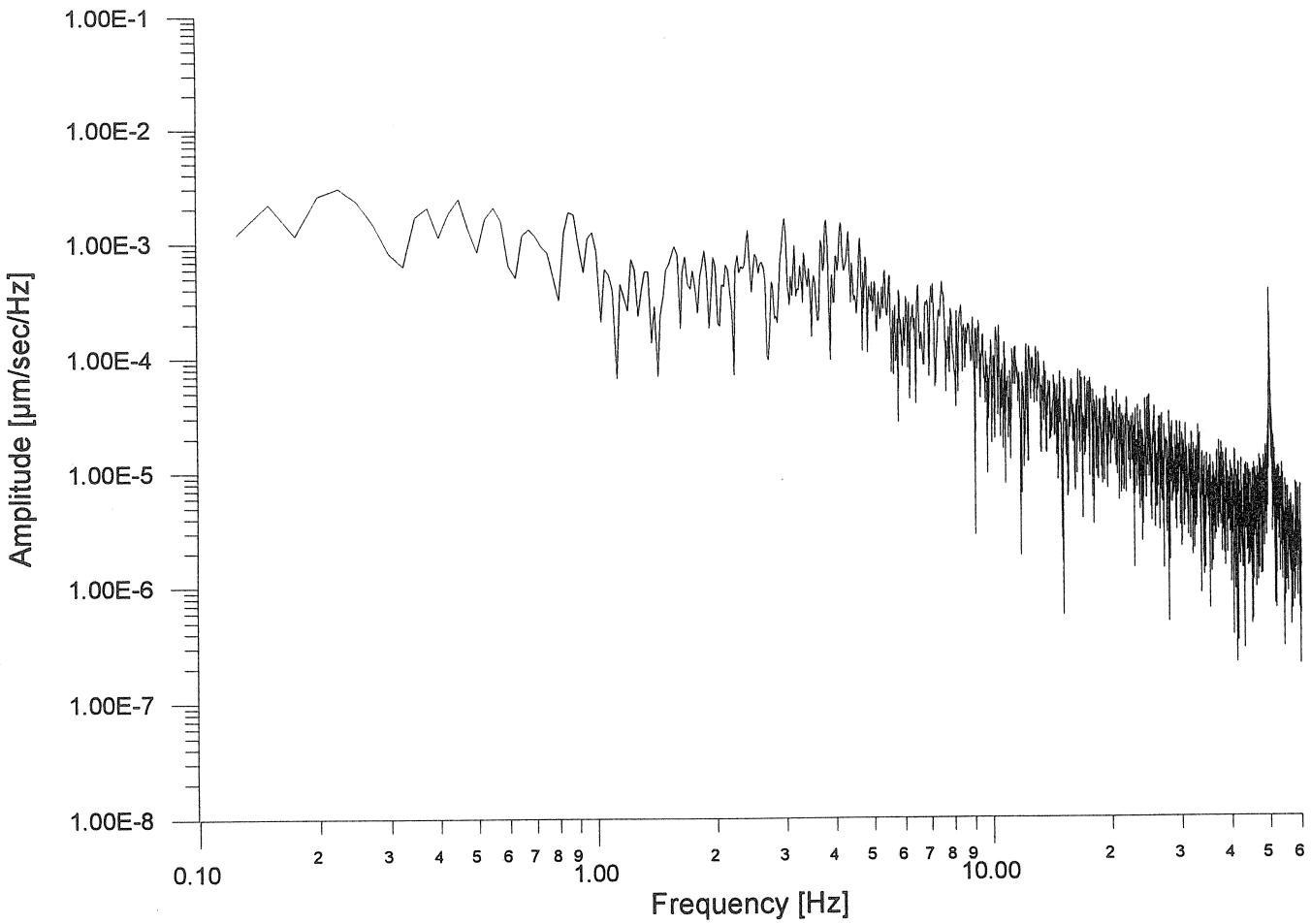

Fig.5 : Membach, spectrum of the noise (vertical component), when the refrigerating device is off. Note the presence of the 50 hz peak and the absence of the 47.2 Hz one.

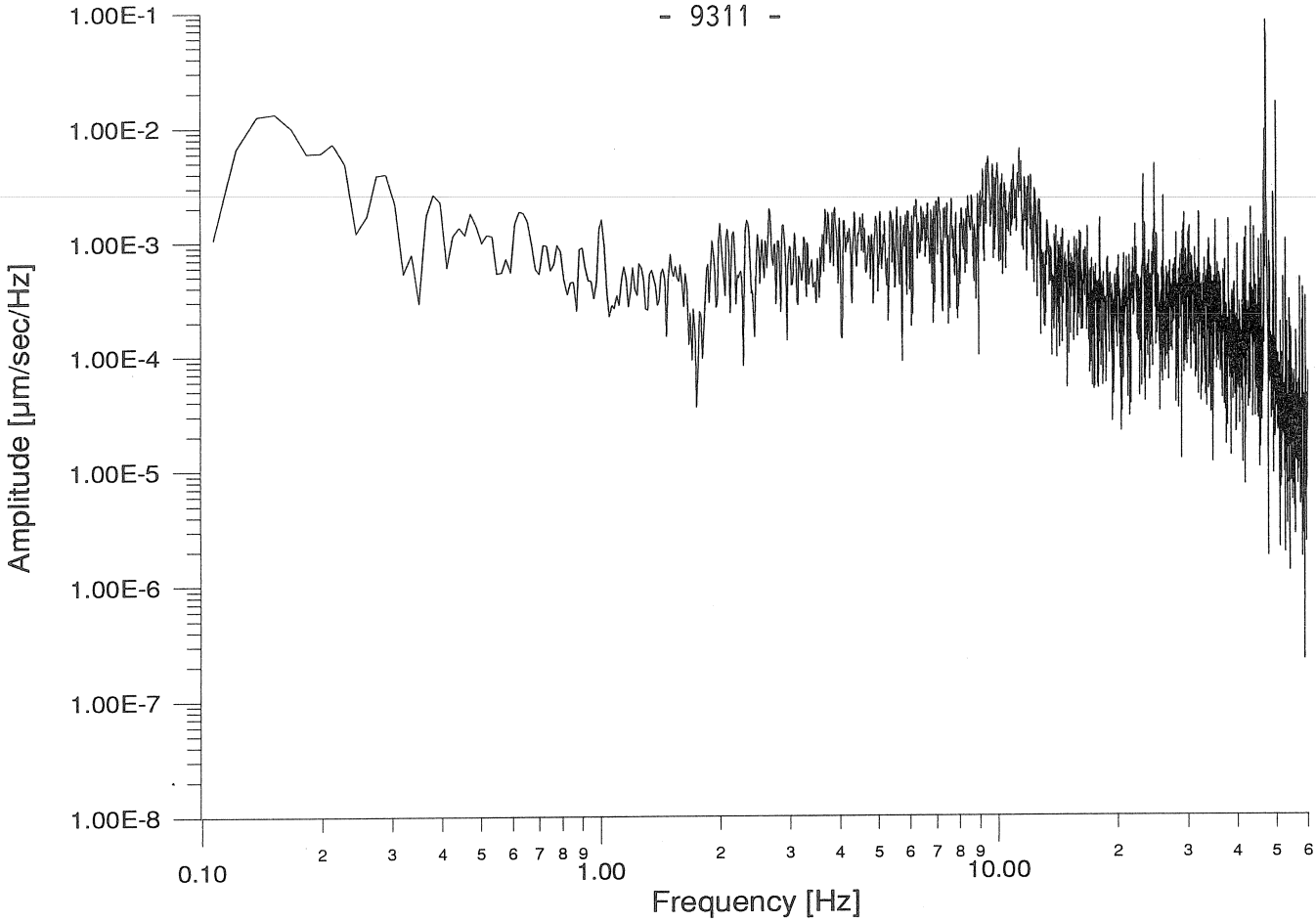

fig. 6: Bad Homburg, spectrum of the noise (vertical component) when the refrigerating device is on. The sismometer is on a pillar at 3 m from the compressor. Note the 47.2 Hz peak.

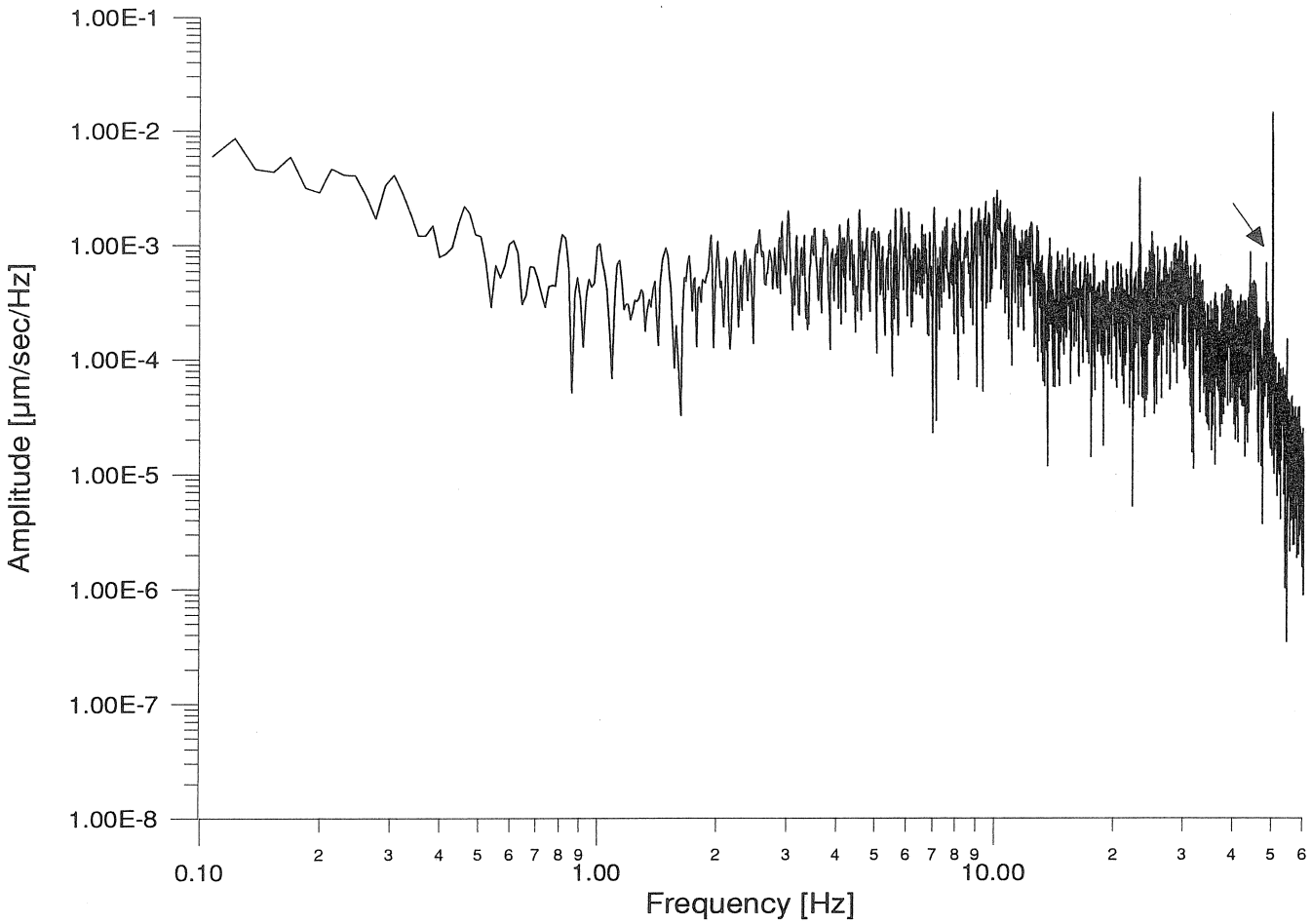

fig. 7: Bad Homburg, spectrum of the noise (vertical component), when the refrigerating device is off. Note the presence of the 50 Hz peak and the absence of the 47.2 Hz one. The peak near the 50 Hz one, indicated by an arrow, is not on 47.2 Hz.

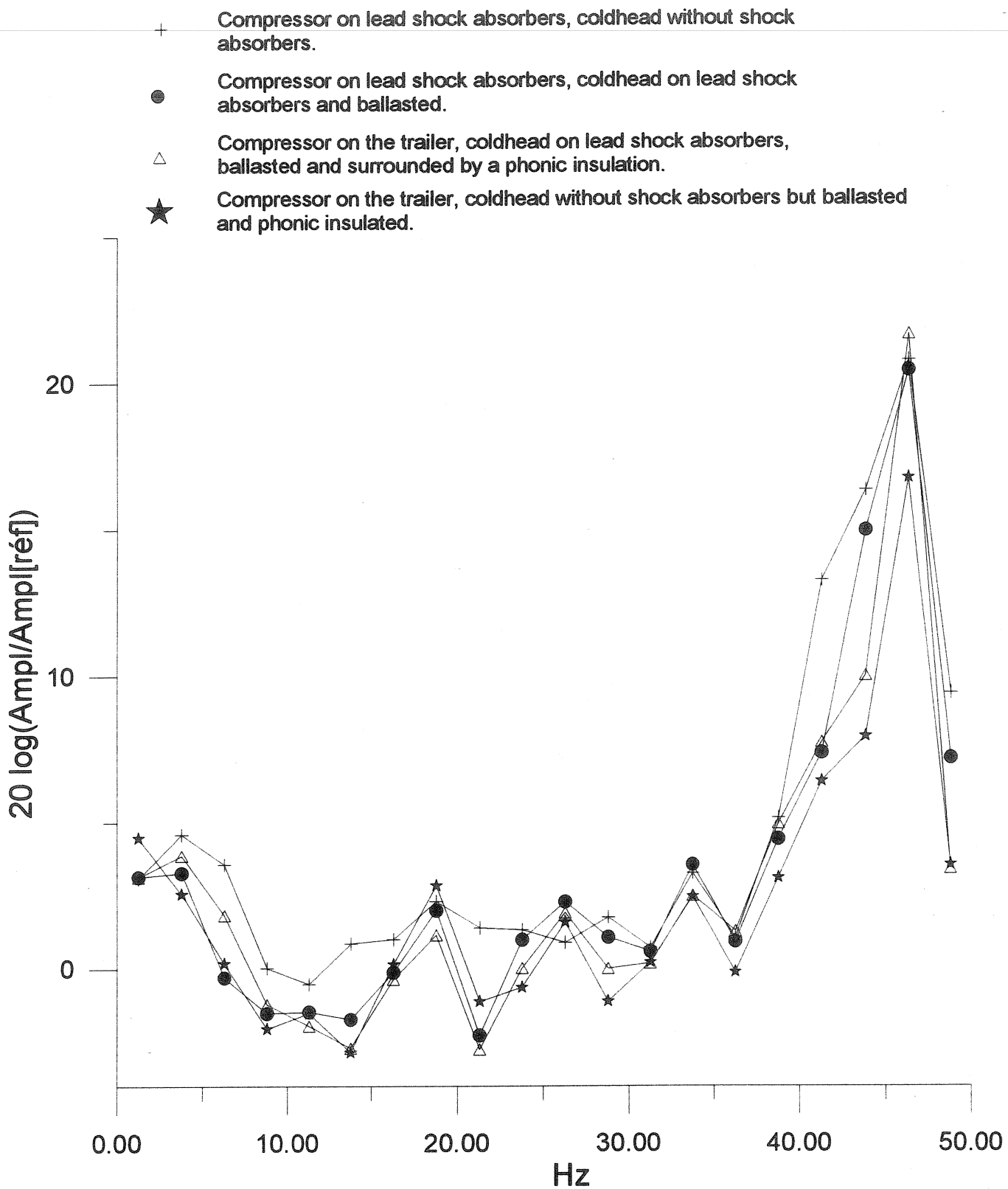

Fig. 8 : Membach : horizontal component (east-west) : compaison (in dB) of a reference spectrum with the spectra calculated for different shock absorbers placed beneath both the compressor and the coldhead. The compressor is at 100 m from the seismometers and the coldhead at 15 m.
The reference spectrum is calculated when no compressor is present.
Each point is an average of the amplitude on a 2.5 Hz interval.

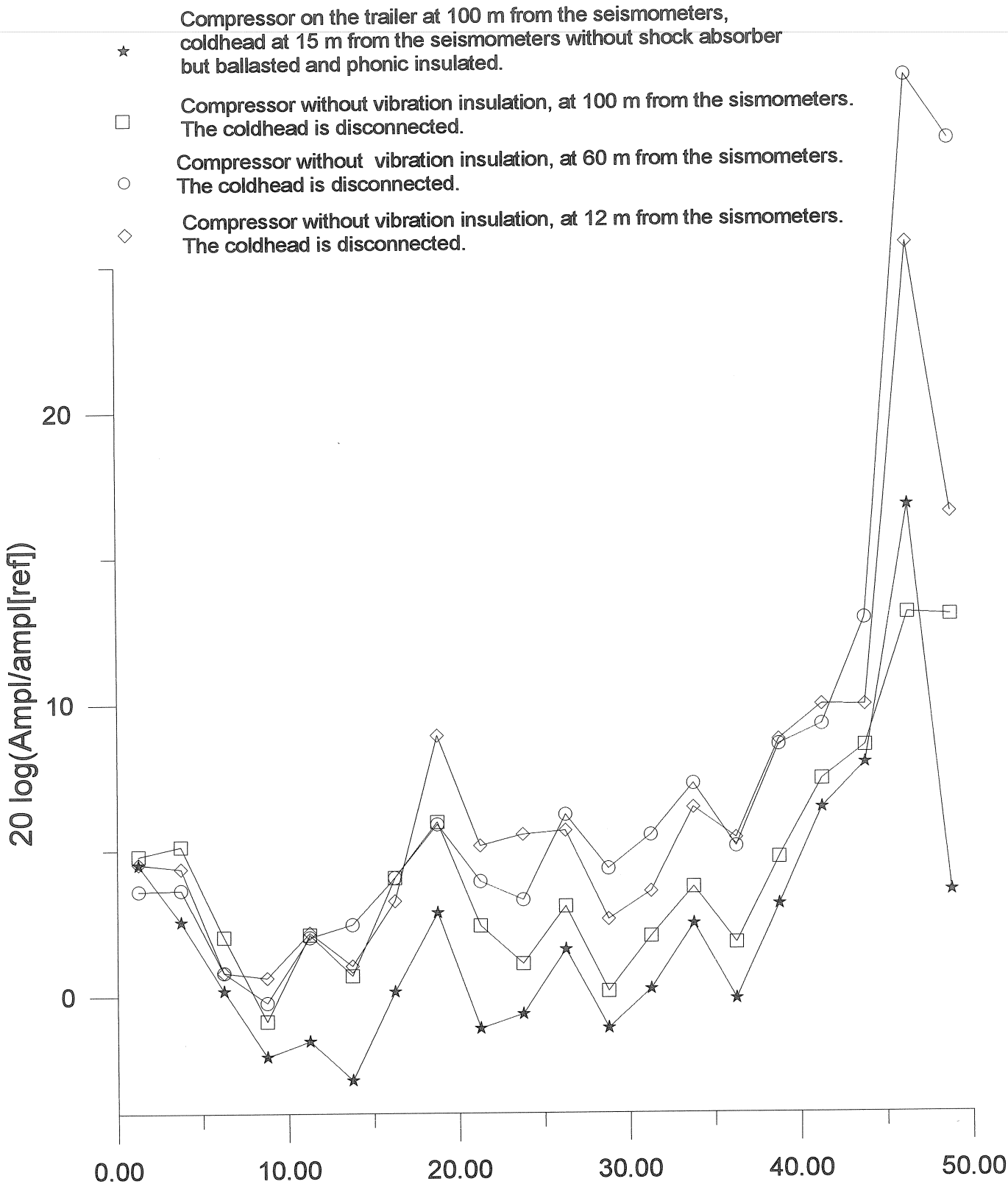

Fig.9 : Membach : horizontal component (east-west) : comparison (in dB) of a reference spectrum with the spectra calculated for different distances of the compressor to the sismometers.
There is no shock absorber below the compressor. The reference spectrum is calculated when no compressor is present.
The comparison when the compressor is on the trailer is also shown as it has the best noise level.
Each point is an average of the amplitude on a 2.5 Hz interval.

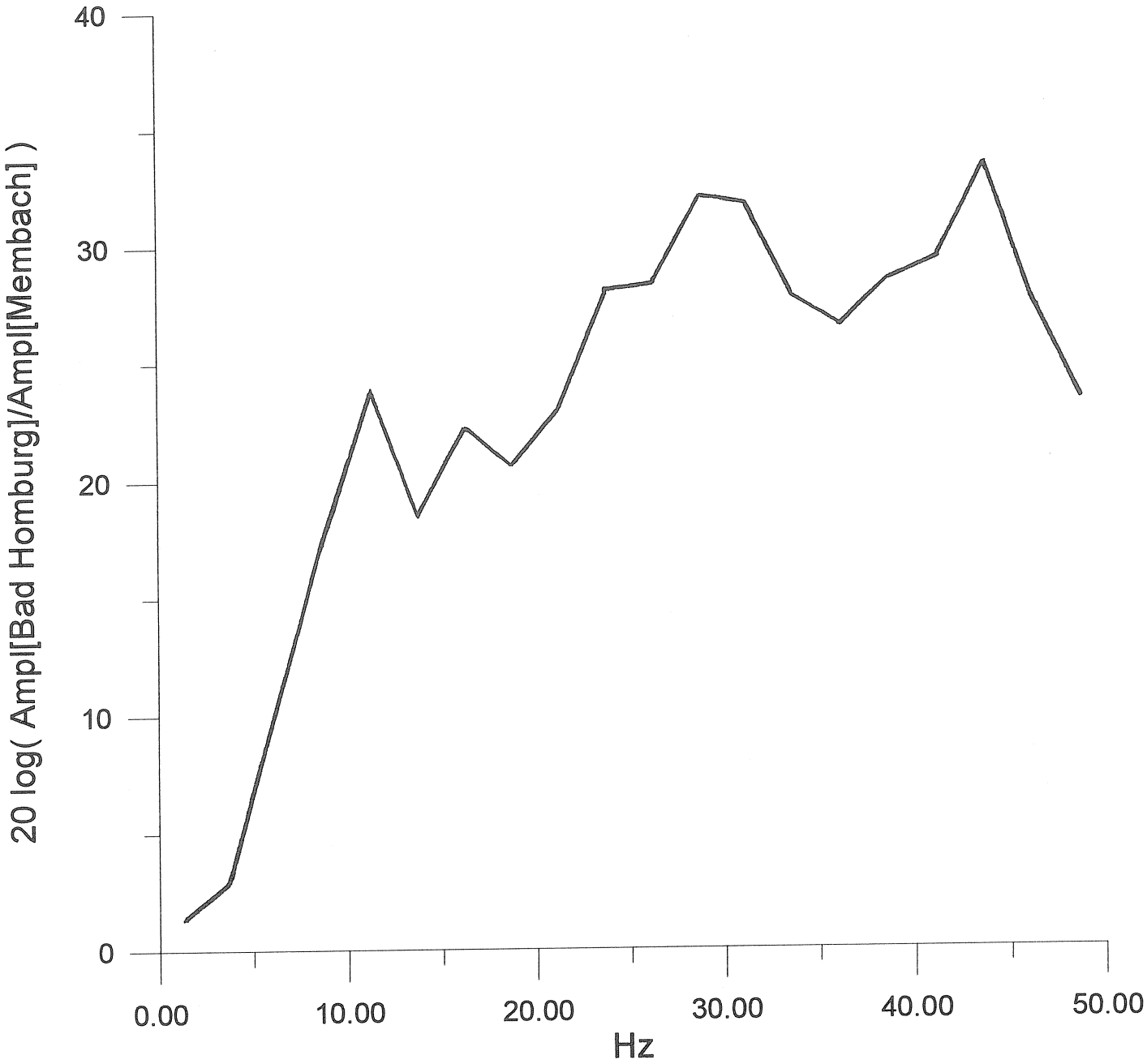

Fig. 10 : comparison (in db) of the noise in Bad Homburg (March 94) with the noise in Membach (June 94) which is the reference. The refrigerating device is off. Each point is an average of the amplitude on a 2.5 Hz interval.

Traduction

ESTIMATION DE LA PRECISION DE CALCUL DES CORRECTIONS DE MAREES.

B.P. Pertsev, M.V. Ivanova.

Institut de géophysique planétaire Schmidt.
Physique de la Terre, 1994 n° 5 pp 78 à 80.

La précision toujours croissante des observations gravimétriques exige le calcul des corrections de marées avec une précision allant jusqu'à 1 à 2 microgals. Mais quelle est la précision réelle des corrections de marées terrestres utilisées lors de la réduction des mesures gravimétriques effectuées aux points non englobés par les observations des marées terrestres ?

Pour évaluer la précision des corrections de marées calculées dans les mesures gravimétriques de haute précision, il est souhaitable d'avoir leurs valeurs propres pour n'importe quels points et intervalles de temps. On peut prendre soit les courbes observées, soit les courbes de corrections élaborées sur la base d'une série de valeurs de haute précision des paramètres de marées terrestres δ, $\Delta\phi$ pour 15 à 20 ondes principales de la marée gravimétrique.

Il apparaîtrait que la courbe observée est l'étalon idéal pour l'estimation de la précision des calculs. Cependant la dérive de l'appareil, les perturbations météorologiques et le bruit de fond déprécient dans une mesure importante la prédominance des enregistrements continus du phénomène. C'est pourquoi, à notre avis l'existence de paramètres gravimétriques de marées terrestres obtenus par de longues séries d'observations réalisées par des gravimètres de marées de haute précision, donnent une base plus sûre pour faire une estimation de la précision de calcul des corrections de marées.

On est conduit à cette même conclusion par l'analyse des autres courbes c'est à dire les différences entre la courbe observée et la courbe calculée sur la base des paramètres des marées terrestres obtenus par l'analyse harmonique de longues séries d'observations. De plus il est plus simple de faire la comparaison avec les courbes précalculées. Nous avons adopté cette méthode de réalisation de courbes "observées" dans les calculs ultérieurs. Nous noterons que cette méthode de calcul des corrections de marées s'applique à présent universellement dans les cas où les mesures gravimétriques se font dans des endroits pour lesquels les valeurs des paramètres de marées terrestres sont bien connus sur base des observations.

Pour résoudre le problème posé on a choisi quelques stations de marées terrestres dans lesquelles on possède de longues séries d'observations gravimétriques effectuées par les gravimètres de marées les plus modernes. A cet effet on a pris: 1) Bad Homburg (Allemagne) où on a obtenu une série de trois ans d'observations avec un gravimètre cryogénique GWR [1]. 2) Pecni (R. Tchèque) une série de sept ans d'observations avec un GS-15 [2]. 3) Potsdam (Allemagne) une série de douze années d'observations avec un GS-15 [3]. 4) Uccle (Belgique) une série de quatre années d'observations avec un gravimètre cryogénique GWR [4]. 5) Pinon Flat (USA) une série d'un an et demi d'observations avec un gravimètre cryogénique GWR [5]. 6) Sèvres (France) environ un an et demi d'observations avec un gravimètre Western modernisé [6]. Il convient de noter que dans les observations à Sèvres il y avait beaucoup de coupures et qu'en outre on n'a pas pu utiliser le même gravimètre. Nous avons

pris ce point uniquement parce que Sèvres est un point gravimétrique fondamental où on effectue, depuis plusieurs années, des déterminations absolues de la pesanteur.

Pour toutes ces stations on possède des paramètres de marées terrestres pour un grand nombre d'ondes, obtenus par l'analyse harmonique de longues séries d'observations. Mais, pour la plupart des stations, malgré la grande durée des observations, les paramètres relatifs aux ondes à longue période n'ont pas été déterminés. Pour celles-ci on a pris $\delta = 1.16$ et $\Delta\phi = 0$. Etant données les faibles amplitudes de ces ondes ceci ne peut un tant soit peu sensiblement perturber les résultats cherchés.
Ces paramètres ont été aussi utilisés pour construire les courbes de marées gravimétriques "observées". Ensuite on a calculé pour chaque point les valeurs des paramètres de marées terrestres dans les trois variantes. Dans deux de celles-ci on a tenu compte de l'influence des marées océaniques sur la base des cartes cotidales globales de Schwiderski [7] pour les neuf ondes principales: M_2, S_2, N_2, K_2, O_1, K_1, P_1, Q_1 et Mf. En outre, on a tenu compte des corrections de Wenzel [8] sur le caractère ellipsoïdal de la Terre, des corrections d'inertie [9] de résonance [10] et des corrections de nutation [11]. Ces dernières ont été prises dans les deux variantes correspondant aux modèles I et II de Molodenski [10]. On a pris pour le second modèle la valeur non perturbée $\delta = 1.1567$ conforme au modèle de Terre n° 508 et non la valeur donnée dans le travail de M.S. Molodenski. A titre de troisième variante on a pris le modèle généralement adopté à savoir que, pour toutes les ondes on a pris $\delta = 1.16$ et $\Delta\phi = 0$.

En outre, on a encore calculé pour trois stations une quatrième variante dans laquelle on a pris $\delta = 1.17$ et $\Delta\phi = 0$ employées souvent lors des calculs des corrections de marées. Cependant, comme on le constate par la table 2 cette variante a donné des résultats très voisins des précédentes et c'est pourquoi elle n'a pas été appliquée pour les autres stations. Enfin, on a encore calculé pour trois points une cinquième variante dans laquelle on a pris les paramètres de marées terrestres calculés par Dehant [12] pour le modèle de Terre PREM en tenant compte de l'aplatissement et de la rotation de la Terre et nous avons naturellement tenu compte des corrections de l'influence des marées océaniques d'après les cartes cotidales de Schwiderski. Comme le montre la table 2 cette variante a donné des résultats très voisins des valeurs obtenues d'après le modèle II de Molodenski.

A titre d'exemple nous avons donné dans la table 1 les paramètres de marées terrestres pour Bad Homburg calculés dans les deux variantes indiquées plus haut (modèle I et II de M.S. Molodenski) et également les paramètres obtenus par les observations [1].

Ensuite pour des intervalles de deux à trois mois pris arbitrairement pour chacune des 6 stations on a calculé des séries de corrections de marées avec les valeurs des paramètres de marées terrestres correspondant au catalogue obtenu par les observations et à la quatrième variante indiquée plus haut. On a alors formé les différences: le catalogue moins chacune des quatre variantes et on les a comparées. Dans la table 2 on a donné pour chaque point (pour une série de un à trois mois) le nombre des ordonnées "de différences" dépassant ou égales à 1, 2 et 3 μgals. Là également sont indiquées les valeurs des ordonnées "de différences" maximale (d'après le modèle). Le nombre des ordonnées dans une série de un à trois mois est égal à 2160.

Il résulte de la table que le calcul préliminaire des corrections de marées fait avec un facteur δ constant et un écart de phase nul permet de garantir la précision du calcul dans les limites de 10 μgals, même pour les points situés sur les côtes. Le calcul de tous les effets énumérés plus haut et principalement des marées océaniques permet d'élever la précision du calcul préliminaire des corrections de marées jusqu'à 2 à 3 μgals. Pour obtenir des

valeurs plus précises il faut disposer des valeurs des paramètres de marées terrestres des ondes principales déterminées par l'analyse d'une longue série d'observations obtenues par des gravimètres de haute précision près du point pour lequel il faut calculer les corrections.

Toutes les remarques indiquées se rapportent à un même calcul. Mais comme lors des déterminations absolues de la pesanteur, les observations se font sur une longue durée en un même point alors les corrections de marées, comme les mesures individuelles sont moyennées aussi dans la valeur résultante de la pesanteur, la valeur de la corrections de marée moyennée sera plus précise.

Le problème du calcul des constantes des composantes de la marée (correction de Honkasalo) pour la latitude donnée ne se posait pas ici puisque ces composantes non déterminées par les observations de marées terrestres, sont constantes et disparaissent dans les différences.

Table 1

Valeurs calculées et observées des paramètres de marées terrestres à la station de Bad Homburg

Onde	$\varphi = 50°2285$ $\lambda = 8°6113$					
	Modèle I		Modèle II		Observations	
	δ	$\Delta\varphi$	δ	$\Delta\varphi$	δ	$\Delta\varphi$
Mm	1.1360	0.00	1.1320	0.00	1.1274	0.13
Mf	1.1357	−0.07	1.1324	−0.07	1.1462	0.33
Mtm	1.1360	0.00	1.1320	0.00	1.1305	−1.53
Q_1	1.1515	−0.25	1.1485	−0.25	1.1443	−0.31
O_1	1.1516	0.07	1.1485	0.07	1.1449	−0.07
M_1	1.1540	0.00	1.1510	0.00	1.1433	0.22
P_1	1.1520	0.19	1.1492	0.19	1.1459	0.05
K_1	1.1371	0.17	1.1350	0.17	1.1331	0.10
J_1	1.1580	0.00	1.1550	0.00	1.1517	−0.03
OO_1	1.1580	0.00	1.1540	0.00	1.1456	0.04
$2N_2$	1.1700	2.00	1.1700	2.00	1.1619	2.30
N_2	1.1772	2.52	1.1739	2.53	1.1700	2.07
M_2	1.1893	2.01	1.1860	2.02	1.1835	1.65
L_2	1.1900	1.50	1.1870	1.50	1.1975	1.93
S_2	1.1912	0.75	1.1879	0.76	1.1857	0.21
K_2	1.1900	0.65	1.1865	0.65	1.1864	0.46
M_3	1.0700	0.00	1.0700	0.00	1.0687	0.03

Table 2 Quantité de "différences" d'ordonnées dépassant la limite donnée

Observ.	−1.16	−1.17	Modèle I	Modèle II
		Pecni		
≥1 мкГал	934	1152	0	0
≥2	214	439	0	0
≥3	2	71	0	0
max мкГал	3.0	3.7	0.6	0.7
		Potsdam		
≥1 мкГал	881	1018	0	23
≥2	146	324	0	0
≥3	0	43	0	0
max мкгал	2.7	3.6	0.7	1.1
		Sèvres		
≥1 мкгал	1598	1485	498	671
≥2	883	792	54	123
≥3	336	311	0	0
max мкГал	5.1	5.2	2.5	2.9

Observ.	−1.16	Modèle I	Modèle II	Dehant
		Bad Homburg		
≥1 мкГал	1194	48	5	5
≥2	404	0	0	0
≥3	36	0	0	0
max мкГал	3.3	1.3	1.0	1.1
		Uccle		
≥1 мкГал	1259	194	298	296
≥2	358	0	1	1
≥3	23	0	0	0
max мкГал	3.5	1.6	2.0	2.0
		Pinon Flat		
≥1 мкГал	1814	431	598	578
≥2	1369	0	38	24
≥3	955	0	0	0
max мкГал	9.7	1.9	2.4	2.4

Références

1. *Richter B.* The spectrum of a registration with a superconducting gravimeter // Proc. of the X Intern. Symp. on Earth Tides. Madrid, 1985. P. 131 - 139.
2. *Holub S., Simon Z.* Results of long-term Earth tide measurements with the GS - 15 N 228 gravimeter at the station Pecny // Proc. of the X Intern. Symp. on Earth Tides. Madrid, 1985. P. 223 - 230.
3. *Dittfeld H.-J.* Tidal results of the gravimetric observatory Potsdam // Proc. of the XI Intern. Symp. on Earth Tides. Helsinki, 1989. P. 623 - 636.
4. *Ducarme B., Van Ruymbeke M., Poitevin C.* Three years of registration with a superconducting gravimeter at the Royal Observatory of Belgium // Proc. of the X Intern. Symp. on Earth Tides. Madrid, 1985. P.113 - 129.
5. *Warburton R., Goodkind J.* Detailed gravity-tide spectrum between one and four cycles per day // Geophys. J. R. A. S. 1978. № 52. P. 117 -136.
6. *Ducarme B., Melchior P.* Tidal gravity profiles in Western Europe, Asia, Australia, New Zealand and Pacific Islands // Bulletin d'Observations: Marees Terrestres. 1977. V. IV. Fasc. 4. P. 49 - 50.
7. *Schwiderski E.* On charting global ocean tides // Rev. Geophys. & Space Physics. 1980. V. 18. № 1. P. 243 - 268.
8. *Wenzel H.* The correction of tidal force developement to ellipsoidal normal // BIM. 1974. № 68. P. 3784 - 3790.
9. *Парийский Н.Н., Перцев Б.П.* Влияние инерционных сил на наблюдаемые приливные изменения силы тяжести и наклонов // Изучение земных приливов. М.: Наука, 1980. С. 22 - 35.
10. *Молоденский М.С.* Теория нутации и суточных земных приливов // Молоденский М.С., Крамер М.В. Земные приливы и нутация Земли. М.: Изд. АН СССР, 1961. С. 40.
11. *Молоденский С.М.* Влияние вынужденной нутации Земли на результаты приливных наблюдений // Изучение земных приливов. М.: Наука, 1980. С. 36 - 41.
12. *Dehant V.* Tidal parameters of an inelastic Earth // Phys. Earth Planet. Inter. 1987. № 49. P. 97 - 116.

Traduction

OBSERVATIONS DE MAREES TERRESTRES ET HYPOTHESE DE L'EFFET D'ECRAN DE L'ATTRACTION

B.P. Pertsev, M.V. Kouznetsov, M.V. Ivanova,
O.V. Kovaleva, L.V. Kouznetsova.

Institut planétaire de géophysique
O.You Schmidt. PAH
Edité le 12.04.94.

Physique de la Terre, 1994 n° 50 pp. 70 à 72
Communications scientifiques

Durant ces dernières décennies les chercheurs se sont préoccupés à maintes reprises de l'existence possible d'un effet d'écran du champ de gravitation et un grand effort a été fait pour découvrir un tel effet par des observations gravimétriques au moment des éclipses solaires. Dans ce cas la Lune apparaît comme écran. Il serait plus utile d'utiliser dans le rôle d'écran un corps céleste plus massif. A cet égard on peut utiliser la Terre, ce qui a été fait par Z. Simon et d'autres [1] après avoir utilisé les résultats de l'analyse spectrale d'une série de trois ans d'observations de marées terrestres gravimétriques obtenues à Bruxelles à l'aide du gravimètre cryogénique GWR [2].

A l'inverse des éclipses solaires très rares et de durée très courte, les observations de marées terrestres de durée non limitée permettent d'éliminer une quantité de bruits accidentels et d'effets perturbateurs. En outre à l'inverse des observations gravimétriques coûteuses faites spécialement au moment des tremblements de terre on utilise ici les observations de routine dont le but est de préciser la structure interne de la Terre.

La formule de base pour le calcul de l'absorption donné en [1] a été obtenue comme une précision supérieure à la formule donnée dans le travail de Y.A. Ditchko et P.P. Chliakovoi [3]. A l'inverse de [3] on a tenu compte en [1] d'un ordre plus élevé de l'hétérogénéité de la Terre, ce qui a influencé sensiblement les résultats des calculs.

Dans ce cas, la formule de base apparaît sous la forme [1] :

$$G_\lambda = \frac{fM\lambda}{r^2}\left[\bar{\rho}x\left(\cos z - \frac{R}{r} + 3\frac{R}{r}\cos^2 z\right) - \bar{\rho}_0 R\cos z\right].$$

Où f est la constante d'attraction, M est la masse du Soleil, λ est le coefficient d'absorption, ρ et ρ_0 sont les valeurs effectives de la densité de la Terre aux points x et R à l'intérieur de la Terre. x, τ, R et Z sont données à la figure 1. Par la formule (1) on voit clairement pourquoi il faut examiner uniquement l'effet du Soleil. Si en (1) on introduit les valeurs des paramètres et si on prend $\lambda = 10^{-15}$ cm^2 γ^{-1} nous obtiendrons la valeur de l'absorption (en μgal)

$$G_\lambda = 2.0844\frac{c^2}{r^2}\left[(\bar{\rho}x - \bar{\rho}_0 R)\cos z - \right. \qquad (2)$$
$$\left. - 4.2588\times 10^{5}\bar{\rho}x\frac{c}{r}(1-3\cos^2 z)\right],$$

où c est la valeur moyenne de la distance du centre du Soleil au centre de la Terre. En (2) la valeur ρ est exprimée en unités de la densité moyenne et x en unités du rayon moyen de la Terre.

Nous avons calculé ρ x et ρ_0 R en fonction de r_1 (fig. 1) entrant dans cette formule et qui dépendent de la structure de la Terre selon le modèle n° 508 de Gilbert F. et Dziewonski A. [4]. Elles sont données dans la table 1.

Les données astronomiques intervenant dans les formules (1) et (2) ont été calculées conformément aux annuaires.

A partir de représentations géométriques simples et aussi d'après la table 1 il résulte que l'absorption de l'attraction (si elle existe) doit se manifester d'autant plus qu'est proche de l'équateur le point d'observation. Parmi toutes les stations gravimétriques de marées terrestres accessibles ayant de longues séries d'observations de haute précision on a choisi la station la plus proche de l'équateur et éloigné du bord de la mer dont le nom de code est BDF, située dans la région tropicale du Brésil (ϕ = 15°6639 S et λ = 47°9033 W). Les observations y ont été faites avec un gravimètre LaCoste Romberg du 6.5. 77 au 5.9.78 dans le cadre du projet américain IDA (réseau mondial de stations gravimétriques).

De petites interruptions dans les enregistrements ont été complétées sur la base des valeurs des paramètres de marées terrestres obtenus par l'analyse harmonique de ces enregistrements. L'analyse harmonique a été faite d'après la méthode de Venedikov.

La comparaison de ces résultats avec les résultats obtenus dans la même région par les collaborateurs de l'Observatoire Royal de Belgique [5] montre que les paramètres de marées terrestres de δ obtenus à la station BDF sont sensiblement plus bas que les valeurs analogues données en [5]. Apparemment il y a une petite erreur systématique dans l'étalonnage du gravimètre LaCoste Romberg. Mais pour notre but cela n'est pas très important puisque le problème porte sur la présence ou l'absence d'une absorption dans le spectre des observations gravimétriques de marées terrestres.

La série continue obtenue de cette façon a été soumise à l'analyse spectrale en utilisant les fenêtres de Haning avec un pas en fréquence $\Delta\omega$ = 0.01537 degré/h. dans la gamme des ondes diurnes, semi-diurnes, ter-diurnes et quart-diurnes.

Pour le même intervalle de temps et le même point on a calculé une marée théorique qui a été également soumise à l'analyse spectrale avec le même pas et dans les mêmes gammes de fréquence.

Essentiellement, sur la base des formules données plus haut nous avons calculé une série de valeurs de l'absorption de la gravitation pour $\lambda = 10^{-15}$ cm^2 γ^{-1} pour le même point et le même intervalle de temps. Cette série de valeurs de la fonction d'absorption a été également soumise à l'analyse spectrale dans les mêmes gammes de fréquence.

Les lignes spectrales d'absorption obtenues, comme il convient de l'espérer, sont situées rigoureusement dans des périodes diurnes, semi-diurnes, ter-diurnes etc. diminuant avec l'augmentation du numéro de l'harmonique. Les amplitudes des lignes spectrales principales d'absorption (en μgal) pour les différentes périodes sont données dans la table 2. Nous y donnons aussi les amplitudes des lignes d'absorption pour la station de Bruxelles tirées du travail [1] et également calculées par nous pour le même point et le même intervalle de temps.

Pour des raisons incompréhensibles en [1] les lignes spectrales d'absorption dans les fréquences semi-diurnes et quart-diurnes obtenues sont érodées ce qui a amené apparemment à une divergence sensible avec nos résultats. En outre, nous donnons dans la table les amplitudes de la marée gravimétrique dans les mêmes fréquences que nous avons obtenues par analyse des observations de la station BDF. Comme on le constate, les amplitudes des lignes spectrales

d'absorption à la station BDF sont sensiblement plus grandes que les valeurs analogues pour la station de Bruxelles, plus éloignée de l'équateur. Il convient de noter que pour la même valeur du coefficient λ l'effet d'écran de l'attraction de la Lune au moment de l'éclipse solaire n'atteint pas plus de 0.7 cos z μgal, z étant la distance zénithale du Soleil et de la Lune au moment de l'éclipse.

La comparaison de trois spectres (théorie, absorption et observations) dans chacune des bandes de fréquence indiquées a confirmé la conclusion de Z. Simon [1] qu'étant données les perturbations météorologiques possibles des ondes nettement diurnes et semi-diurnes possédant de plus de grandes amplitudes, la partie du spectre convenant le mieux pour mettre en évidence l'absorption est la partie du spectre voisine des ondes ter-diurnes. D'autant plus qu'il n'y a pas d'onde de marée nettement ter-diurne. La comparaison des spectres dans cette gamme a montré que le spectre d'absorption doit ici dépasser sensiblement le bruit blanc pour $\lambda = 10^{-15}$ cm^2 γ^{-1}. L'absence de la ligne spectrale remarquable à cet endroit montre que si il y a aussi absorption, alors le coefficient d'absorption λ ne doit pas dépasser 2×10^{-16} cm^2 γ^{-1}. La raie d'absorption dans la gamme des ondes de 6 heures bien que plus de deux fois trop petite que dans la gamme de 8 heures, peut être également employée pour estimer l'effet d'absorption étant donnée l'absence d'ondes de marées dépassant 0.01 μgal dans cette partie du spectre [6].

Sur les figures 2 et 3 sont indiqués les spectres d'absorption et les spectres des observations dans la gamme des ondes de huit à six heures.

En conclusion les auteurs expriment leur profonde reconnaissance à leurs collègues américains de l'Université de Californie, San Diego pour les enregistrements mis à leur disposition des enregistrements de marées terrestres à la station de BDF.

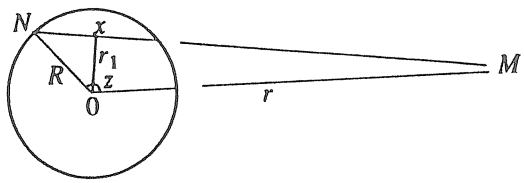

Рис. 1.

1. *Simon Z., Kostelecky J., Zeman A.* On the Gravitation Absorption Hypothesis // Studia geoph. et geod. 32. Praha, 1988. P. 16 - 23.
2. *De Mayer F.* Spectral analysis of the Observations of a superconducting gravity meter // Marees Terrestres Bulletin d'Informations. 1983. № 93. P. 6157 - 6183.
3. *Дычко И.А., Шляховой В.П.* Оценка эффекта экранирования в наблюдениях земных приливов // Вращение и приливные деформации Земли. Киев: Наук. думка, 1978. Вып. 10. С. 39 - 48.
4. *Gilbert F., Dziewonski A.* An application of normal mode theory to the retrieval of structural parameters and source mechanisms from seismic spectra // Phil. Trans. Roy. Soc. London A, 1975. № 1280. P. 187 - 269.
5. *Melchior P., Ducarme B., Van Ruymbeke M., Poitevin C.* Trans World Tidal Gravity Profiles II (West Africa and South America) // Observatoire Royal de Belgique, Bull. d'observations: Marees Terrestres, 1989. V. V. Fasc. 2. P. 67 - 68.
6. *Tamura Y.* A Harmonic Development of the Tide-Generating Potential. Marees Terrestres Bulletin d'Information. 1987. № 99. P. 6813 - 6855.

Table 1 Valeurs ρx (r_2) pour le modèle de Terre n° 508

r_1	$\bar{\rho}x$	r_1	$\bar{\rho}x$	r_1	$\bar{\rho}x$
0.00	3.1347	0.35	2.5498	0.70	1.1770
0.05	3.1225	0.40	2.3765	0.75	1.0606
0.10	3.0855	0.45	2.1761	0.80	0.9321
0.15	3.0207	0.50	1.9315	0.85	0.7836
0.20	2.9055	0.55	1.4806	0.90	0.5895
0.25	2.8136	0.60	1.3909	0.95	0.3844
0.30	2.6954	0.65	1.2888	1.00	0.0000

$\bar{\rho}_0 R = 1.56734$

Table 2. Amplitudes des lignes spectrales principales de l'absorption.

Fréquence (degré/h)	15	30	45	60
Amplitudes d'absorption à BDF (μgal)	1.53	1.00	0.52	0.21
Idem à Bruxelles [1] (μgal)	1.29	0.22	0.14	0.02
A Bruxelles d'après nos données (μgal)	1.32	0.35	0.13	0.03
Amplitudes de la marée à BDF (μgal)	20,.58	35.45	$\langle$ 0.10	$\langle$ 0.10

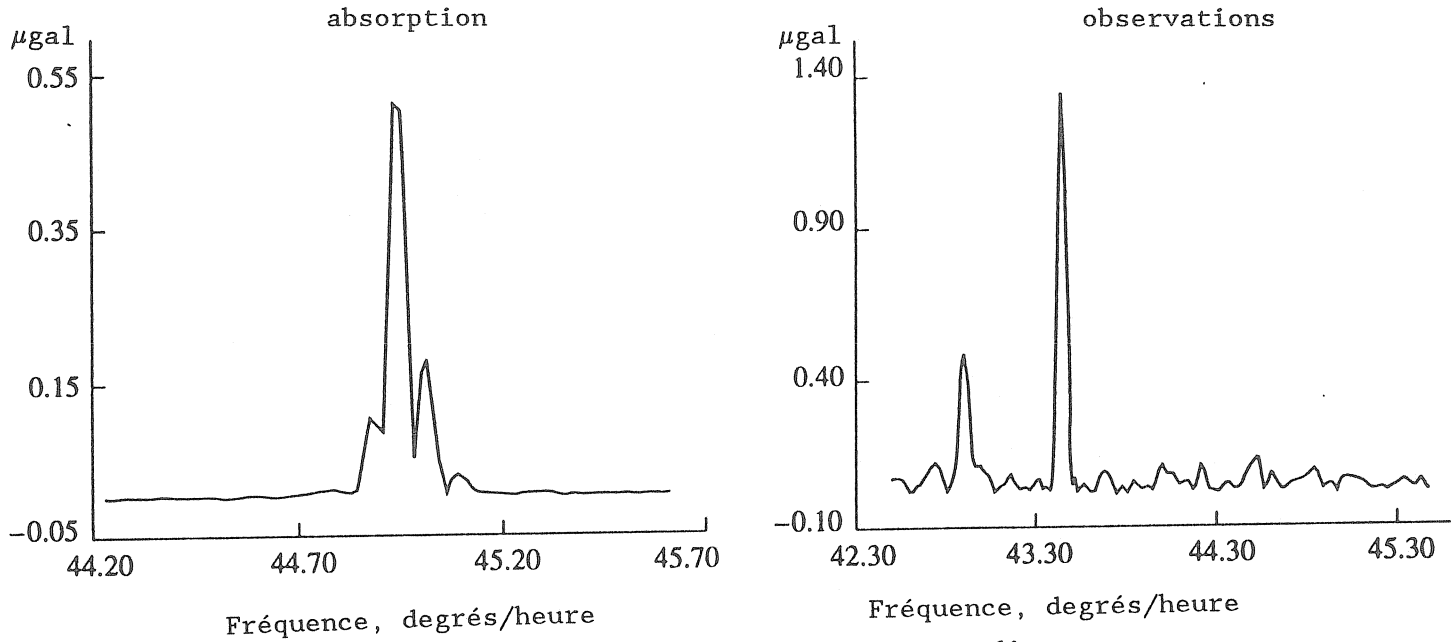

Fig. 2. Spectres des ondes ter-diurnes

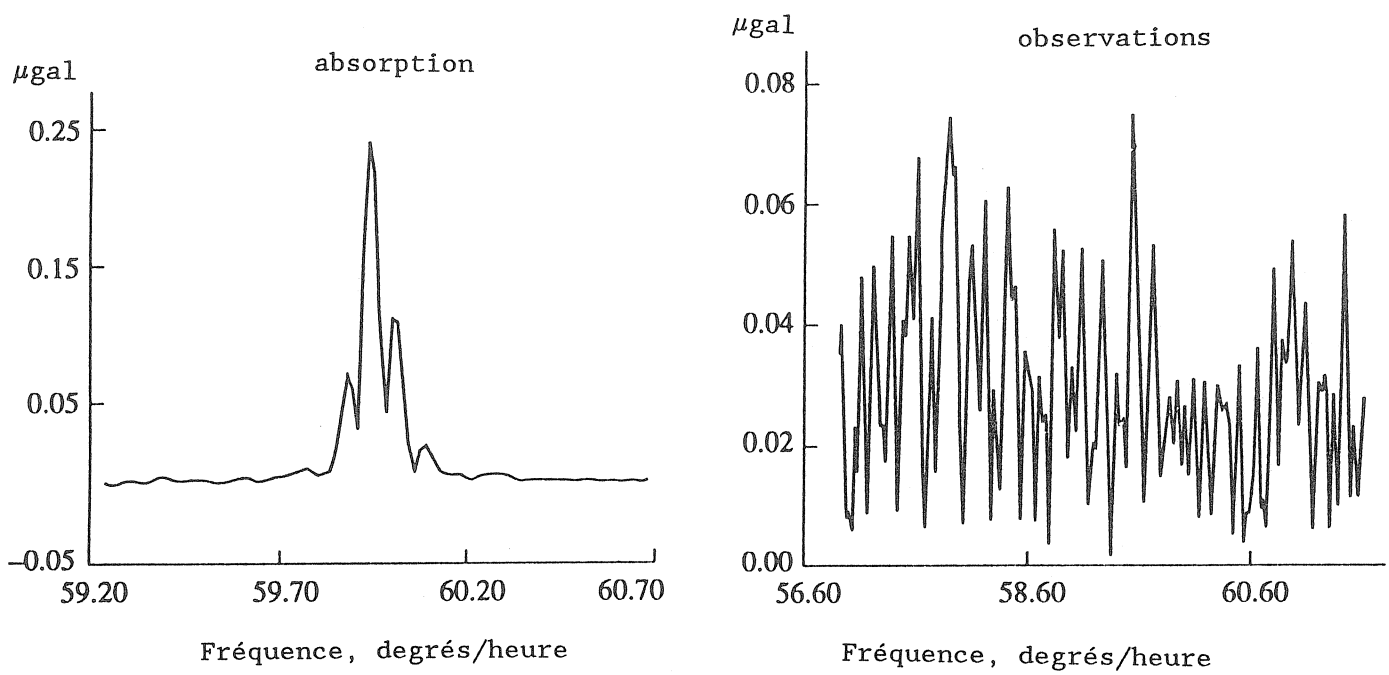

Fig. 3 Spectre des ondes quart diurnes

OBSERVED TIDAL GRAVITY CHANGES AT THE COMPRESSION REGION AND AT THE EXTENSION-SHIFT REGION GARM-BAIKAL

Timofeev V.Yu. *, Gridnev D.G. **, Sarycheva Y.K. *,
Anisimova L.V. ***, Panin S.F. ***

*Institute of Geophysics UIGG & M SB RAS,
Novosibirsk, Russia
**Institute of the Physics of the Earth RAS
Moscow, Russia
***BEMSE of Institute of Earth Crust SB RAS,
Irkutsk, Russia.

1. Introduction

Observations of tidal gravity variations allow to study elastic properties of the Earth when deforming under the action of the Moon and Sun attraction of known magnitude. The investigation of tidal parameters in different regions is an interesting task (Melchior, 1994). We consider here the results of tidal gravity observations in contrast zones, as the Baikal rift (extension in the centre and shift in the flanks) and at the contact zone of the Eurasian lithospheric plate (including South Tien Shan) and of the Pamirs microplate (compression at the Garm area). The geological structure of the region, its recent movements are considered from modern geophysical investigations. Tidal gravity measurements were performed at the Garm station, at the Irkutsk stations and at the Talaya station.

2. The structure of the test regions.

Tides are a planetary phenomenon. It affect the whole body of the Earth from it's centre to it's surface. As we know (Alekseev et al., 1971), the upper mantle structure of the test regions is much about the same. Main differences are the Earth crust properties of the test regions. The active continental Baikal rift system is situated in the centre of the Asian continent. From geological and geophysical data, there are extension conditions in the centre of the rift (northern part of the Baikal lake) and shift conditions at these flanks. The Baikal rift seismicity is concentrated mainly at a depth of 10 to 20 kilometres. The Talaya station is situated in the South-West part of the Baikal rift, 6 km to the West from Baikal lake. To the North of the station, at a distance of about 5 km, is the Main Sayan fault, which has here a sublatitudal stretching. Tilt and strain observations carried out during last years at the underground gallery of the Talaya station display the shift nature of horizontal recent deformations and the cyclic nature of vertical recent movements (Timofeev et al., 1994). In this case, we mainly note, that values of the volume deformation and shift deformation have a cyclic nature and did not accumulate to big amounts during the observation period [Fig. 2, 3, 4].

The territory of the Garm test region, including the adjacent part of Pamirs, Tien Shan and of the Tadjik depression separating them, are under compression and have intensive recent movements (Bokanenko et al., 1992; Guseva, 1986; Guseva et al., 1993) horizontal and vertical, have intensive

seismicity, which are in a broad interval of depths (from kilometres to a hundred kilometres). In this case, we note mainly that the values of the volume deformation accumulate to a big amount (Fig. 5). Consequently, the properties of rocks are exchanged. There is cracking at the Garm territory, as noted in the article by Antonova et al (1994).

3. Tidal gravity observations.

The equipment for tidal gravity observations carried out in Irkutsk consists of static high-precision gravimeters Askania GS-12 n° 186, n° 180, GS-11 n° 159 (at Irkutsk I) (Gridnev et al., 1986) and GS-12 n° 186, 180 and SQG (developed by Gridnev D.G.) (at Irkutsk II). The equipment for gravimetric tidal observations carried out in Talaya and Garm stations consists of static quartz gravimeters - "SQG" type. We used recorders based on reflection galvanometers and electric measuring devices providing stable power supply to the instrument sensor and thermostats. At Irkutsk I station, we used a time-mark system with precision 10 (-12) second. The recording was made on oscillographic paper at a scale of 2.0 - 4.0 μgal/mm. At the station we used the known method of coupled shifts and the special large shifts method (Gridnev et al., 1982). At that station we had a stable temperature in the stabilization equipment room. At the other stations (Irkutsk II, Talaya, Garm), we had passive temperature stabilization equipment. At these stations (Irkutsk II, Talaya, Garm), we used the new record scaling method. The new procedure is based on the inclination technique (Sarycheva, Timofeev, 1992; Gridnev et al., 1992). The record was made on oscillographic paper at a scale of 3.0 - 11.0 gal/mm.

The results of harmonic analyses (by Venedikov 74 procedure), are given in tables 1, 2, 3, 4, 5, 6. For the passive temperature stabilization stations, we used results only for the semi-diurnal sectorial wave M_2. For the tidal vectors related to one tidal wave under consideration (in this paper the semi-diurnal sectorial wave M_2), we use here the same notations as in the paper by Melchior (1994), the Irkutsk results are given in Tables 1, 3.

$\mathbf{X}$ (X, x) = B - L = A - R - L is the final residue vector expected to represent the observations noise (about 0.3 μgal for the M_2 wave). At Irkutsk stations, it does not exceed this noise level. At the Garm station, $X(M_2)$ greatly exceeds this noise level (table 6). The maximum latitude difference (from Melchior, 1994, see tables 10, 11) from different tidal models do not exceed 0.0068 for the $\delta(M_2)$ factor.

4. Conclusions.

The analyses of the measurements show an effect of the earth crust. The value of the effect may reach 2% of the gravimetric factor value. The effect for the Garm station (about 1 μgal for the M_2 wave) is the final residue from the gravimetric factor expected to represent the properties of the crust rocks changed under the contact tectonic plate conditions (fig. 6), (table 7).

5. Acknowledgements.

This work has been a part of the scientific programmes of the Institute of Geology and Geophysics (Novosibirsk) and the Institute of Physics of the Earth (Moscow) since 1979.

The investigation were partly supported by grants of the Russian Fund for Scientific Research n 93-05-14021, n 094-05-17060-a, additional support being given by the Siberian Branch of Russian Academy of Sciences.

We are indebted to Prof. P. Melchior, Brussels for stimulating discussions, constructive critical comments and wise advice.

References

Alekseev A.S., Lavrentiev M.M., Mukhametov R.G. et al., 1971.
Numerical method for determination of upper mantle Earth structure. In the book: Mathematical problems of geophysics. V.II, Novosibirsk, 143-165 (in Russian).

Antonova L.V., Aptikayev F.F., Krestnikov V.N. et al., 1994.
Evaluation of Seismic Activity from Rock Fracturing Examination. Fizika Zemli. 5, 3-10 (in Russian).

Bokanenko L.I., Perederin V.P. Galaganov O.N., 1992.
Local Deformations of Garm Area and Possibilities of Earthquake Prediction. Fizika Zemli, 10, 27-41 (in Russian).

Gridnev D.G., Kuznetsov M.V. Kuznetsova L.V., Sarycheva Yu.K., Timofeev V. Yu, 1986.
Regional tidal investigation at Asian part of USSR. In the book: Modern Geodynamics of Siberia Lithosphere. Novosibirsk, 63-79 (in Russian).

Gridnev D.G., Naumenko-Bondarenko L.I., Sidorin A.Ya, et al., 1992.
Observation of tidal gravity changes at the Garm. Fizika Zemli, 9, 121-124 (in Russian).

Gridnev D.G., Sarycheva Yu.K., Timofeev V. YU., 1982.
The determination of tidal gravimeter GS-12 n° 186 record scaling. Geologia i Geofizika, 3, 96-101 (in Russian).

Guseva T.V., 1986.
Recent movement of the Earth crust at the Pamir-Tien Shan boundary zone. Moscow, Inst. Phys. Earth AS USSR, 171 (in Russian).

Guseva T.V., Lukk A.A., Trapeznikov Yu. A. et al. 1993.
Measurement of distances and the Geodynamics of the Garm Test Area (Tadjikistan). Journal of Earthquake prediction research, 2, 3, 445-458.

Melchior P., 1994.
A new data bank for tidal gravity measurements (DB 92). Phys. Earth Planet. Inter., 82, 125-155.

Sarycheva Yu.K., Timofeev V. Yu., 1992.
Tidal parameters of the Earth from Gravimetric Observations in Novosibirsk. Geologia i Geofizika, 2, 37-44 (in Russian). (BIM, 1993, 114, 83).

Solonenko A.V., 1993.
About the symmetry of the stress field in the Earth crust of Baikal rift. DAN, 328, 6, 674 (in Russian).

Timofeev V. YU., Panin S.F., Sarycheva Yu.K., et al., 1994.
Investigation of Earth surface tilts and strains in the Baikal rift zone (st. Talaya). Geologia i Geofizika, 3, 119-129 (in Russian).

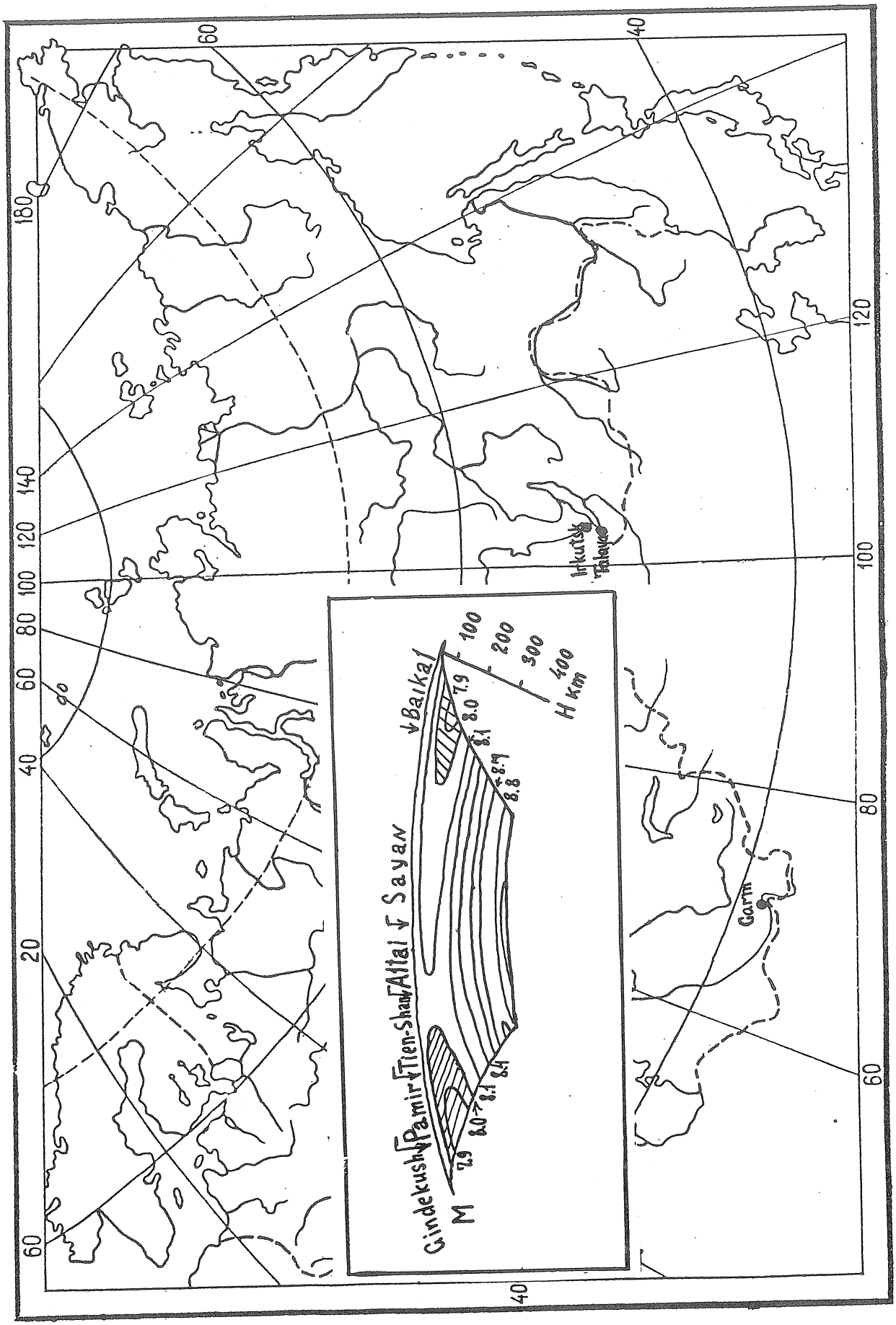

Fig.1. Map of tidal gravity stations (Irkutsk, Talaya, Garm). Inside the insertion - the seismic profile Pamir-Baikal (Alekseev et al., 1971).

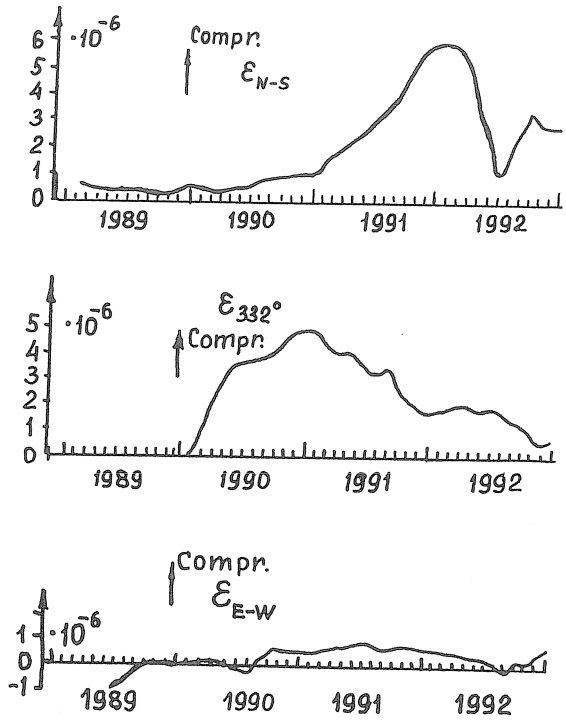

Fig. 2. The results of strain observation with the three extensometers at the Talaya station (1989-1992).

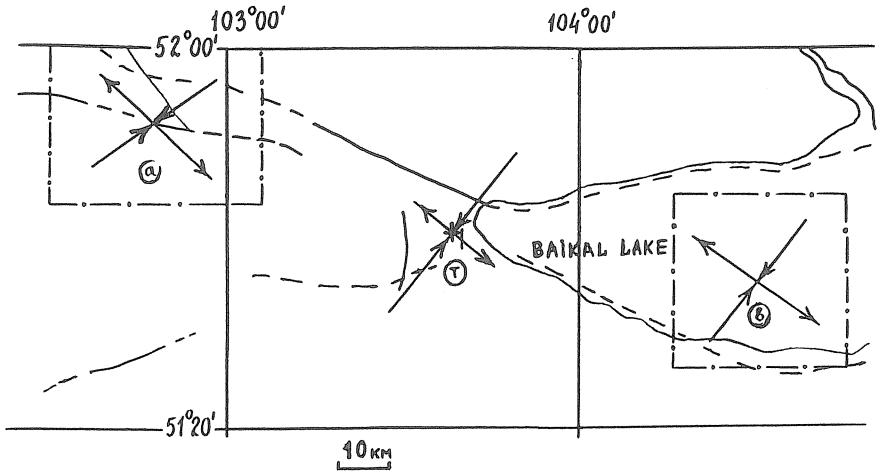

Fig. 3. The orientation of stress axes (a, b) from seismology data (A. Solonenko, 1993) and (T) from the strain observation at the Talaya station (1990-1991).

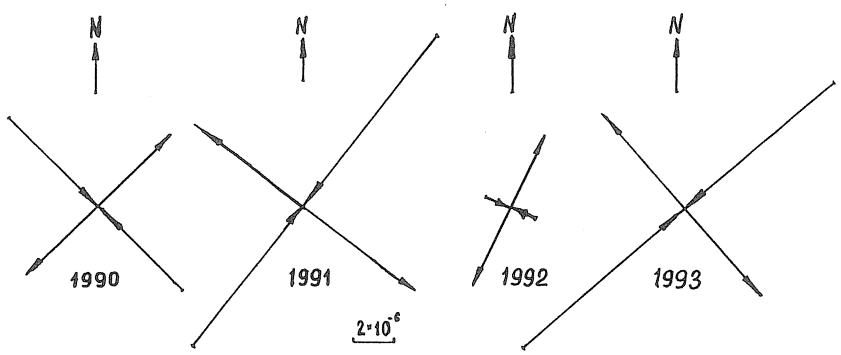

Fig. 4. The yearly orientation of main strain axes from the observations a the Talaya station.

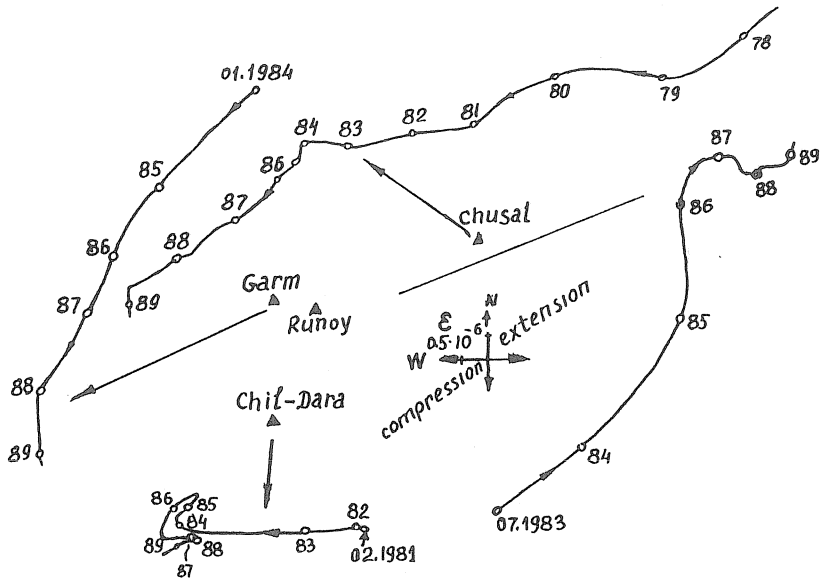

Fig. 5. Strain vector diagrams from the observations at the underground station in the Garm region (Bokanenko et al., 1992). South Tien Shan - Garm, Chusal and Pamir - Chil-Dara, Runoy.

Irkutsk	δ	α	X	χ
I	1.1589	-0.47°	0.27	-97.2°
II	1.1558	-0.56°	0.34	-111.0°
Talaya	1.1503	-1.03°	0.66	-115.7°

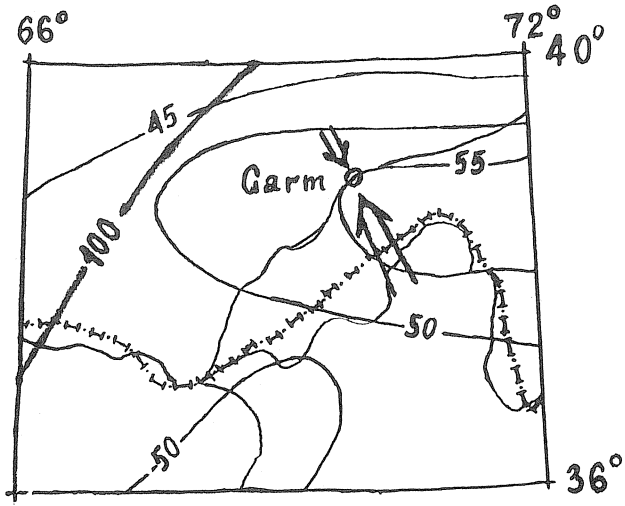

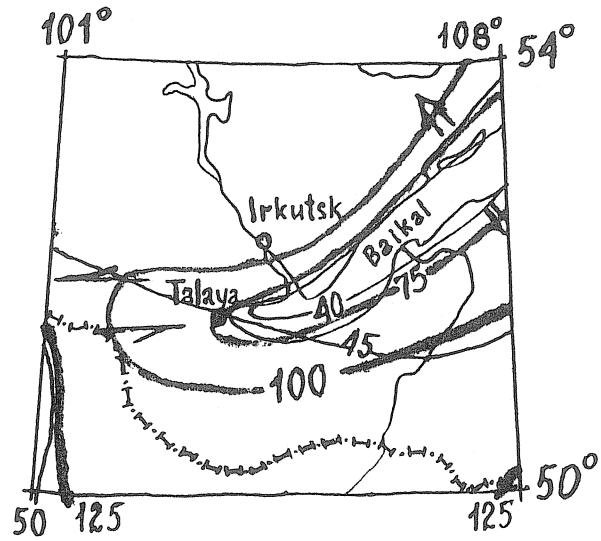

Garm	δ	α	X	χ
	1.1868	-0.04°	1.21	-1.9°

Fig. 6. The map of tidal gravity stations with crustal thickness (km), lithospheric thickness (km) ("Map of active faults of the USSR and the adionining areas", scale 1: 8 000 000, Editor-in Chief V.G. Trifonov, A S USSR, Moscow-Irkutsk, 1986, shift and compression conditions and our tidal results (M_2 wave).

Table 1 Instrumental phase lag in degrees

Gravimeters	Epoch	in minutes	M2	S2	O1	K1
N 186	02.06.81	0.32	-0.15	-0.16	-0.07	-0.08
N 180	14.03.80	0.24	-0.12	-0.12	-0.06	-0.06
		0.30	-0.14	-0.15	-0.07	-0.08
			-0.13	-0.14	-0.07	-0.07
N 159	13.05.81	0.34	-0.16	-0.17	-0.08	-0.09
		0.40	-0.19	-0.20	-0.09	-0.10
			-0.18	-0.19	-0.09	-0.10
SQG (with shunt)	18.05.83	0.67	-0.32	-0.33	-0.16	-0.17

Table 7 Corrected Results

Wave M2

Station		δ	α	X	χ
1300	Irkutsk I	1.1589	-0.47°	0.27µgal	-97.2°
1300*	Irkutsk II	1.1558	-0.56°	0.34µgal	-111.0°
1301	Talaya	1.1503	-1.03°	0.66µgal	-115.7°
1272	Garm	1.1868	-0.04°	1.21µgal	-1.9°

Wave O1

1300	Irkutsk I	1.1490	-0.09°	0.32µgal	189.7°
1300*	Irkutsk II	1.1589	-1.95°	1.19µgal	268.2°
1301	Talaya	1.1728	-2.41°	1.54µgal	-76.1°
1272	Garm	1.1786	-0.12°	0.58µgal	-7.5°

Table 2 Station 1300-Irkutsk I (52.03°N, 104.31°E, H=520m)

Gravimeters	Number of days and epoch	Gravimetric factor phase lag in degrees			
		M2	S2	O1	K1
GS-12 N 186	834 days	1.1622 ± 65	1.1339 ± 135	1.1552 ± 71	1.1447 ± 48
	24.09.1979-27.02.1983				
		-0.83° ±.33	-0.48° ±.72	0.23° ±.35	-0.51° ±.24
GS-12 N 180	826 days	1.1634 ± 40	1.1429 ± 84	1.1546 ± 81	1.1425 ± 55
	22.09.1979-27.02.1983				
		-0.38° ±.20	4.20° ±.43	0.15° ±.40	0.40° ±.27
GS-11 N 159	286 days	1.1544 ± 43	1.1951 ± 94	1.1591 ± 141	1.1486 ± 88
	17.04.1980-28.02.1981				
		-0.16° ±.21	0.38° ±.46	0.24° ±.71	0.71° ±.43
Mean gravity factor		1.1600		1.1563	
Corrected for inertial forces		1.1562		1.1555	
Observed amplitude in µgal		32.8571		34.8243	
Phase lag in degrees		-0.30°		0.28°	
Load vector L					
Amplitude in µgal		0.1242		0.2986	
Phase in degrees		128.50°		48.72°	
Corrected gravity factor		1.1589		1.1490	
Amplitude in µgal		32.9350		34.6269	
Phase		-0.47°		-0.09°	
Residue vector X (µgal) χ (in degrees)		 0.27 -97.2°		 0.32 189.7°	

Table 4 Calibration of N186 gravimeter by tilt procedure

Time	Ki (μgal/mm)	(Ki-Kmean)/Kmean(%)
12.12.83	5.3901	-0.38
5.01.84	5.3689	-0.69
11.01.84	5.4040	-0.04
3.02.84	5.3877	-0.34
7.02.84	5.4099	0.07
17.02.84	5.4159	0.18
20.02.84	5.4000	-0.11
23.02.84	5.4159	0.18
27.02.84	5.4500	0.81
6.03.84	5.4355	0.54
12.03.84	5.3921	-0.26
14.03.84	5.3763	-0.55
16.03.84	5.3646	-0.77
21.03.84	5.4480	0.78
22.03.84	5.4139	0.14
17.04.84	5.4159	0.16
19.04.84	5.4179	0.19
7.05.84	5.4079	0.00
Kmean	5.4079	
Mean sq.er	0.0066	
in %	0.12 %	

Table 3 Station 1300-Irkutsk II (52.06°N, 104.27°E, H=460m)

Gravimeters	Number of days and epoch	Gravimetric factor phase lag in degrees			
		M2	S2	O1	K1
GS-12 N 186	219 days	1.1581 ± 39	1.1381 ± 83	1.1660 ± 124	1.0985 ± 90
	02.05.1983-03.07.1984				
		-0.23° ±.20	3.30° ±.46	-1.64° ±.61	0.16° ±.49
GS-12 N 180	140 days	1.1569 ± 71	1.1978 ± 136	1.1811 ± 192	1.0846 ± 138
	05.07.1983-21.05.1984				
		-1.04° ±.35	4.76° ±.71	-1.07° ±.96	-0.14° ±.72
SQG	87 days	1.1556 ± 82	1.1666 ± 196	1.1074 ± 337	1.1277 ± 282
	18.06.1983-28.04.1984				
		-0.50° ±.88	3.13° ±2.08	6.10° ±3.50	4.30° ±2.62

Mean gravity factor	1.1569	1.1660 (N 186 only)
Corrected for inertial forces	1.1531	1.1652
Observed amplitude in µgal	32.7242	35.1095
Phase lag in degrees	-0.39°	-1.57°
Load vector L		
Amplitude in µgal	0.1242	0.2986
Phase in degrees	128.50°	48.72°
Corrected gravity factor	1.1558	1.1589
Amplitude in µgal	32.8022	34.9195
Phase	-0.56°	-1.95°
Residue vector		
X (µgal)	0.34	1.19
χ (in degrees)	-111.0°	268.2°

Table 5 Station 1301-Talaya (51.68°N, 103.65°E, H=580m) SQG gravimeter

Gravimeter	Number of days and epoch	Gravimetric factor phase lag in degrees			
		M2	S2	O1	K1
SQG	30 days	1.1508 ± 134	1.3152 ± 319	1.1734 ± 318	1.1601 ± 218
	10.07.1989-08.08.1989				
		-1.41° ±.70	8.21° ±1.48	-2.13° ±1.54	-0.96° ±1.00
SQG	108 days	1.1517 ± 65	1.2906 ±223	1.1860 ±222	1.1320 ±152
	06.02.1987-31.05.1987 29.04.1989-21.06.1989 10.07.1989-08.08.1989				
		-1.00° ±.65	0.16° ±1.30	-2.29° ±1.50	-1.66° ±.94
Mean gravity factor		1.1513		1.1797	
Corrected for inertial forces		1.1475		1.1789	
Observed amplitude in μgal		33.1192		35.6358	
Phase lag in degrees		-0.88°		-2.05°	
Load vector L					
Amplitude in μgal		0.1210		0.2904	
Phase in degrees		132.54°		48.07°	
Corrected gravity factor		1.1503		1.1728	
Amplitude in μgal		33.2025		35.4503	
Residue vector X (μgal) χ (in degrees)		0.66 -115.7°		1.54 -76.1°	

Table 6 Station 1272-Garm (39.01°N, 70.31°E, H=1500m) SQG gravimeter

Gravimeters	Number of days and epoch	Gravimetric factor phase lag			
		M2	S2	O1	K1
SQG	183 days	1.1817 ± 86	0.9898 ± 165	1.1789 ± 242	1.2797 ± 175
	23.05.1988-08.12.1988				
		-0.85° ±.43	-3.44° ±.96	0.41° ±1.25	4.21° ±.74
SQG	114 days	1.1886 ± 82	1.2353 ± 169	1.1757 ± 164	1.1994 ± 128
	23.05.1989-23.10.1989				
		-1.39° ±.39	-18.18° ±.89	-0.27° ±.76	5.97° ±.63
SQG	90 days	1.1910 ± 63	0.9600 ± 160	1.1772 ± 116	1.1495 ± 79
	20.11.1989-18.02.1990				
		-0.63° ±.33	-4.40° ±.93	0.05° ±.61	-4.00° ±.40
Mean gravity factor		1.1871		1.1773	
Corrected for inertial forces		1.1833		1.1765	
Observed amplitude in μgal		53.6380		35.7570	
Phase lag in degrees		-0.63°		0.22°	
Load vector L					
Amplitude in μgal		0.5726		0.2222	
Phase in degrees		-106.51°		106.36°	
Corrected gravity factor		1.1868		1.1786	
Amplitude in μgal		53.6380		35.8194	
Phase		-0.04°		-0.12°	
Residue vector X (μgal) χ (in degrees)		1.21 -1.9°		0.58 -7.5°	

Traduction

RECHERCHES CLINOMETRIQUES A NIEFTEIOUGANSK

V. You Timofeev, You K. Saritcheva.

Méthode et résultats de l'étude des variations spatio-temporelles des champs géophysiques.

Rosskiiskaia Akad. Nauk. Sibirskoe Otdellenie
Novosibirsk 1992, page 208-220.

Depuis ces dernières années, on note très fréquemment, des phénomènes tectogéniques - abaissement de la surface terrestre et augmentation de la séismicité dans les régions d'exploitations pétrolières [1, 8]. Une étude doit se faire pour la prévision de conséquences catastrophiques, la nature des phénomènes et la recherche de conditions de sécurité de l'exploitation. Une méthode est poursuivie à l'aide de clinomètres.

Les inclinaisons mesurées par les clinomètres à petite base constituent des indications des mouvements actuels [2, 4-6]. Nos mesures dans la région de Niefteiougansk ont été faites pour déterminer l'importance, le caractère et la nature possible des inclinaisons sur un gisement se trouvant en exploitation depuis plusieurs années. Elles ont débuté en automne 1989. Depuis le printemps 1990, les observations ont été faites en régime continu. Le point de mesure est situé dans un local souterrain dans la cour d'un jardin d'enfants dans la micro région de T-M de Niefteiougansk à quelques centaines de mètres de la rive du fleuve (fig. 1).

On a utilisé des clinomètres en quartz (base 15 cm) avec suspension Zöllner construits par D.G. Gridniev [6] (fig. 2).
Les appareils ont été étalonnés à la station de marée "Klioutch" (Novosibirsk). La précision de la détermination de la constante électrodynamique des clinomètres est élevée: l'erreur de détermination ne dépasse pas 0,1 - 0,2%. Les recherches ont montré que la constante du clinomètre reste invariable (dans les limites de 1%) lors d'inclinaisons de sa base au moins jusqu'à ± 50". Sur l'enregistreur H399 l'échelle atteint 1000 mm/" c'est à dire que dans des conditions déterminées il est possible d'enregistrer les variations de marées (dans les conditions normales l'amplitude atteint 0,05"). La sensibilité du clinomètre dépend de la période propre de son pendule. Les périodes de fonctionnement sont de 2 à 8 s. L'échelle d'enregistrement a été choisie en fonction du niveau général des inclinaisons dans la région. On a utilisé des échelles de 50 à 3 mm/" en fonction de la vitesse de variation des inclinaisons.

Le point de mesure à Niefteiougansk est à une profondeur d'environ 3 m. Les deux clinomètres (azimut NS et EW) sont placés sur un socle en béton (tuyau métallique d'une dimension de 2000 x 600 mm rempli de béton, un mètre au-dessus de la surface), séparé du sol. Un chauffage électrique fonctionnait dans le sous-sol, débranché uniquement dans les mois d'été. L'enregistrement a été fait avec un enregistreur H399 avec une vitesse de 20 mm/heure (une bande par mois d'enregistrement) et dans des cas séparés 180 à 5400 mm/h avec une marque horaire automatique à partir d'horloges électroniques. Le choix de l'échelle d'enregistrement a été fait en fonction du niveau des inclinaisons thermiques diurnes provoquées par la déformation thermique de la surface terrestre. Des exemples des inclinaisons thermiques dans les mois d'été sont

donnés sur la figure 3. Les lectures horaires des inclinaisons dans les mois d'hiver ont été soumises à l'analyse de marée (sur BM. EC 1066 d'après le programme Venedikov-74). Nous donnons sur la figure 4 les résultats de l'analyse et indiquons le niveau des inclinaisons de marées normales. On peut dire, en fait, que le niveau des inclinaisons thermiques atteint 1" dans les mois d'hiver (des dixièmes de secondes d'arc). Les hétérogénéités dans l'échauffement de la surface de la Terre dans la région de la station apparaissent à cause du relief, dépendant des coefficients de conductibilité thermique etc... Les inclinaisons thermiques et les déformations (périodiques non provoquées par les marées) sont dues en fait au réchauffement périodique irrégulier de la surface lors de la rotation diurne et annuelle de la Terre et par les hétérogénéités de la surface [3]. Les inclinaisons thermiques de la surface terrestre ψ sont approximativement décrites par la formule où x est la profondeur d'enfouissement en mètres; α est le coefficient d'accroissement thermique (degré -1); σ est le coefficient de Poisson; ω est la fréquence de l'onde de température (s^{-1}) le long de l'arc Y; ϑ_0 est son amplitude en degrés; a est le coefficient de l'allure de la température (M^2/s); l est le démembrement du relief et de l'hétérogénéité en mètres; $k = \sqrt{\omega/2a}$.

$$\psi = \frac{\alpha \vartheta_0}{1-\sigma}\left\{P_\psi \cos\left(ut - \frac{\pi}{4}\right) - Q_\psi \sin ut\right\} \cdot l^{-\frac{2\pi}{l}\cdot x} \cdot \sin\left(\frac{2\pi}{l}\cdot y\right) +$$

$$+ (1+\sigma)\cdot \frac{\sqrt{2}\pi}{\kappa l} \cdot l^{-\kappa x}\left[\sin\left(ut - \kappa x + \frac{\pi}{4}\right) -\right.$$

$$\left. -(1+\sigma)\cdot \frac{2\pi^2}{l^2\kappa^2} \cdot \cos\left(ut - \kappa x + \frac{\pi}{4}\right)\right] \cdot \sin\frac{2\pi y}{l} ;$$

$$P_\psi = (1+\sigma)\frac{\sqrt{2}\pi}{l\cdot\kappa}\left[\frac{2\pi}{l}x + (1-2\sigma)\right],$$

$$Q_\psi = \frac{2\pi^2}{l^2\kappa^2}\left[2(1-\sigma) + (1+\sigma)\frac{2\pi}{l}x\right],$$

D'après les résultats des recherches précédentes les inclinaisons thermiques diurnes d'été et d'hiver sont à peu près les mêmes à Niefteiougansk, Novosibirsk et Irkoutsk [3, 4]. Ce n'est pas étonnant puisque ces stations, jusqu'à la surface, sont situées dans les terres submersibles de fleuves importants et sur des roches analogues (sables, grès, acrolyte). Les inclinaisons thermiques annuelles sont quelquefois plus grandes en amplitude que les variations diurnes car la chute annuelle des températures est de 30 à 40° et la variation diurne de seulement 10 à 15°. Un exemple du processus cyclique annuel d'après les données de la station "Klioutchi" est donné sur la figure 5. Ainsi, l'allure annuelle des inclinaisons thermiques à Niefteiougansk doit atteindre quelques secondes d'arc et présente sur le diagramme vectoriel un caractère cyclique elliptique.

Sur le fond de ces inclinaisons périodiques on note de brusques variations par exemple en avril 1990. C'est l'époque de la fonte rapide de la neige et de la rentrée de l'eau par le mur Sud Est dans la vallée. Ici pour quelques heures

d'enregistrement du 21.04.90 on a noté une inclinaison de 9,0" vers le Sud Est. Il est évident que cet effet est lié à l'entrée d'eau sur le mur et à l'irrigation de la base du socle portant les appareils. L'allure générale de l'inclinaison de mars à mai est liée également à la fonte des neiges et du sol dans la région par la variation du régime des eaux souterraines.

Lors du débranchement du chauffage électrique on a noté des variations rapides des inclinaisons et de la température. Les inclinaisons locales thermiques sont indiquées sur la figure 6 (juin 1990).

Des variations rapides sont notées également lors de l'enregistrement des ondes de surface des tremblements de terre lointains.
La comparaison de l'enregistrement des ondes de surface des forts tremblements de terre à Niefteiougansk avec les enregistrements obtenus dans la cave de la station séismologique de Talaïa (rive sud du lac Baïkal) a montré que l'amplitude des ondes de surface à Niefteiougansk est plus grande de plus d'un ordre (fig. 7). Ce fait reflète une différence dans la structure de l'écorce terrestre et également des roches dans la région.

Une brusque variation de l'allure de l'inclinaison de la surface terrestre est donnée sur la figure 8. D'après ces enregistrements le vecteur anormal de l'inclinaison est de 1, 6 " et est dirigé vers le Nord Ouest. Il est possible que dans ce cas on ait observé un brusque affaissement de la surface terrestre, provoqué par les processus dans les couches rocheuses sous le point de mesure. L'anomalie n'est pas liée aux variations climatiques naturelles (voir fig. 8).

Les résultats des mesures pour les deux composantes pour la période de décembre 1989 à février 1991 sont donnés sur la figure 9 du diagramme vectoriel des variations d'inclinaison. La dérive la plus faible de l'inclinaison suivant les mois a été notée au début des mesures - l'automne tard 1989 et en hiver 1989 à 1990. Dans cette période la dérive de l'inclinaison ne dépasse pas 0,5-2" par mois (fig. 10). La plus haute vitesse a été notée dans les mois de printemps 1990 jusque 25" par mois. En été et en automne 1990 la dérive est de 5 à 10" par mois. L'allure générale pour la période des observations d'après les deux composantes de décembre 1989 à février 1991 atteint 107" vers le Sud Est. Si on élimine la dérive dans les mois de printemps (mars à mai 1990) alors elle atteint 57" vers le sud pour toute la période (voir fig. 9). Sur l'enregistrement d'une période de plus d'un an de mesures il est évident que ne se manifeste pas d'onde annuelle. Apparemment le niveau des inclinaisons thermiques annuelles ne dépasse pas 10" et est plus petit que la dérive. Il convient de noter une grande variabilité de la dérive dans les mois de printemps et d'été ce qui reflète la variation du niveau des eaux souterraines dans cette période et est lié au fait que la ville de Niefteiougansk est construite sur des sables alluvionnaires et est située sur le gisement pétrolier de Oust-Balsiki.

Sur la base des mesures clinométriques d'octobre 1989 à février 1991 on peut tirer comme conclusions:

1. L'allure des inclinaisons thermiques dont l'amplitude moyenne n'est pas plus de 1 à 2" est habituelle pour les points du même type (période T = 1 jour).

2. On note bien de forts tremblements de terre lointains. L'amplitude des ondes de surface est d'un ordre plus élevé que les amplitudes notées dans la région de la zone de rift du Baïkal ce qui est lié à la différence de structures géologiques des régions.

3. Dans le processus d'observation on a enregistré quelques cas de variations rapides (heures) de l'allure de l'inclinaison. Cela est lié à la fonte des sols, de la neige et à l'entrée de l'eau dans la salle en avril 1990, également au moment du branchement et du débranchement du chauffage électrique de la salle de mesures.
Il convient particulièrement de noter la variation brusque (minutes) de l'allure de l'inclinaison du 16.02.91 non liée aux effets de température et atmosphériques (voir fig. 8). Il est possible que cette anomalie soit provoquée par l'affaissement du sol dans le processus d'exploitation du gisement Oust-Baliski. Le même effet instantané peut provoquer un effet de tremblement de terre.

4. L'allure de l'inclinaison sur une période de plus d'un an d'observations indique la présence d'une composante systématique dans l'azimut S.E. La composante périodique provoquée par les déformations annuelles thermiques est quelquefois moindre que la composante systématique et, en amplitude, ne dépasse pas 10" ce qui est un ordre plus petit que la composante systématique.
L'allure systématique peut être partiellement liée à la variation dans le temps du régime hydrodynamique et hydrostatique des eaux souterraines du territoire adjacent et particulièrement avec la variation du niveau du sol par infiltration et le degré d'irrigation des sols, bien que les mesures ont été faites dans le même point et il est difficile de juger de l'échelle du phénomène. Les variations systématiques du niveau des eaux du sol peuvent être provoquées par les variations climatiques saisonnières de plusieurs années. On peut également supposer la présence de mouvements qui ont lieu à cause de l'exploitation du gisement de pétrole. La vitesse élevée de l'allure systématique de l'inclinaison exige une grande attention, un enregistrement continu et l'analyse méticuleuse de l'allure de l'inclinaison dans le temps et l'espace.

Références

I. Болт Б. Землетрясения. - М.: Мир, I98I. - 256 с.

2. Гриднев Д.Г., Сарычева Ю.К., Тимофеев В.Ю., Савиных А.В. Аномальные наклоны земной поверхности перед некоторыми землетрясениями // Геология и геофизика. - I987. - № I2. - С. 78-82.

3. Гриднев Д.Г., Сарычева Ю.К., Тимофеев В.Ю. Квазисуточные неприливные наклоны земной поверхности в районе Новосибирска и Иркутска. - Новосибирск, I988. - I2 с. - Деп. в ВИНИТИ 3I.08.88, № 678I-В88.

4. Гриднев Д.Г., Сарычева Ю.К., Тимофеев В.Ю. Наклоны земной поверхности в районе водохранилища Иркутской ГЭС // Геология и геофизика. - I989. - № 3. - С. II6-I22.

5. Гриднев Д.Г., Тимофеев В.Ю., Сарычева Ю.К. и др. Наклоны земной поверхности на юге Байкала (Талая) // Геология и геофизика. - I990. - № 5. - С. 95-I04.

6. Гриднев Д.Г., Тимофеев В.Ю. Кварцевый наклономер с магнитным управлением // Геология и геофизика. - I99I. - № 3. - С. I42.

7. Тимофеев В.Ю., Гриднев Д.Г., Сарычева Ю.К. и др. Наклономерные исследования в Байкальской рифтовой зоне // Геолого-геофизические исследования в сейсмоопасных зонах СССР. - Фрунзе, I989. - С. 76-77.

8. Arich E., Merrer A.M. Fluctuations in oil flow before and after earthqvakes // Nature. - 1974. - V.247. - P. 534-535.

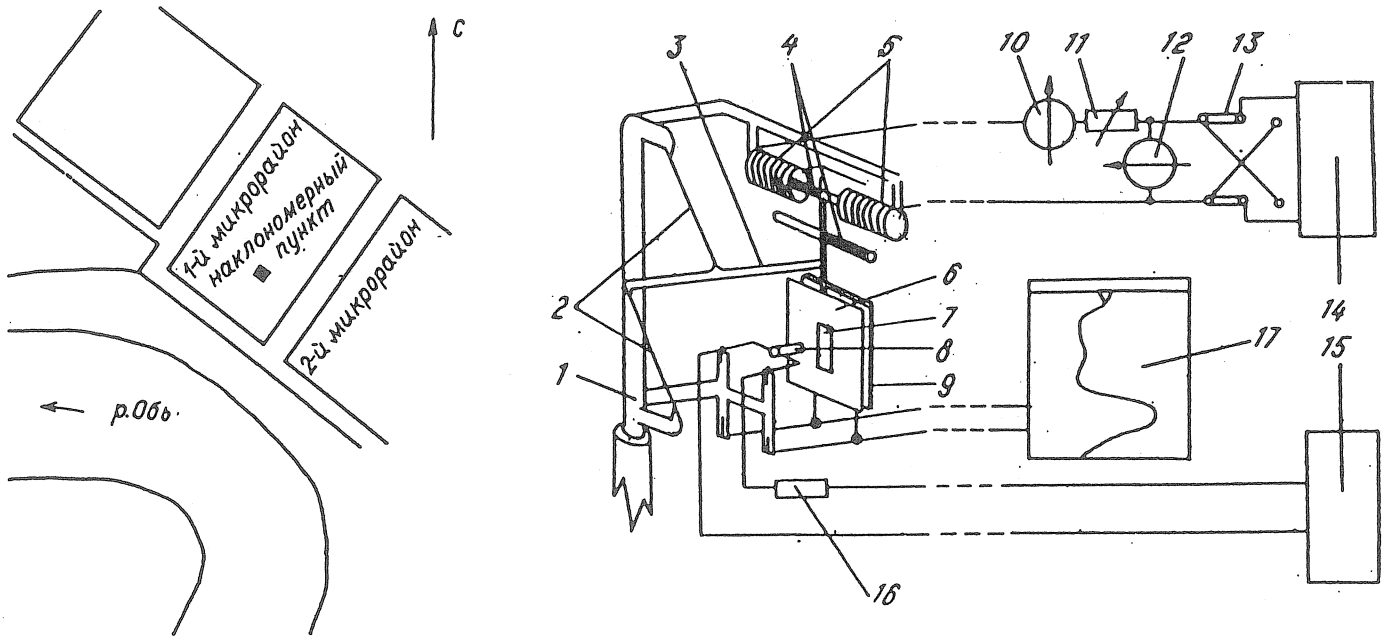

Figure 1. Schéma de la position du point clinométrique à Niefteiougansk.

Figure 2. Construction du clinomètre à quartz avec commande magnétique.

1.- Châssis de montage en quartz; 2.- fils de quartz; 3.- pendule en quartz; 4.- aimants principaux constants (les moments magnétiques sont les mêmes et sont dirigés à la rencontre l'un de l'autre); 5.- solénoïdes, attachés solidement au châssis de montage; 6.- écran métallique avec ouverture rectangulaire placée verticalement; 7; 8.- diode lumineux; 9.- photoélément différentiel; 10.- microampèremètre; 11.- magasin de résistances; 12.- voltmètre; 13.- interrupteur; 14., 15.- sources d'alimentation hautement stabilisées; 16.- résistance d'atténuation; 17.- enregistreur.

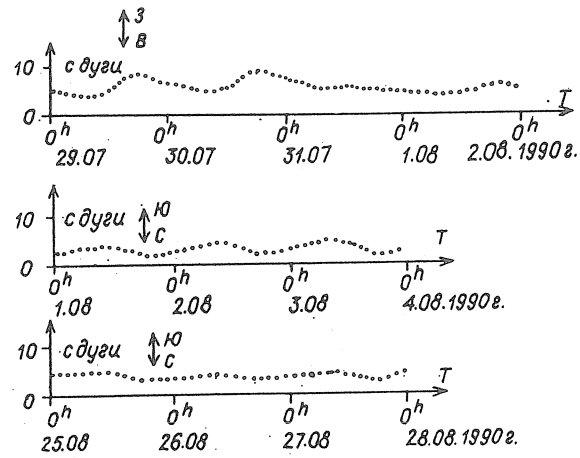

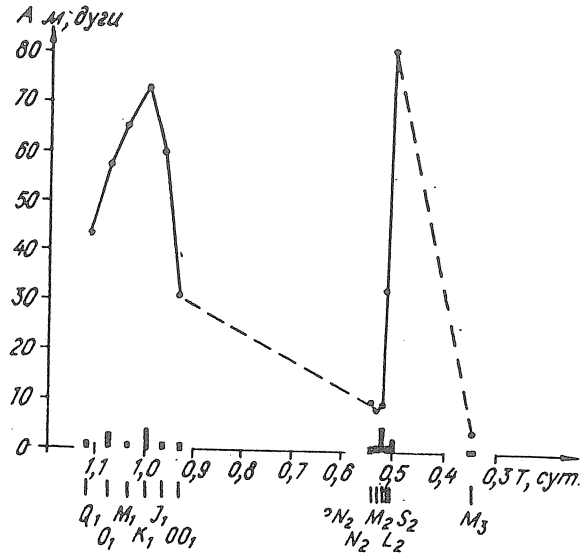

Figure 3. Inclinaisons diurnes théoriques de la surface de la Terre à la station de Niefteiougansk dans les mois d'été.

Figure 4. Résultats de l'analyse de marée des inclinaisons pendant les mois d'hiver (décembre 1990 à février 1991) à la station de Niefteiougansk (composante Nord-Sud) - courbe brisée. Les lignes verticales le long de l'axe des périodes sont les amplitudes normales des ondes de marées (diurnes - Q_1, O_1, M_1, K_1, J_1, OO_1, semi-diurnes $2N_2$, N_2, M_2, L_2, S_2, terdiurnes M_3). A est l'amplitude des ondes en millisecondes d'arc.

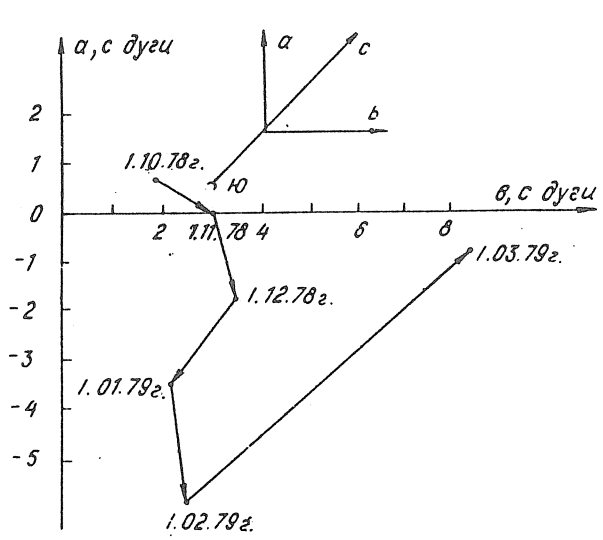

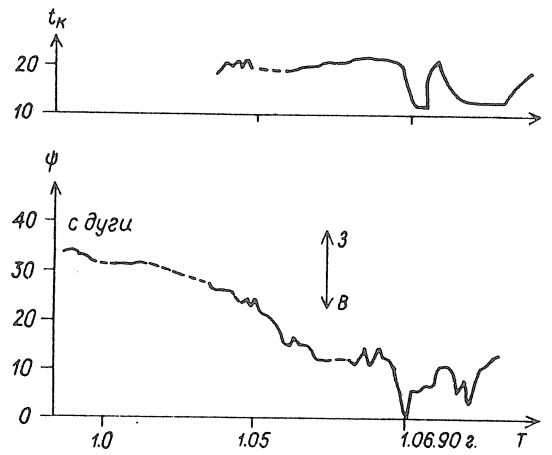

Figure 5. Diagramme vectoriel des variations de l'inclinaison de la surface terrestre à la station de marée "Klioutchi", région de Novosibirsk.

Figure 6. Variations de température dans la salle (t_k) lors du débranchement du chauffage. L'allure de l'inclinaison au printemps-été 1990 est donnée en dessous.

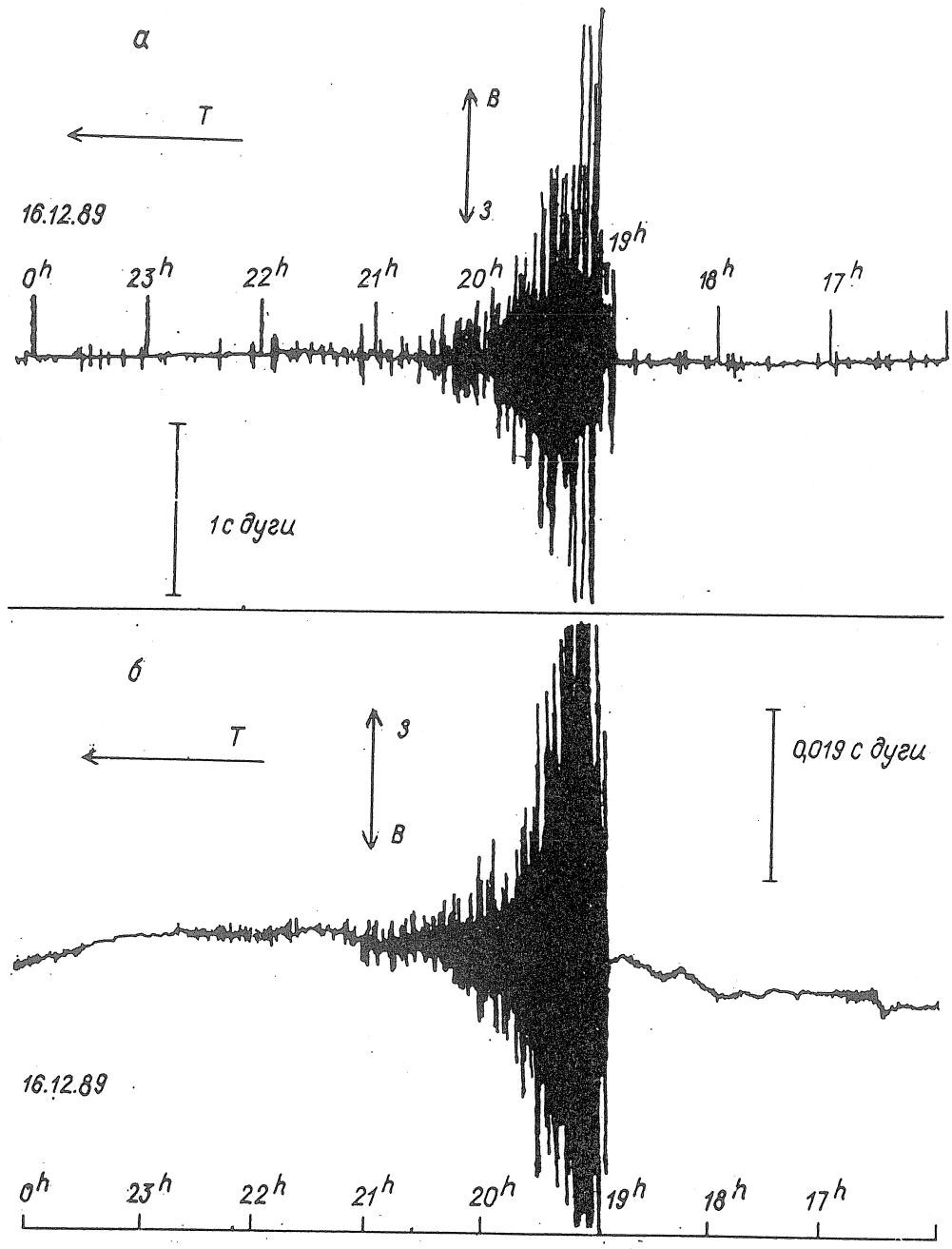

Figure 7. Ondes de surface d'un fort tremblement de terre éloigné (le temps d'arrivée dans la station séismique d'Irkoutsk à 18h 43 min 46,6 s. le 15.12.89 à Mindanao, Philippines 8,38°N, 126.65°E, M = 7,1) enregistrées par les clinomètres dans les stations de Niefteiougansk (a) et Talaïa (b) (Baïkal, 51.68°N, 103.65°E).

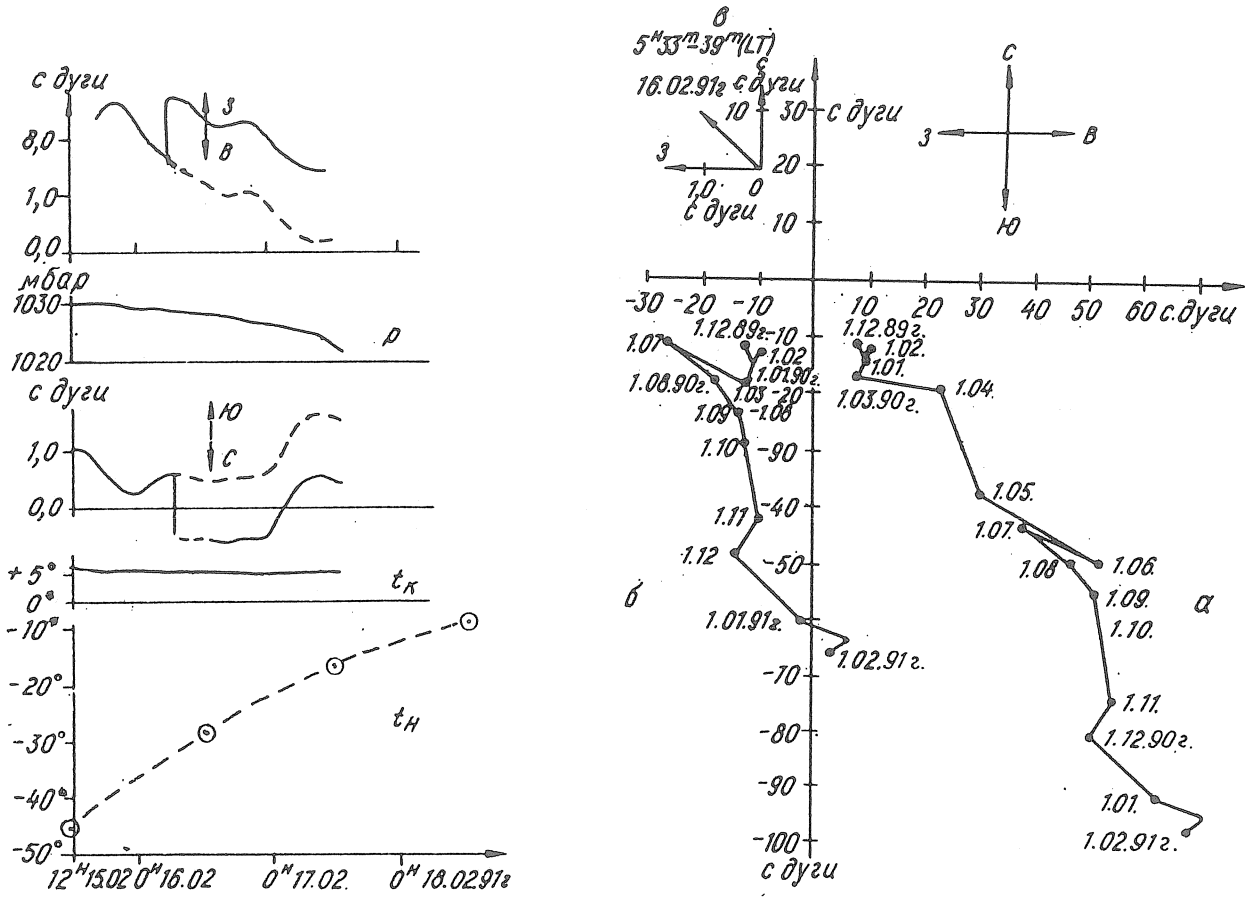

Figure 8. Enregistrement de la dérive de l'inclinaison au point de Niefteiougansk d'après les composantes NS et EW le 16.02.91. Les brusques variations ont eu lieu à 5h 33 min. temps local. De haut en bas: dérive de l'inclinaison (E.W.), pression atmosphérique P, dérive de l'inclinaison (N.S.), variation de la température de l'air dans la salle (t_k), variation de la température perturbée de l'air dans la période du 15 au 18 février 1991 (t_n). Sur les courbes de dérive de l'inclinaison on a noté le choc enregistré et l'allure supposée de l'enregistrement.

Figure 9. Diagrammes vectoriels de la dérive à Niefteiougansk:

a- diagramme vectoriel de la dérive du 01.12.89 au 01.12.91;
b- diagramme vectoriel de la dérive sans les mois de printemps de 1990 réunis, du 01.03.90 au 01.06.90;
c- vecteur de la variation anormalement rapide de l'inclinaison du 16.02.91 avec leurs axes des coordonnées (1 s. d'arc = $4,8.10^{-6}$).

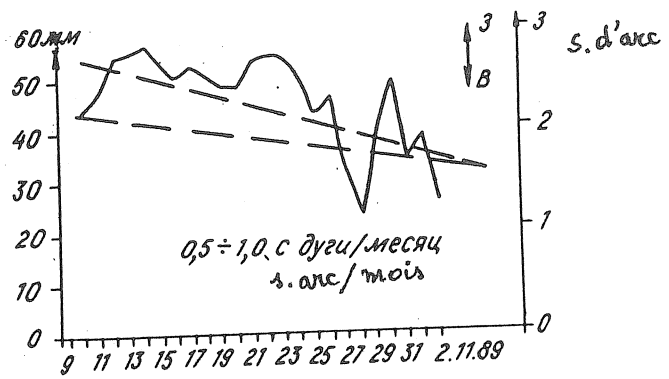

Figure 10. Dérive de l'inclinaison en octobre 1989 à Niefteiougansk.

Traduction
Abrégé

EFFET DYNAMIQUE DU NOYAU LIQUIDE DANS LES OBSERVATIONS DE MAREES TERRESTRES DANS LES STATIONS DE SIBERIE (Novosibirsk, Talaïa, Irkoutsk).

V. You Timofeyev, You K. Saritcheva,
L.V. Anisimova*, S.F. Panine*, S. You Khomoutov

Institut réuni de géologie de géophysique et de minéralogie COPAH, 630090, Novosibirsk, Prof. Université 3 Russie

* Institut de la lithosphère COPAH, 664033 Irkoutsk, Lemonov 128, Russie.

On examine ici les résultats de l'analyse de plusieurs mesures par gravimètres, clinomètres et déformographes. Dans les amplitudes obtenues pour les ondes diurnes O_1 et K_1 on observe une dépendance en fréquence provoquée par la résonance avec une fréquence presque diurne des oscillations libres de la Terre (nutation quasi diurne de la Terre). Ces oscillations libres sont liées aux mouvements du noyau liquide et aux conditions à l'interface noyau-manteau. On a généralisé les résultats des mesures dans les stations de Novosibirsk 1966-1989 (1 gravimètre), 1977 à 1979 (4 gravimètres), Irkoutsk 1979 à 1982 (3 gravimètres) et Talaïa (zone Baïkal de rift) 1985 à 1990 (2 clinomètres), 1989 (1 gravimètre) et 1989 à 1992 (3 déformographes). La fréquence de résonance d'après neuf déterminations indépendantes est de 15,0782 ± 0,0037 degrés/heure et d'après les déformographes (dans les trois azimuts) : 15,0759 ± 0,0017 degrés/heure. Les déterminations les plus précises par quatre gravimètres à Novosibirsk et par les trois déformographes à Talaïa donnent en moyenne 15,0755 ± 0,0004 degrés/heure.

L'étude de l'effet dynamique du noyau liquide est l'une des tâches actuelles de la géophysique et de l'astronomie. En particulier, la résonance de la marée terrestre diurne est un problème important ainsi que la nutation quasi diurne provoquée par les oscillations du noyau liquide. On sait que dans le champs d'attraction luni-solaire le corps de la Terre subit des déformations et le même potentiel de marée engendre aussi bien les marées terrestres diurnes que le phénomène de la nutation-précession de l'axe de rotation de la Terre. L'étude du caractère de ces déformations et des paramètres des nutations aide à préciser les modèles de la structure interne de la Terre. Ainsi, partant des modèles du type "un liquide en rotation dans une enveloppe élastique" [1], les chercheurs passent à de plus compliqués tenant compte du caractère de l'effet réciproque à la limite noyau-manteau, des processus hydrodynamiques dans le noyau de forme non ellipsoïdale et également de la topographie de l'interface noyau-manteau [2, 3] précisée par les méthodes de tomographie séismique [4]. L'importance de ces processus résulte de leur lien avec les phénomènes globaux comme l'apparition du champ magnétique propre de la Terre et la géotechnique.

Les méthodes expérimentales actuelles (interférométrie à très longue base, mesure des déformations de marées) permettent de déterminer les paramètres liés à l'effet dynamique du noyau liquide avec une précision suffisante pour améliorer et départager les modèles existants.

Le but de notre travail est l'estimation de l'effet du noyau liquide dans les observations de marées effectuées dans les stations de Sibérie (Novosibirsk, Irkoutsk, Talaïa), la comparaison avec les modèles théoriques actuels du phénomène et ainsi l'obtention de la valeur de la fréquence de résonance et l'estimation de l'aplatissement du noyau.

Le phénomène étudié consiste en ce qui suit. L'axe de rotation de la Terre, pour une série de raisons, accomplit un mouvement complexe dans l'espace et dans le corps de la Terre qu'on peut considérer comme composant de la précession, nutation et du déplacement dans le corps de la planète auquel correspond la période du mouvement des pôles de Chandler.

Une des perturbations du mouvement de précession-nutation de l'axe de rotation est liée aux oscillations du noyau liquide par rapport à l'enveloppe puisqu'elle est également soumise à l'action des marées tesserales [5, 6]. Conformément à la théorie hydrodynamique de la rotation du noyau liquide [5] il faut s'attendre à une résonance des variations presque diurnes (appelées nutation diurne) avec la marée terrestre diurne. Les observations des marées terrestres confirment cette hypothèse. Ainsi, d'après les résultats des observations gravimétriques et clinométriques on note une dépendance en fréquence des amplitudes des ondes de marées, en particulier la présence d'une différence systématique entre les facteurs d'amplitudes des ondes principales diurnes. Par conséquent, l'effet de résonance est présent aussi dans les nombres de Love h, k, ℓ déterminés par les facteurs d'amplitude.

La théorie de M.S. Molodenski [5] développée pour la nutation de la Terre donne une relation entre les nombres de Love, la fréquence de la marée et la fréquence de la nutation provoquée par les oscillations du noyau liquide. C'est pourquoi, en utilisant les données des observations de marées et en s'appuyant sur la composition spectrale de la marée bien connue par l'astronomie, on peut préciser la fréquence de la nutation libre et la valeur de la période correspondante.

L'effet dynamique du noyau liquide pour les modèles de Terre correspondant aux données séismiques a été examiné par M.S. Molodenski [5]. Dans ses modèles il a pris la répartition des densités de Bullen, un noyau liquide avec aplatissement $\delta = 0.0026 = 1/384,6$ (M I) ou un noyau liquide avec un noyau intérieur solide (M II). Selon la théorie de Molodenski l'effet du noyau liquide est déterminé par les seconds membres des relations :

$$h = 0,6206 + 0,4711 \cdot 10^{-3} \frac{\sigma(\sigma + 2\omega)}{\omega^2}\beta ,$$

$$k = 0,3070 + 0,2384 \cdot 10^{-3} \frac{\sigma(\sigma + 2\omega)}{\omega^2}\beta , \qquad (1)$$

$$l = 0,0904 - 0,0112 \cdot 10^{-3} \frac{\sigma(\sigma + 2\omega)}{\omega^2}\beta ,$$

où σ est la fréquence de l'onde de marée; ω est la fréquence de la rotation diurne de la Terre, $\beta = 41.87/(02136 - 100\ (\sigma_0 - 100\ (\sigma_0 + \omega)/\omega) + 1,9$ est le facteur de résonance; σ_0 est la fréquence de résonance (fréquence de la nutation libre du noyau). Pour les ondes diurnes les plus fortes O_1 et K_1 la valeur de β est respectivement égale à : + 197,9 et + 7,1. La fréquence de résonance pour le modèle M I est égale à 1,0021405 cycle par jour sidéral ce qui correspond à une vitesse horaire de 15,073264 degrés/heure. Pour le modèle M II les relations sont plus complexes [5] et la fréquence est de 1,0021628 cycle/jour sidéral (15,0736 degrés/heure). Les valeurs théoriques des nombres de Love pour les modèles M I et M II sont :

Modèle	h_{O_1}	h_{K_1}	k_{O_1}	k_{K_1}	l_{O_1}	l_{K_1}
MI	0,617	0,527	0,305	0,260	0,0905	0,0926
MII	0,614	0,534	0,300	0,261	0,0809	0,0838

Le facteur de résonance diffère de deux ordres pour O_1 et K_1 ce qui donne la possibilité de déterminer l'effet dynamique du noyau liquide par la différence des facteurs d'amplitude de ces ondes. On considérant le rapport $\delta\ (K_1)/\delta\ (O_1)$ on élimine le coefficient de calibration dont les erreurs de détermination peuvent sensiblement altérer l'exactitude.

Comme il apparaît par la table 1, l'effet du noyau liquide atteint 2% dans les variations de marées de la pesanteur, 6% dans les inclinaisons de la lithosphère, 19 à 39% dans les déformations en fonction de l'azimut. La figure 1 montre que la valeur de l'effet est différente aux diverses fréquences.

Le modèle de Molodenski a été construit au début des années 60 et correspondait aux données expérimentales de l'époque. Dans les années 80 la précision des travaux expérimentaux a augmenté et des modèles plus complexes de la structure de la Terre sont apparus.

Wahr [7, 8] a élaboré un modèle dans lequel on examine la Terre en rotation ellipsoïdale avec un noyau interne élastique, un noyau externe liquide et un manteau élastique. Les paramètres rhéologiques correspondent aux modèles 1066 A, PEM-C et C2 [9]. Avec l'aplatissement hydrostatique du noyau $\epsilon = 1/392$, la fréquence de résonance est de 1.0021739 cycle/jour sid. (15,073767 degrés/heure). Les rapports pour les nombres de Love ont la forme

$$k_0(\omega_n) = k_0(\omega_{o_1}) + k_1 \frac{\omega_n - \omega_{o_1}}{\omega_1 - \omega_n},$$

$$h_0(\omega_n) = h_0(\omega_{o_1}) + h_1 \frac{\omega_n - \omega_{o_1}}{\omega_1 - \omega_n}, \qquad (2)$$

$$l_0(\omega_n) = l_0(\omega_{o_1}) + l_1 \frac{\omega_n - \omega_{o_1}}{\omega_1 - \omega_n},$$

où $\omega\pi$ est la fréquence de marée; $\omega_{01} = 0,92700$, $\omega_{K1} = 1$ cycle/jour sid.; ω_π est la fréquence de résonance; les valeurs des coefficients pour les différents modèles de structure de la Terre sont les suivants :

Modèle	$k_0(\omega_{o_1})$	k_1	$h_0(\omega_{o_1})$	h_1	$l_0(\omega_{o_1})$	l_1
1066A	0,298	-0,00123	0,603	-0,00246	0,0842	0,0000781
PEM-C	0,298	-0,00124	0,602	-0,00246	0,0839	0,0000769
C2	0,298	-0,00123	0,602	-0,00245	0,0846	0,0000758

Les valeurs des nombres de Love pour les modèles théoriques de Wahr et de Molodenski sont données dans la table 2. Comme nous le verrons, les valeurs de l'effet dans les différentes formes des variations de marées sont voisines puisque les nombres de Love concordent dans les différents modèles.

Avec les appareils actuels l'analyse harmonique de séries d'une durée de 3 mois et plus se fait avec une erreur de un pour-cent en fonction des valeurs du facteur d'amplitude. Lors de l'utilisation du déformographe, la

grande valeur de l'effet de résonance pour l'onde K_1, permet de tenir compte des mesures avec une erreur d'un ordre plus grand que dans les mesures gravimétriques. La détermination de l'effet du noyau liquide a été faite pour les différents aspects des mesures que nous avons faites depuis plusieurs années. On a utilisé les résultats des mesures dans les stations de Klioutch (Novosibirsk), Irkoutsk et Talaïa (partie Sud-Ouest de la zone de rift du Baïkal, 51,68° lat. Nord, 103,65° long. Est) fig. 2). Les mesures gravimétriques à Novosibirsk sont représentées par les résultats obtenus au cours de différentes périodes (1966 à 1989) avec le gravimètre Askania GS-12 n° 186 [10]. Comme nous l'avons noté plus haut, pour éliminer l'influence des erreurs de calibration on a utilisé le rapport des facteurs d'amplitude des deux ondes diurnes O_1 et K_1, l'une hors et l'autre dans la zone d'influence de la résonance. Ce rapport est égal à 0,9825 ± 0,0030 pour la station de Novosibirsk. Pour cette même station on a analysé les résultats des mesures de 1977 à 1979 avec un groupe de quatre gravimètres: Askania GS-11, n° 159, GS-12 n° 180 et n° 186, CKR (gravimètre à quartz statique, Gridniev). D'après ces mesures, le rapport pour les ondes O_1 et K_1 est égal à 0,9831 ± 0,0019 [11].

Avec ce même groupe d'appareils on a fait des mesures à Irkoutsk de 1979 à 1982. Des résultats de qualité [12] ont été obtenus pour les trois gravimètres GS-11 n° 159, GS-12 n° 180 et GS-12 n° 186; on a obtenu ici un rapport 0,9904 ± 0,0055. Ces observations ont été faites dans des salles thermostabilisées spécialement équipées.

Une grande quantité de mesures a été faite à la station de Talaïa: variations de la pesanteur et des inclinaisons. Les mesures gravimétriques ont été faites en 1987-1989 avec le gravimètre CKR dans la cave avec thermostabilisation passive, située sous le bâtiment de la station séismique. Le résultat de l'analyse pour les ondes O_1 et K_1 satisfaisant en précision n'a été obtenu que dans une courte période (10.07-08.08) 1989; avec pour rapport :

$$\delta_{K1}/\delta_{O1} = 0,989 \pm 0,019.$$

L'utilisation du rapport des facteurs d'amplitude des deux ondes permet, outre l'élimination de l'erreur de calibration, de diminuer l'influence des effets météorologiques sur les résultats des mesures. Ainsi, l'influence de la pression atmosphérique sur les résultats des mesures gravimétriques a été prise en considération à partir des données d'un barographe de haute précision, microbarographe H-75 avec échelle d'enregistrement de 1 mbar. sur 20 mn d'enregistrement. Pour traduire la pression en μgal on a utilisé le coefficient 0,3 μgal/mbar. Les résultats sont donnés sur la figure 3. L'influence de la pression ne dépasse pas 1% de l'amplitude des marées. Ces perturbations pour les ondes O_1 et K_1 sont en phase et ont la même amplitude. L'utilisation d'une série de deux mois en comparaison avec une série mensuelle diminue l'influence de la pression d'un facteur deux. Ainsi, l'utilisation du rapport des facteurs d'amplitudes à titre de paramètre résultant permet de diminuer sensiblement l'influence des variations climatiques sur les résultats des mesures.

Par rapport à l'influence des marées océaniques sur les résultats des mesures il faut noter que, pour les stations continentales intérieures éloignées de 1 000 km des océans, les corrections des marées océaniques atteignent des dixièmes de pour-cent. L'utilisation du rapport des facteurs d'amplitudes des deux ondes permet de diminuer l'influence des marées océaniques sur les résultats des mesures.

Les mesures à l'aide de clinomètres à quartz de Gridniev se font en continu dans la galerie de la station de Talaïa depuis 1985. On utilise une paire d'appareils pour les mesures dans les azimuts NS et EW. Leur sensibilité atteignait 0,5 mseca/mm. Le régime de température dans la galerie est très stable: la température au cours de l'année est de + 10°C, les variations annuelles restent dans les limites de 1°C, les variations diurnes sont de millièmes de degré. Pour un intervalle de mesures de cinq ans le rapport des facteurs d'amplitudes γ_{K1} / γ_{O1} est 1,0639 (± 9%) pour l'azimut NS et 1,0845 (± 3,3%) pour l'azimut EW.

Les mesures des déformations linéaires dans la galerie de Talaïa ont été faites à l'aide de déformographes à tige avec transducers de déplacements. Pour les mesures dans l'azimut NS on a utilisé un tube en quartz d'une longueur d'environ 1.5 m [11] et, dans l'azimut 332° N, une tige d'invar intégrante sur des billes d'une longueur d'environ 9 m. Dans l'azimut EW les mesures ont été faites à l'aide d'un tube de quartz d'une longueur d'environ 2 m. L'une des extrémités de la tige est fixée dans un petit socle dans la roche. Les mesures ont été faites à l'extrémité libre par un transducer. L'échelle d'enregistrement varie dans les limites de (1 à 4).10^{-9}/mm. Les résultats pour les paramètres L_{KO}/L_{O1} sont les suivants: dans l'azimut NS (1989 à 1991, 10 séries) - 0,670 ± 0,031; dans l'azimut 332° (1990 à 1992, 4 séries) - 0,737 ± 0,70; dans l'azimut EW (1989 à 1991 - 7 séries) - 0,794 ± 0,058.

La table 3 donne pour l'azimut NS et pour des périodes de plusieurs mois, les résultats de l'analyse harmonique et de la détermination des nombres de Love h et . Dans les limites des erreurs elles sont voisines des valeurs données par les modèles théoriques (voir table 2). En fait les rapports des facteurs d'amplitudes obtenus pour les ondes O_1 et K_1 sont voisins des valeurs calculées à partir des modèles présentés plus haut (table 1).

Pour comparer les données selon les différents aspects des mesures, les résultats obtenus ont été recalculés aux valeurs de la fréquence de résonance. Dans le travail [15] on utilise aussi bien les caractéristiques d'amplitude que de phases des ondes de marées: on détermine la fréquence de résonance directement par la dépendance en fréquence des facteurs d'amplitude des ondes de marées et avec l'application du retard de phase on détermine la validité. Nous utilisons uniquement les caractéristiques d'amplitude et la forme de la courbe de résonance qui se conserve pour les différents modèles. Nous nous servirons des expressions (2) (avec les paramètres du modèle C2 pour évaluer le rapport des ondes K_1 et O_1. Nous obtenons ensuite les relations pour le calcul de la valeur de la fréquence de résonance ω_1, par les mesures gravimétriques

$$\omega_1 = 1 + 0{,}38238.10^{-4}\ (1 - \delta_{K1}/\delta_{O1}),$$

par les mesures clinométriques

$$\omega_1 = 1 + 1{,}27959.10^{-4}\ (\gamma_{K1} / \gamma_{O1} - 1),$$

par les mesures déformographiques dans l'azimut NS

$$\omega_1 = 1 + 7.62245.10^{-4}/(1- L_{K1}/L_{O1}),$$

dans l'azimut EW

$$\omega_1 = 1 + 4.38809 \times 10^{-4}/(1 - L_{K1}/L_{O1}),$$

dans l'azimut 332°N

$$\omega_1 = 1 + 6{,}60016.10^{-4}/(1 - L_{K1}/L_{O1}).$$

Pour les différents aspects des mesures, nous obtenons les valeurs de la fréquence de résonance ω_1 et de la vitesse horaire correspondante f_0 (table 4). Nous examinerons les résultats selon différents aspects et groupes de mesures:

a) la moyenne pour 9 déterminations différentes $f_0 = 15{,}0782 \pm 0{,}0037$ degr./h;

b) une détermination la plus précise selon l'aspect séparé des mesures (2): $f_0 = 15{,}0751 \pm 0{,}0026$ degré/h.;

c) moyenne selon les stations gravimétriques de Novosibirsk et Irkoutsk (1, 2, 3) $f_0 = 15{,}083 \pm 0{,}008$ degré/h.;

d) moyenne pour toutes les formes de mesures à la station de Talaïa (4, 5, 6, 7, 8, 9) $f_0 = 15{,}0757 \pm 0{,}0037$ degrés/h.;

e) moyenne d'après les mesures avec les déformographes (7, 8, 9) $f_0 = 15{,}0759 \pm 0{,}0017$ degrés/h.

Les valeurs suivantes : 15,078; 15,076; 15,075 et 15,0759 étaient les meilleures en précision. A la dernière valeur de f_0 correspondent

$\omega_1 = 1{,}00231 \pm 0{,}00011$ et la période $T_0 = 432 \pm 20$ jours.

Par le rapport [3]

$$\omega_1 = 1 + (\epsilon_r - \beta_h)\, A/A_M$$

A et A_M sont les moments d'inertie principaux de la Terre et du manteau, ϵ_r est l'aplatissement du noyau, β_M est le coefficient reflétant les propriétés inélastiques à la base du manteau, ($\beta_M \approx 0{,}25\ \epsilon_r$) en utilisant la valeur obtenue plus haut de la fréquence de résonance on peut obtenir la valeur de l'aplatissement du noyau $\epsilon_r = 1/366$.

Selon les deux groupes d'appareils (gravimètre et déformographe) mesurant les manifestations différentes des déformations avec la plus grande précision nous obtenons la valeur moyenne de la fréquence

$\omega_1 = 1{,}00229 \pm 0{,}00003$ et de la vitesse $f_0 = 15{,}0755 \pm 0{,}0004$ degrés/h.

à laquelle correspond $T_0 = 436 \pm 4$ jours et $\epsilon_r = 1/370$ ou 9,3 km.

La dernière valeur coïncide bien avec les données de l'interférométrie à très longue base ($f_0 = 15{,}07587$ degrés/h et $T_0 = 431$ jours [15]) avec les résultats des mesures par les gravimètres à supraconductivité [2]: Bruxelles ($f_0 = 15{,}0760 \pm 0{,}0009$ degrés/h et $T_0 = 430 \pm 12$ jours), Bad Homburg ($f_0 = 15{,}0759 \pm 0{,}0006$ degré/h et $T_0 = 431 \pm 8$ jours) et également des mesures par déformographes à tige au Japon [16] ($f_0 = 15{,}0758 \pm 0{,}0009$ degrés/h et $T_0 = 432 \pm 11$ jours).

Ainsi, d'après nos déterminations, la fréquence de la résonance est (1 + 1/436) cycle/jour. D'après les travaux [2, 3, 7, 8] si la Terre a une structure correspondant aux représentations actuelles et à la rhéologie et a un aplatissement hydrostatique, la marée terrestre diurne et les nutations

luni-solaires doivent être en résonance avec la fréquence (1 + 1/460) cycle/jour. Les différences dans ces valeurs s'expliquent par la topographie dynamique de l'interface noyau-manteau; la disparité est probablement déterminée par la structure asphérique du noyau provoquée par les forces de gravitation dans le manteau [3, 17]. Le problème n'a pas jusqu'à présent de bonne solution théorique. Pour les travaux expérimentaux, face aux exigences quant à l'augmentation de la précision des mesures constitue un problème intéressant sur la mesure des variations de l'effet de résonance dans le temps.

Le travail a été fait avec le soutien financier du Fonds Russe des Recherches Fondamentales (projet 93-05-14021).

Les auteurs remercient le professeur P. Melchior (Observatoire Royal de Belgique) pour sa collaboration dans ce travail.

Références

1. Бакулин П. И., Кононович Э. В., Мороз В. И. Курс общей астрономии. М., Наука, 1966, 527 с.
2. Melchior P. Tidal interactions in the Earth Moon System // IUGG, Chronicle. Luxembourg, IUGG, 1992, № 210, p. 76—114.
3. Dehant V. On the nutations of a more realistic Earth model // Geophys. J. Int., 1990, № 100, p. 477—483.
4. Forte A. M., Dziewonski A. M., Woodward R. L. Structure of lowermost mantle and CMB topography // XX general Assembly IUGG. Union Program and Abstracts. Graz, Austria, 1991, p. 72.
5. Молоденский М. С., Крамер М. В. Земные приливы и нутация Земли. М., Изд-во АН СССР, 1961, 40 с.
6. Мельхиор П. Физика и динамика планет. М., Мир, 1972, 484 с.
7. Wahr J. Body tides of an elliptical, rotating, elastic and oceanless Earth // Geophys. J. Roy. Astron. Soc., 1981, № 64, p. 677—703.
8. Wahr J. The forced nutation of an elliptical, rotating, elastic and oceanless Earth // Geophys. J. Roy. Astron. Soc., 1981, № 64, p. 705—727.
9. Dziewonski A. M., Anderson D. L. Preliminary reference Earth model // Phys. Earth Planet. Inter., 1981, v. 25, p. 297—356.
10. Сарычева Ю. К., Тимофеев В. Ю. Приливные параметры Земли по результатам новосибирских гравиметрических наблюдений // Геология и геофизика, 1992, № 2, с. 37—44.
11. Баленко В. Г., Барсенков С. Н., Булацен В. Г. и др. Приливные изменения силы тяжести в Новосибирске в 1977—1979 гг. // Медленные деформации Земли и ее вращение. М., Радио и связь, 1985, с. 40—59.
12. Гриднев Д. Г., Кузнецов М. В., Кузнецова Л. В. и др. Региональные приливные исследования в азиатской части СССР // Современная геодинамика литосферы Сибири. Новосибирск, ИГиГ СО АН СССР, 1986, с. 63—79.
13. Сарычева Ю. К., Тимофеев В. Ю. Приливные наклоны в Талой (Байкальская рифтовая зона) // Методика и результаты изучения пространственно-временных вариаций геофизических полей. Новосибирск, ОИГГиМ СО РАН, 1992, с. 173—194.
14. Тимофеев В. Ю., Сарычева Ю. К., Панин С. Ф., Анисимова Л. В. Приливные параметры по результатам деформографических наблюдений в районе Байкальской рифтовой зоны (Талая) // Методика и результаты изучения пространственно временных вариаций геофизических полей. Новосибирск, ОИГГиМ СО РАН, 1992, с. 202—207.
15. Herring T. A., Gwinn C. R., Shapiro I. I. Geodesy by Radio Interferometry: Studies of the Forced Nutations of the Earth. I. Data Analysis; II. Interpretation // J. Geoph. Res., 1986, v. 91, B5, p. 4745—4765.
16. Sato T. Fluid core resonance measured by quartz tube extensometers at the Esashi Earth Tides station // Proceedings of the Eleventh International Symposium on Earth Tides. Stuttgart, 1991, p. 573—582.
17. Sasao T., Wahr J. An excitation mechanism for the „free core nutation" // Geophys. J. Roy. Astron. Soc., 1981, № 64, p. 729—746.

Table 1

Effet dynamique du noyau liquide sous différentes formes des observations de marées selon la théorie de Molodensky.

Aspect des observations de marées	Ao/At dans les nombres de Love	Valeur Ao/At pour les ondes O_1		K_1		Différences pour les ondes O_1 и K_1		Rapports d'amplitude des facteurs des ondes O1 et K1		Effet en pourcent	
		MI	MII	MI	MII	MI	MII	MI	MII	MI	MII
Variations de la pesanteur	$\delta = 1 + h - 3/2k$	1,1590	1,1640	1,1375	1,1435	+0,0215	+0,0205	0,9814	0,9823	1,86	1,77
Inclinaisons	$\gamma = 1 - h + k$	0,688	0,686	0,731	0,727	-0,043	-0,041	1,0625	1,0597	6,25	5,97
Déformations											
Azimut NS	$L = h - 4l$	0,2550	0,2904	0,1568	0,1988	+0,0982	+0,0916	0,6149	0,6846	38,51	31,54
" EW	$L = h - 2l$	0,4360	0,4522	0,3419	0,3664	+0,0941	+0,0858	0,7842	0,8103	21,58	18,97
" 33° N	$L = h - 3,56l$	0,2948	0,3260	0,1975	0,2357	+0,0973	+0,0903	0,6700	0,7229	33,00	27,70

Remarque Ao sont les observations, A_T est l'amplitude théorique

Table 2 Nombres de Love k, h, ℓ pour les ondes O_1 et K_1 conformément aux calculs théoriques de Molodensky et Wahr.

Параметр		1066A	PEM-C	C2	MI	MII
Частота	град/ч	15,073728	15,073813	15,073923	15,073263	15,073610
k	O_1	0,298 (1,000)	0,298 (1,000)	0,298 (1,000)	0,305 (1,000)	0,300 (1,000)
	K_1	0,256 (0,859)	0,256 (0,859)	0,257 (0,862)	0,260 (0,862)	0,261 (0,870)
h	O_1	0,603 (1,000)	0,602 (1,000)	0,602 (1,000)	0,617 (1,000)	0,614 (1,000)
	K_1	0,520 (0,862)	0,519 (0,862)	0,512 (0,865)	0,527 (0,854)	0,534 (0,871)
l	O_1	0,0842 (1,000)	0,0839 (1,000)	0,0846 (1,000)	0,0905 (1,000)	0,0809 (1,000)
	K_1	0,0869 (1,032)	0,0865 (1,031)	0,0872 (1,031)	0,0926 (1,023)	0,0838 (1,036)

Table 3

Résultats de l'analyse harmonique des mesures de déformations dans l'azimut NS pour la période du 04.03 au 30.06.81 et détermination des nombres de Love.

Onde de marée	Valeur du facteur d'amplitude	Erreur
N_2	0,732	0,059
M_2	0,680	0,012
S_2	0,727	0,022
O_1	0,311	0,020
K_1	0,206	0,014

Remarque

Pour les ondes de marées M_2 et O_1 - le rapport des nombres de Love:

$L_{M2} = h + 1.21\,\ell$

$L_{O1} = h - 4\,\ell$

En utilisant les résultats de l'analyse, nous obtenons les valeurs des nombres de Love: $\ell = 0,071 \pm 0,005$ et $h = 0,59 \pm 0,04$.

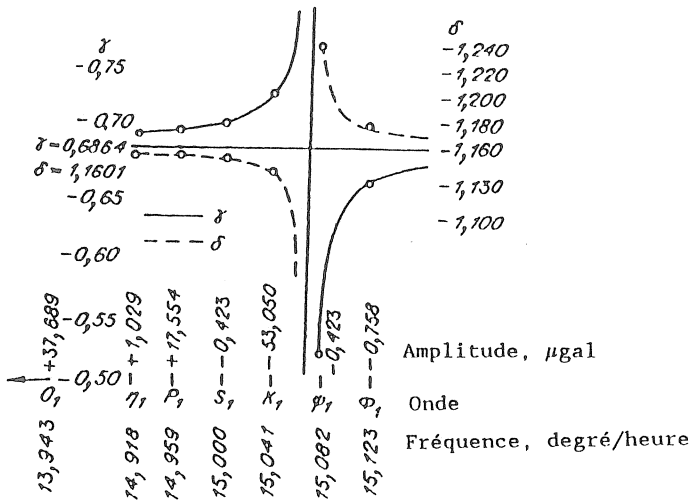

Figure 1 Courbes de résonance pour les facteurs d'amplitude de δ et γ conformément à la théorie de Molodensky.

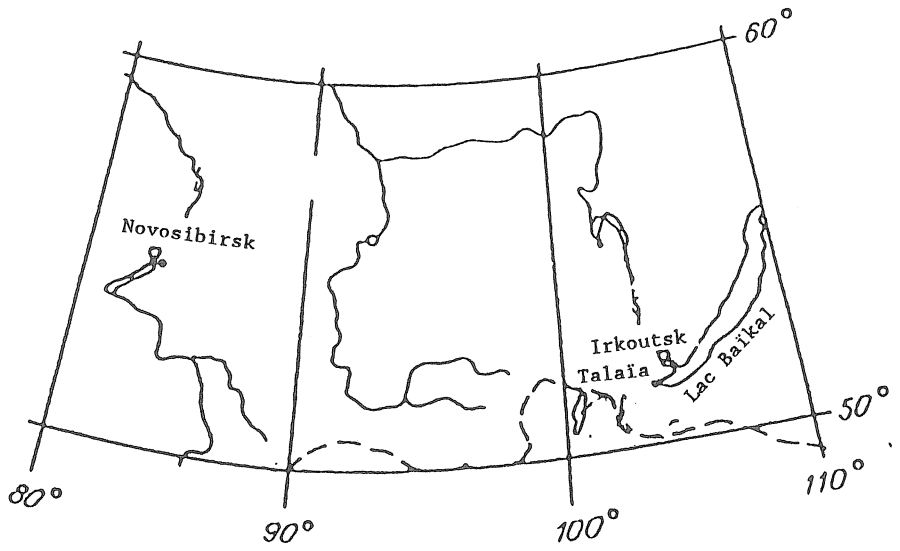

Figure 2 Situation des points des mesures de marées.

Table 4

Valeurs de la fréquence (ω_1) et de la vitesse horaire (f_0) selon les différentes composantes des variations de marées dans les stations de Novosibirsk, Irkoutsk, Talaïa (zone de rift du Baïkal).

N° II/II	Type d'appareil, période, station	ω_1 (cycle/jour)	f_0 (degr./h)
1.	Gravimètre GS-12 n°186, 1966-1989, Novosibirsk	1,00218	15,0738
2.	Gravimètres GS-11 n°159, GS-12 n°180 et n°186 CKT 1977-1979, Novosibirsk	1,00226	15,0751
3.	Gravimètres GS-11 n°159, GS-12 n°180 et 186, 1979-1982, Irkoutsk	1,00398	15,1010
4.	Gravimètre CKR, 1989, Talaïa	1,00333	15,0911 15,0638
5.	Clinomètre quartz (EW) 1985-1990, Talaïa	1,00151	15,0711
6.	Clinomètre quartz (NS) 1985-1990, Talaïa	1,00200	15,0731
7.	Déformographe quartz (EW) 1989-1991, Talaïa	1,00213	15,0788
8.	Déformographe invar (332°) 1990-1992, Talaïa	1,00251	15,0758
9.	Déformographe quartz (NS) 1989-1991, Talaïa	1,00231	
	Moyenne	1,00247	15,0782 ± 0,0037

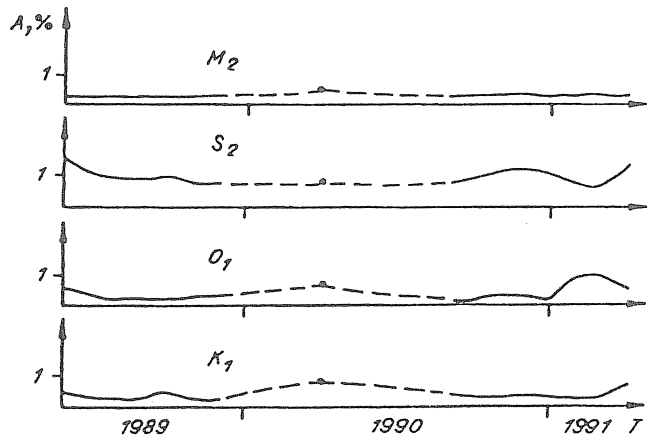

Figure 3 Apport de la pression atmosphérique dans l'amplitude des ondes de marée M_2, S_2, O_1, K_1 pour la période 1989 à 1991. L'influence a été prise en considération d'après les résultats des mesures continues avec le microbarographe à la station de Talaïa.

TIDAL PARAMETERS FROM THE RESULTS OF LASER DEFORMOGRAPHIC MEASUREMENTS IN THE SOUTH - WEST PART OF THE BAIKAL RIFT Talaya station.

Semibalamut V.M., Fomin Yu. N., * Timofeev V. Yu, Rybushkin A. Yu., Gribanova E.I., Kuznetsov S. Yu., Popov M.E., * Sarycheva Y.K.

Institute of Laser Physics SB RAS
Lawrentjewa 13/3, Novosibirsk, 630090, Russia.

* Institute of Geophysics UIGGM SB RAS
Universitetskii pr. 3, Novosibirsk, 630090, Russia.

ABSTRACT

Results of harmonic analysis of tidal oscillations that were registered with the help of a laser deformograph in the South - West part of the Baikal rift are presented.

INTRODUCTION

Investigation of the Earth crust deformations are of great interest for studying the development of present day geological processes, the tidal phenomena and natural oscillations of the Earth. The creation of an apparatus which would enable these investigations to be carried out on long bases and with high sensitivity is one of the main problems in geodynamics.

The Institute of Laser Physics of the Siberian Division of the Russian Academy of Sciences (SB RAS), jointly with the Siberian Experimental Methodical Laser Party of the SB RAS has developed a He-Ne laser deformograph ensuring a substantial gain in sensitivity as compared with the traditional means of registration of the Earth crust deformations [1]. The developed set in contrast to analogous devices [2, 3] does not require a special hermetic sealing of the measuring leg of the interferometer which makes it more mobile and allows easy installation of the measuring optical system in mine and combines it with the existing utility systems, facilities, research set ups and devices. Since 1988, experimental specimens of the laser deformograph have been put through tests at the seismological Talaya station located in the South West part of the Baikal rift. A very interesting material concerning rock deformation before some earthquakes has been accumulated during this period [4, 5] and at present these measurements are being continued. In this paper the results of analysis of tidal oscillations that were recorded in the South West part of the Baikal rift with a modernized laser deformograph are presented.

APPARATUS

The operation of the measuring system of the deformograph is based on continuously registering time phase variation caused by the Doppler effect when the radiation reflects from a moving object. Transformation phase information from the optical into the radiofrequency range (with the method of optical heterodyning) provides for the substantial gain in sensitivity as compared with the traditional means of registration of deformations [6, 7, 8]. To obtain heterodyning optical radiation in deformographs being developed, the method of synchronization of radiations of lasers that has been devised at the

Institute of Laser Physics of the SB RAS in used. The method is covered by patent RF 1362923, ICI 4 CO1 B 21/00.

The modification of the deformograph described in [1] enabled only differential rock deformation along measuring legs to be registered. The introduction of a compensating leg in the interferometer scheme has enable us to exclude the influence of the atmosphere and frequency variations of the laser upon the deformation observations and register the rock deformation along each of the independent directions in the open air [9]. The schematic diagram of the laser deformograph, with one measuring leg, for simplicity, is depicted in Fig.1.

The basis of the set up is two lasers and an automatic phase frequency tuning system thanks to which the difference of frequencies and phases of radiations of the lasers developing across the photodetector D1 is maintained with a constant precision determined by a frequency stability of the reference radiogenerator. Radiation of measuring laser 1 is transmitted to the measuring path and the compensating leg; the returned beams cluster with radiation of laser-heterodyne 2 on the photodetectors D2 and D3. The compensating leg is an inwar rod that is installed on the base near the interferometer. Measurements of the difference of phases of the radio signals is performed on the phase shift meters (PSM), specially developed digital devices with a great dynamic range and high sensitivity $\sim\pi/512$. The change of the wave length of the measuring laser is determined from the analysis of the difference of phases between radio signals of the detectors D1 and D2 which develops across PSM-1. The phase difference of the optical signal on the measuring path is due to the change of the probing radiation wave length, and, besides, the phase difference due to the variation of the path length is added Fig. 2a. Knowing the proportionality factor between the length of the compensating leg and the length of the measuring leg, one extracts from the phase difference signal on PSM-2 that part which is only due to the change of the measuring path length Fig.2b.

Primary treatment of information coming from the measuring devices, a mapping of the registered process on the monitor screen in real time scale and it's preservation is provided with the help of the computer.

The software of the system of collecting data presents a set of real time programs providing for interaction of an operator with the task being performed and control of the course of its performance. The computing system operates in background operative conditions under the control of a RT11FB monitor that executes the distribution of the time of the central processor between background and operative problems. The operative problem is designed for recording the results of measuring into external devices with synchronisation of the events by a system timer.

REGION OF THE WORK.

The Talaya seismo station where the testing of a laser apparatus is being carried out is situated in the South-West part of the Baikal folded region, 6 km from Baikal Lake.
According to the map of the seismic division into districts, it is a zone of possible 8 - 9 magnitude earthquakes. To the North from the station, at a distance of about 5 km, the principal Sayans fault runs along, they has here a sublatitudinal stretching. The adit of the Talaya seismo station has been drilled fifteen meters up from the Talaya brook. The holding rocks are crystalloschits and marble of Archean age. The location of the apparatus in the adit is shown in Fig.3.

RESULTS OF FIELD MEASUREMENTS AND TIDAL ANALYSIS.

During 1992 investigations of deformations of earth crust had been carried out in the adit Talaya s/s. The measurements were performed in two measuring legs each 25 meters long. The sensitivity of the system to deformation along the measuring legs is 5 * (10**(-9)), and registration of the two measuring legs was performed with a response of 3 * (10**(-10)). The discretization frequency was 0.5 Hz. The plots of rock deformations along the measuring legs over the period from 19.08 to 09.12 subjected to low frequency filtering are displayed in Fig. 4. High sensitivity of the laser deformograph ≈ (10**(-10)) enables us to register both slow deformation processes and tidal deformations of the earth surface. A fragment of the record of tidal deformations is depicted in Fig. 2b.

The tide theory has been developed to fit the spherically homogeneous Earth [8]. Tidal deformations in the Earth are proportional to the potential of tidal forces. The components of the deformation of the Earth surface are expressed through the Love number h and the Shida number ℓ, these numbers are connected with the distribution of density and rigidity modulus in the Earth. According to the models these numbers are :

Earth Model	h	ℓ
Gutenberg	0.6055	0.0829
Gilbert-Dziewonsky	0.6130	0.0853

After averaging the experimental data over the world net, Melchior [8] got h = 0.584 and ℓ = 0.045. From the sputnik measurements, Lageos (1983 - 1985) [4] has found h = 0.605 ± 0.004 and ℓ = 0.097 ± 0.002.

A deformograph of meridian orientation registers the tidal deformation $e\phi\phi$, that of latitude orientation the deformation $e\theta\theta$. An instrument oriented in an arbitrary azimuth with the cosine directions m and n registers the component

$$e = m^2 * e\,\theta\theta + n^2 * e\phi\phi + m * n * e\theta\phi \qquad (1)$$

Substituting the components of the deformations from [6-8] into the expressions we get for the semi-diurnal wave M_2 :

$$e = 38{,}222 * 10^{-9} * (A \cos 2H + B \sin 2H) \qquad (2)$$

where

$$A = h * \sin^2\theta + 2 * \ell\,(m^2 * \cos^2\theta - n^2 - \sin^2\theta)$$

$$B = 4 * \ell * m * n * \cos\theta$$

for the diurnal wave O_1 :

$$e = 15{,}863 * 10^{-9}\,(A \cos H - B \sin H) \qquad (3)$$

where

$$A = (h - 2 * \ell * (1 + m^2)) * \sin 20;$$

$$B = 4 * \ell * m * n * \sin\theta;$$

H - is the hour angle of the Moon or the Sun.

The results of deformographical measurements obtained in 1992 were analyzed with the standard program "Venedikov - 74" according to the version "Analysis of tidal variations of force of gravity", since the expression for

the tidal measurements of deformations coincides with the expression for the results of gravimetrical measurements up to a constant factor (-2g). As is known, tidal waves M_2 and O_1 are the least susceptible to meteorological effects. The results are presented in Tables 1 and 2. Having determined the ratio of the observed amplitudes of waves M_2 and O_1 to the theoreticals, from (2) and (3) we get two equalities to determine the numbers h and . As for the analysis of differential tidal deformations from two measuring legs, only the Shida numbers is determined. In this case the amplitude factor for our measuring circuit is 8.2371 for semi-diurnal waves and 2.391 for the diurnal waves. The numbers h and obtained by the material of 1992 (110 - twenty - four - hours series of observations) are given in Table 3.

As is seen from Table 3, the Shida number deduced from the difference of the measuring legs is determined with the lowest error, which indicates a good compensation of atmospheric pressure differences and frequency change of the laser radiation for this measuring circuit.

Unfortunately, the counting errors of determining tidal parameters from the data obtained along measuring legs 1 and 2 are rather large which is determined by the effect of deformation on wave O_1 which occur with daily temperature and pressure fluctuation and by the small amplitudes of the tidal oscillations along the second leg.

The number obtained from the differential deformation by the wave M_2 (= 0.0658 ± 0.0006) and h calculated along the first leg over the period from 19.08 to 09.12 (h = 0.5105 ± 0.0182) agree rather well with the Love numbers determined from the results of deformation measurements that were carried out with the help of an invar bar North - South oriented deformograph in March - May, 1989 in the same adit. One may compare the Shida numbers we have obtained with those calculated from the tiltmeter data presented in [10, 11]. The amplitude factor for the tiltmeter observations is

$$\gamma = 1 + k - h \qquad (5)$$

On the average, over the six years period of observations we have got for the principal tidal wave M_2 :

$\gamma = 0.777$ (N - S) and $\gamma = 0.702$ (E - W).

From the theoretical relationships [8], $k = 0.495 * h$, then under the assumption that k is global we have h = 0.4416 (N - S), and h = 0.5901 (E - W); k = 0.301 (from the sputnik measurements) and then we get h = 0.524 (N - S) and h = 0.599 (E - W).

To diminish the influence of meteorological factors on our determination of h and , let's substitute the number obtained after analysis of data from the difference of two legs for wave M_2 (from 19.08 to 09.12) : = 0.0658 ± 0.0006) into equation (2) and solve it for wave M_2. In this case we get h = 0.5120 ± 0.0154.

CONCLUSION.

With the help of a laser deformograph on the measurement basis of 25 meters, the values of the tidal parameters h and have been obtained for the first time for the South - West part of the Baikal rift zone (the Talaya seismo station). They are close to the Love and Shida numbers determined from the recording of deformations of rocks obtained with a bar deformograph (1.5 m) and tiltmeters, but these results have better precisions.

Since the Love and Shida numbers are connected with distribution of density and rigidity modulus in the Earth, systematic observations of the time variations in the numbers h and enables one to watch variations of these characteristics of the Earth [8].

In conclusion it may be noted that the automatic laser deformographical system allows measurements to be carried out on bases of up to 200 m and has great promise for applications not only in the field of investigation of physics of the Earth, but also enables control over the deformations of engineering structures (nuclear power plants, dams and mines) to be realized.

ACKNOWLEDGEMENTS.

This work was partly supported by the Russian Science Fund - grants n° 93-05-14021, n° 94-05-17060-a and the grant of the Siberian Branch of RAS.

REFERENCES.

1. S.N. Bagayev, V.A. Orlov, Yu.N. Fomin and V.P. Chebotayev.
Laser Deformographes for Precision Geophysical Measurements.
Physics of the Earth, 1992, 1 (in russian).

2. V.A. Aleshin, M.N. Dubrow and A.P. Yakovlev.
Laser Interferometer for Measuring Earth Crust Deformations.
Reports of the Academy of Sciences of the USSR AS USSR, 1980, V 253, 6, pp 1343-1346 (in russian).

3. J. Levine, J.L. Hall.
Design and Operation of a Methane Absorption Stabilized Laser Strainmeter.
J. of Geoph. Research, May 10, 1972.

4. S.N. Bagayev, O.Z. Vakhrushev, Yu. M. Kirin, S.Yu. Kusnetsov, O.V. Nekipelov, V.A. Orlov, S.F. Panin, O.A. Plotnikova, Yu.N. Fomin.
Observation of Peculiarities of Earth Crust Deformations on the Eve of Earthquakes with Laser Deformograph.
Investigations on Creating Scientific Foundations of Prediction of Earthquakes in Siberia, Irkutsk, 1989, pp. 70-71, (in russian).

5. S.N. Bagayev, Yu.M. Kirin, A.E. Ohm, V.A. Orlow, S.F. Panin, O.A. Plotnikova, Yu.N. Fomin.
Observations of Anomalies of Earth Crust Deformations on the Eve of Spitak Earthquake with High Sensitive Heterodyne Laser Apparatus.
Deformational Processes at the Period Preceding the Spitak Earthquake, M. Institute of Physics of the Earth, AS USSR, 1989, pp. 92-98 (in russian).

6. L.A. Latynina.
Determination of the Earth Tide number ℓ from extensometric data.
Study of the Earth Tides, Bulletin n° 6, Budapest, 1985, p. 26-73.

7. L.A. Latynina and P.M. Karmaleyeva.
Deformographical Measurements.
"Nauka", M., 1978, p. 154. (in russian).

8. P. Melchior.
Earth Tides.
M. "Mir", 1968 (in russian).

9. S.N. Bagayev, Yu.M. Kirin, S.Yu. Kuznetsov, I.V. Mescheryakov, V.A. Orlow, A.Yu. Rybuskin, Yu.N. Fomin.
The investigation of the Earth crust deformation dynamic characteristics in BRZ with the help of high sensitive laser equipment. Development of techniques and instrumentation for experimental geophysics. Collection of scientific papers. Volume 1, Moscow, 1993.

10. V.Yu. Timofeev, Yu.K. Sarycheva; S.F. Panin, L.V. Anisimova.
Tidal Parameters form the Results of Deformographical Observations in the Region of the Baikal Rift Zone (Talaya). Methods and Results of Studying of Spatial Time Variations of Geophysical Fields.
Proceedings of the Institute of Geology, Geophysics and Min. SB RAS Novosibirsk, 1992, p. 202-207 (in russian).

11. Yu.K. Sarycheva, V.Yu. Timofeev.
Tidal tilts at Talaya (Baikal rift). Methods and Results of Studying of Spatial Time Variations of Geophysical Fields.
Proceedings of the Institute of Geology, Geophysics and Min. SB RAS Novosibirsk, 1992, p. 173-194, (in russian).

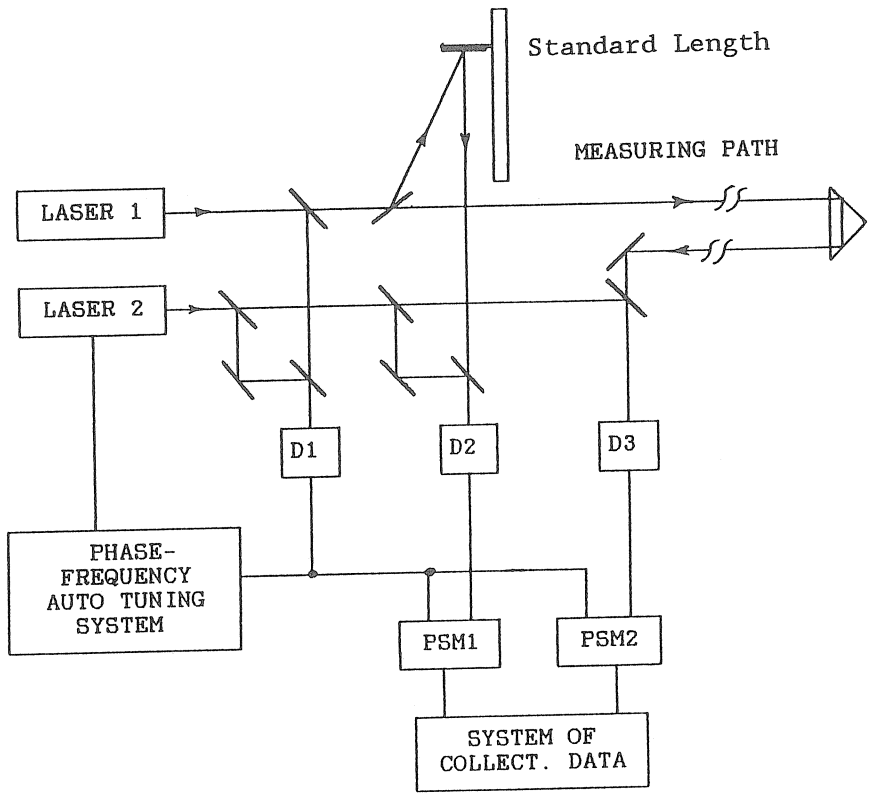

Fig. 1. Schematic diagram of the laser extensometer, with one measuring leg.

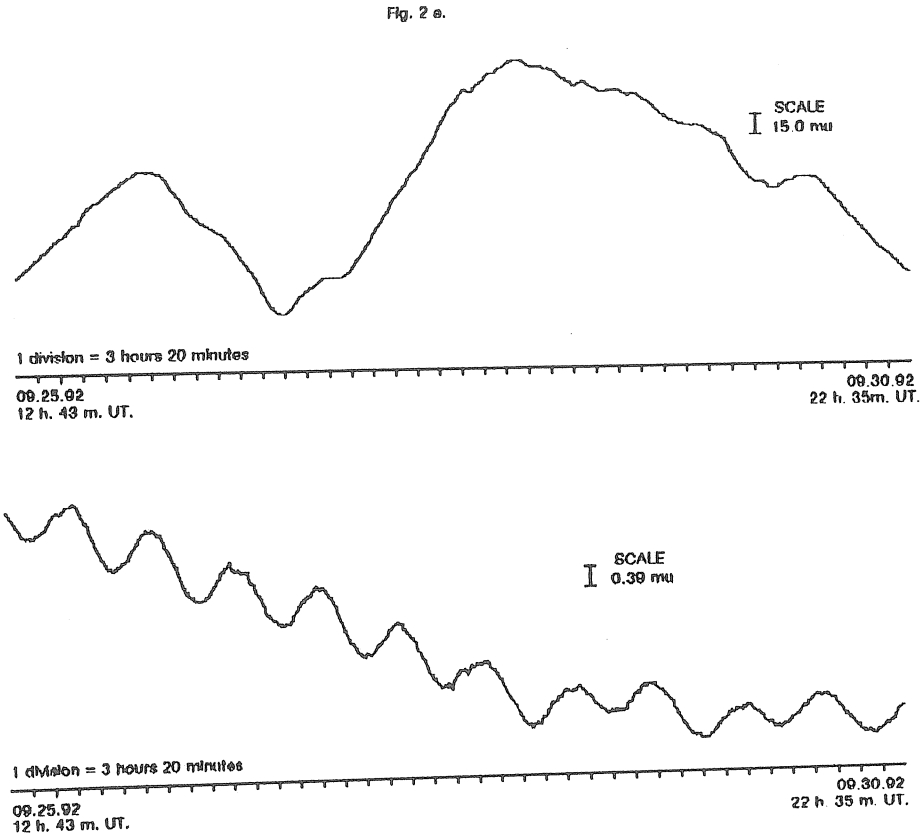

Fig. 2. Illustration of the recording of the measuring leg length variations in time :
a) before compensation;
b) after compensation.

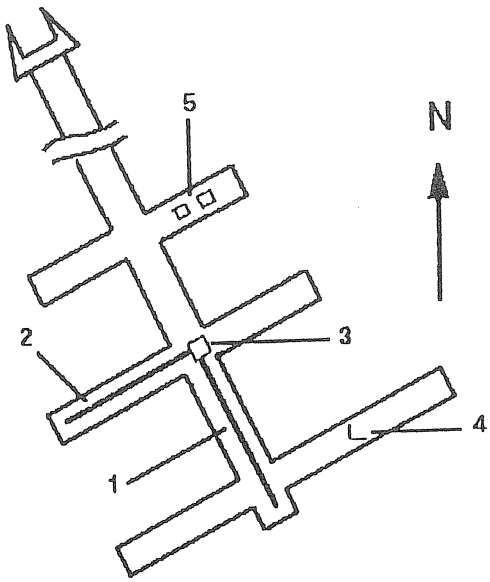

Fig. 3. Schematic diagram of the positioning of the measuring legs of the laser deformograph in the adit of the seismo station of Talaya. 1, 2 are measuring legs; 3 is the interferometer and a compensating leg; 4 rod extensometers; 5 tiltmeters. The adit is 90 meters long; its entrance is closed by double doors. The air temperature in the adit is 1°C. During a year the temperature in the deep part of the adit varies by 0.1°C. The amplitudes of twenty - four - hours' temperature changes do not exceed 0.001°C.

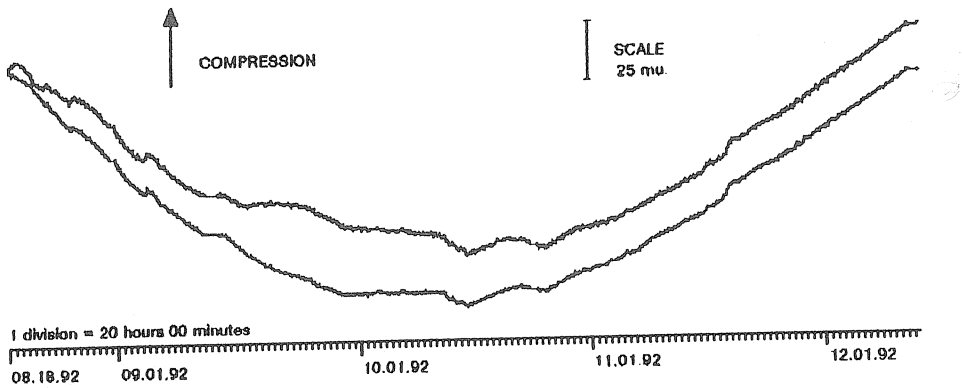

Fig. 4. Time change of relative deformation that was registered along measuring legs 1 and 2 of the laser deformograph from 18.08.92 to 11.12.92.

Table 1.

Tidal analysis results from the difference of the first and second measuring legs (Talaya station 51.68°N, 103°65 E, H = 600 m).

Doodson number	Darwin Code	Numb. Waves	Abs. Ampl.	Amp. Factor	M.S. Error	Phase Diff.	M.S. Error
143-149	01	26	6.84	0.1449	0.0082	-63.50	3.27
161-168	K1	33	9.36	0.1416	0.0052	-71.71	2.35
252-258	M2	26	24.35	0.5428	0.0052	63.94	0.55
271-275	S2	47	11.86	0.5681	0.0104	68.80	1.00

Shida numbers : ℓ(M2) = 0.0658, ℓ(S2) = 0.0690
ℓ(O1) = 0.0605, ℓ(K1) = 0.0592

Table 2.

Tidal analysis results.

	Period	Doodson number	Darwin Code	Abs. Ampl.	Amp. Factor	M.S. Error	Phase Diff.	M.S. Error
1	19.08-	143-149	O1	8.48	0.2804	0.0288	-5.66	5.89
	-09.12	252-258	M2	15.00	0.5192	0.0126	27.36	1.40
	19.08-	143.149	O1	11.01	0.3638	0.0468		
	-22.09	252-258	M2	14.59	0.5052	0.0266		
	18.09-	143.149	O1	10.83	0.3579	0.0445		
	-19.10	252.258	M2	14.81	0.5128	0.0177		
	18.10-	143-149	O1	6.43	0.2123	0.0662		
	-17.11	252.258	M2	14.33	0.4962	0.0307		
	08.11-	143.149	O1	7.51	0.2481	0.0727		
	-09.12	252.258	M2	16.04	0.5552	0.0291		
2	19.08-	143-149	O1	7.05	0.2331	0.0308	25.36	7.55
	-09.12	252-258	M2	9.26	0.3207	0.0125	-47.92	2.25
	19.08-	143.149	O1	8.19	0.2707	0.0547		
	-22.09	252-258	M2	9.48	0.3282	0.0277		
	18.09-	143.149	O1	7.98	0.2636	0.0422		
	-19.10	252.258	M2	8.63	0.2986	0.0176		
	18.10-	143-149	O1	5.93	0.1960	0.0743		
	-17.11	252.258	M2	8.76	0.3030	0.0294		
	08.11-	143.149	O1	5.51	0.1821	0.0626		
	-09.12	252.258	M2	10.37	0.3590	0.0275		
3	19.08-	143-149	O1	4.38	0.1449	0.0082	-63.50	3.27
	-09.12	252-258	M2	15.68	0.5428	0.0052	63.94	0.55
	19.08-	143.149	O1	4.78	0.1579	0.0235		
	-22.09	252-258	M2	15.89	0.5501	0.0104		
	18.09-	143.149	O1	4.53	0.1496	0.0145		
	-19.10	252.258	M2	15.66	0.5421	0.0057		
	18.10-	143-149	O1	4.50	0.1487	0.0199		
	-17.11	252.258	M2	15.40	0.5330	0.0109		
	08.11-	143.149	O1	4.09	0.1352	0.0168		
	-09.12	252.258	M2	15.79	0.5464	0.0107		

1: the first measuring leg of the deformograph (see Fig. 3);
2: the second leg;
3: difference of the first and second measuring legs.

Table 3.

Love and Shida numbers.

	Measuring leg		
	1	2	2-1
h	0.5105 ± 0.0182	0.4386 ± 0.0439	
ℓ	0.0672 ± 0.0104	0.0931 ± 0.0049	M2 0.0658 ± 0.0006 O1 0.0605 ± 0.0034

ABOUT "DATA RESCUE"
AN HISTORICAL TIDAL GRAVITY SERIES OF R. TOMASCHEK

P. Melchior
International Centre for Earth Tides

In BIM 118, page 8780, I wrote that, "at ICET, there is one very old tape that we have not yet been able to read".

Thanks to Dr R. Verbeiren this tape was successfully treated and all the data are now transferred on diskettes. It contained 21 series obtained during the IGY or even before and 21 series obtained between 1960 and 1965. For today geophysical investigations such data are obsolete but they are of real historical interest as the results obtained with these series illustrate the difficulties met in 1957-58 with the calibration of gravimeters. It is thus a duty of ICET to preserve them and pay tribute to those pioneers who sent their data to the World Data Centre C for conservation.

Amongst these 30 old series we found a series of 30 days observed in 1954 at Baltasound by R. Tomaschek.

In 1954 R. Tomaschek installed one Worden and two Frost gravimeters at Baltasound, Unst Island, Shetland to cover the period of a total solar eclipse. Only the 30 days of visual readings obtained with the Frost n° 54 gravimeter, were of sufficient quality to be analyzed. This instrument had been calibrated carefully. Results were published in

R. Tomaschek: Tidal Gravity Measurements in the Shetland. Effect of the Total Eclipse of june 30, 1954. Nature 175, pp 937-942, 1955.

and in

R. Tomaschek: Measurements of Tidal Gravity and Load Deformations on Unst (Shetland). Geofisica pura e applicata, 37, pp 55-78, 1957.

The original data were on our old tape. We analyzed them and got results in fair agreement with those published by Tomaschek who had used the Admiralty method of analysis.
However Tomaschek attributed the big phases found for M_2 (- 15.9°) and for O_1 (- 5.0°) to oceanic loading.
I doubt about this because, nowhere in the World, we have ever observed such a phase for the M_2 wave.
The maximum values amongst 382 stations collected in the ICET Data Bank is 5.1° at Noumea. Moreover, in three stations of the same area the following phases have been observed :

			O_1	M_2	Observer
0800	Laugaskoli	Iceland	1.05	1.98	Wenzel
0821	Torshavn	Faeroe	1.00	-0.43	Ducarme
0843	Bergen	Norway	1.19	-3.30	Bonatz

As the measurements were made every half hour, I suspect that an error of one half hour could have happened by inadvertence in the time reference. Such an error indeed already happened in the preliminary results of four stations of the IGY-UCLA Campaign. (Ness, BIM 22, pp 420-426, 1960 corrected in P. Melchior, BIM 24, p 493, 1961).

A tentative analysis with a 0.5 hour shift has then been made giving, as expected, more convenient results for O_1 and M_2.

As in Tomaschek papers the other waves are abnormal in any case which, according to this author, is most probably due to temperature and pressure variation (even if pressure corrections were applied to the original data).

STATION 0104 BALTASOUND COMPOSANTE VERTICALE GRANDE BRETAGNE

UNST ISLAND, NORTH SHETLANDS, SCOTLAND
60 45 45 N 0 51 10 W H 10 M D 3 KM
GRAVIMETER FROST 54 - OCULAR HALF-HOURLY READINGS
TOTAL ECLIPSE JUNE 30, 1954
BAROMETRIC VARIATIONS OF LARGE AMPLITUDE / CORRECTED 8.70 MICROGAL/MILLIBAR
PROPOSED CORRECTION -0.5 HOUR
INSTALLATION R. TOMASCHEK
CALIBRATION KIRKLINGTON HALL BASE

LEAST SQUARE ANALYSIS / VENEDIKOV FILTERS ON 48 HOURS / PROGRAMMING B.DUCARME
POTENTIAL CARTWRIGHT-TAYLER-EDDEN / COMPLETE DEVELOPMENT
COMPUTING CENTER INTERNATIONAL CENTER FOR EARTH TIDES/FAGS/ BRUSSELS
DATA PROCESSING BY L.VANDERCOILDEN ON 95/06/02
COMPUTER APOLLO DN10000
INERTIAL CORRECTION NOT APPLIED

G 54 54 615/54 713

TIME INTERVAL 30.0 DAYS 720 READINGS 1 BLOKS EFFICIENCY 1.00

WAVE GROUP ARGUMENT	N	WAVE	ESTIMATED AMPL.	R.M.S.	AMPL. FACTOR	R.M.S.	PHASE DIFF.	R.M.S.	RESIDUE AMPL.	PHASE
133.-139.	30	Q1	7.82	0.98	1.5403	0.1933	-8.987	7.186	2.21	-33.6
143.-149.	26	O1	28.24	0.88	1.0654	0.0333	1.946	1.785	2.68	159.1
161.-168.	33	P1S1K1	42.88	0.71	1.1502	0.0191	13.923	0.971	10.35	94.4
243.-248.	24	N2	6.26	0.89	1.8219	0.2589	-12.808	8.159	2.53	-33.2
252.-258.	26	M2	21.38	0.85	1.1918	0.0473	-1.412	2.275	0.77	-43.2
267.-277.	21	S2K2	9.16	1.15	1.0973	0.1381	23.609	7.329	3.89	109.4
327.-375.	17	M3	0.05	0.05	0.2898	0.3020	-34.507	59.587	0.15	-168.8

STANDARD DEVIATION D 15.77 SD 13.92 TD 0.84 MICROGAL

QUALITY FACTORS : Q1= 0.7 Q2= 1.2
O1/K1 0.9263 1-O1/1-K1 0.4357 M2/O1 1.1186
CENTRAL EPOCH TJJ= 2434922.0

ONDE	DELTA	ALFA	B	BETA	L	LAMBDA	X	CHI	DELTA	ALFA
	OBSERVES								CORRIGES	
Q1	1.5403	-8.99	2.20	-33.6	0.23	-148.8	2.31	-28.4	1.5759	-7.90
O1	1.0654	1.95	2.68	159.1	0.79	149.4	1.91	163.0	1.0906	1.11
K1	1.1502	13.92	10.35	94.4	0.95	26.3	10.03	99.4	1.1254	13.65
N2	1.8219	-12.81	2.53	-33.2	0.43	-46.6	2.12	-30.6	1.7203	-10.51
M2	1.1918	-1.41	0.77	-43.1	1.90	-63.0	1.21	104.5	1.1451	3.26
S2	1.0973	23.61	3.89	109.4	0.92	-100.3	4.71	103.8	1.1627	28.14

RE-ANALYSIS OF TOMASCHEK'S GRAVITY TIDE OBSERVATIONS MADE IN 1954 AT BALTASOUND, SHETLANDS ISLANDS

Hans-Georg Wenzel,

Geodätisches Institut, Universität Karlsruhe, Englerstr. 7, D-76128 Karlsruhe.
e-mail: wenzel@gik.bau-verm.uni-karlsruhe.de

Abstract

A group of scientists under R. Tomaschek has recorded in 1954 gravity variations with gravimeter Frost no. 54 at Baltasound on Unst Island (Shetland Islands). They have taken eyepiece readings at integer and half hours over a period of about one month, in order to detect eventual systematic effects during the total solar eclipse on June 30th, 1954. Melchior (1995) proposes to correct the timing of this very old gravity tide data set for half an hour, because of a very strong phase lag of about 15.9^0 at wave group M_2. A very similar phase lag has already been computed and published by Tomaschek (1957), who attributed this phase lag completely to ocean tide loading. My analysis of this data set gives numerically about the same results as published by Tomaschek (1955, 1957) and by Melchior (1995). The quality of the data set is however so poor compared to our modern instruments (about 100 times higher standard deviation), that the data set should in no way be used for any scientific finding. My conclusion is therefore to put the data set unchanged into the historical section of the data base of the International Center for Earth Tides.

1 Introduction

In 1954, a group of scientists (R. Brown, A.N.J. Hales, H.T. Rochelle, C.E. Saul, and R. Tomaschek) have carried out gravity observations with Frost gravimeter no. 54 in a barn at Baltasound on Unst Island (one of the Shetland Islands, see Fig. 1). The instrument set up was done with great care on specially constructed pillars in a room with temperature shielding. They have carried out simultaneous observations with gravimeters Frost no. 54 and 32 at Baltasound, and with gravimeter Worden no. 189 at Skaw island. The observations with the Frost gravimeters were made manually by eyepiece readings at half hourly interval over a period of 32 days. The observations with gravimeter Worden no. 189 were made photographically. The standard deviation of a single reading with gravimeter Frost no. 54 is reported to be about 40 nm/s^2 (Tomaschek 1957). The observations with the other gravimeters were less successfull due to various reasons.

The reason for the observations was to set up limits for gravity absorption or attenuation during the total solar eclipse on June 30, 1954. The gravity observations have been processed and published by Tomaschek (1955, 1957). The main findings from these data were that no systematic effects on gravity due to the eclipse could be seen, which put up an upper limit of the Majorana absorption constant to be less than $1 \cdot 10^{-14}$. As a by-product, a gravimetric factor (amplitude factor of gravity tides) around 1.20 for semidiurnal tides and 1.09 for diurnal tides was derived. The accuracy of these parameters was estimated to about 3%. Tomaschek has reported a strong phase lag of about 15^0 for M_2 (Tomaschek 1957) and attributed this phase lag to ocean tide loading. By a very rough computation using a very rough cotidal chart he has corrected the observations which resulted in ocean tide corrected phase shifts close to zero.

After releasing the data to the International Center for Earth Tides around 1960 (Melchior, personal communication), the data were stored there on a magnetic tape. This tape has recently been recovered and the data were re-analzed by P. Melchior, who also found an anomalous large phase lag around 15.9^0 at wave M_2. Unfortunateley, it is not much known from the currently available data set (e.g. wether the data were recorded at integral hours or at half hours). Melchior (1995) proposes to correct the data set for half an hour "because nowhere in the world we have ever observed such a phase for M_2". I have also re-analyzed the data set using a different method but obtaining almost the same numerical results as Melchior. I come however to the conclusion that the data set should not be used for any scientific finding because of very large noise in the data compared to the precision obtained nowadays with modern instruments. The data set should not be corrected but put unchanged into the historical section of the data base of the International Center for Earth Tides (ICET). If anybody wants to investigate gravity tide parameters at Baltasound, he should observe gravity tides there with a well calibrated modern gravimeter and a modern data acquisition.

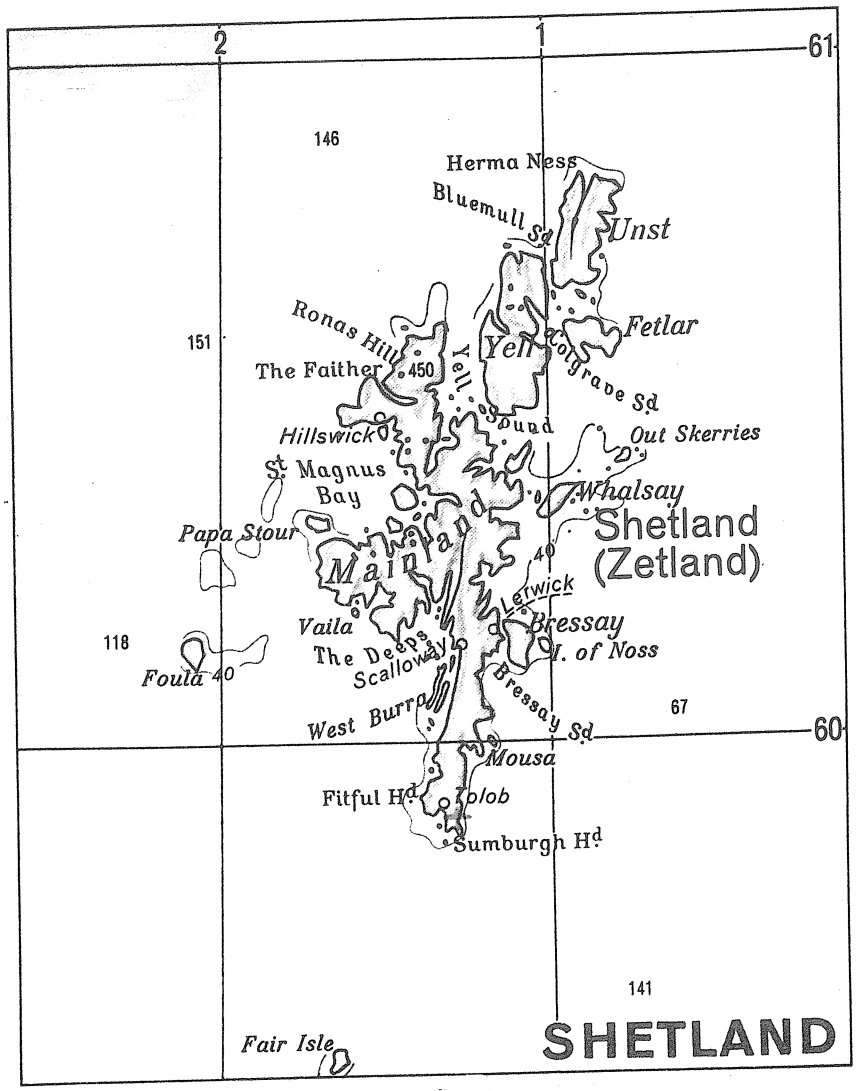

Figure 1: Map of Shetland Islands, taken from Atlas International, Kartographisches Institut Bertelsmann, p. 12-13, 1972, scaled up to 1:1 250 000.

2 Analysis of the Baltasound data

The data set (Fig. 2) supplied by ICET has been reformatted and analyzed using the ETERNA version 3.22 analysis program (Wenzel 1976, 1977, 1994); it is named BAFR5401 in the following. Air pressure, room temperature and outside temperature have been recorded in parallel to the gravity variation, but are not available in digital form. The gravity data have however been corrected for the air pressure effect (instrumental and gravitation plus loading) by Tomaschek (1957) using an empirical coefficient of 87 nm/s^2 per hPa. After a few initial tests, the first day has been deleted because of large residuals. For the earth tide analysis, drift modelling by a 2nd degree polynomial has been used instead of numerical highpass filtering, in order to see the longperiodic contents of the residuals. Due to strong noise in the data and the short length of the data set of 30^d only, there have been used five wavegroups only (O_1 from 0.721500 to 0.974188 cpd, P_1K_1 from 0.989049 to 1.216397 cpd, M_2 from 1.719381 to 1.976926 cpd, S_2 from 1.991787 to 2.182843 cpd and M_3 from 2.753244 to 3.937897 cpd). The tidal potential catalogue of Tamura (1987) has been used. The adjusted parameters are given in Tab. 1, the residuals are shown in Fig. 3, and the Fourier amplitude spectrum of residuals is shown in Fig. 4. We can see from Fig. 3 very large residuals (standard deviation 95.7 nm/s^2) and significant steps and spikes. The comparison of average noise levels (Tab. 1) and Fig. 4 suggests that the error estimation by ETERNA may be too optimistic by a factor of about two, due to the short length of the data set. This is a general problem for all analysis methods when analyzing very short data sets.

Although the strong phase lead of -15.4^0 for M_2 would suggest a timing error of **half an hour time lag**, such a timing error is not supported by the phase leads of the other waves. Especially wavegroup P_1K1 with about twice the amplitude of M_2 would suggest a **time lead** of half an hour. Please not that e.g. the 213.9 nm/s^2 amplitude of wave M_2 is only about twice the standard deviation of 95.7 nm/s^2.

3 Conclusion

The data set recorded by the group of Tomaschek in 1954 at Baltasound on Unst (Shetland Islands) is clearly of great interest from a historical point of view; the continuous observation of eypiece readings over a period of one month reflects the strong scientific engagement of Tomaschek's group. The quality of the data is however so poor compared to our modern instrumentation (about 100 times higher standard deviation), that the data set should not be used for any scientific conclusion.

The analysis of the Baltasound data set has shown a strong phase lag at wavegroup of M_2. Such a phase lag has been found by Tomaschek (1955,1957), Melchior (1995) and in my investigation. Tomaschek (1957) has also analyzed less precise data from two other instruments operated at the same time (one located at Baltasound, another located on Skaw island). Tomaschek (1957) has generally analyzed two data sets for each instrument: One recorded at integral hours and the other recorded at half hours. For the data sets recorded at Baltasound with Frost gravimeter no. 54, he has found no significant difference between both data sets. He has attributed the strong 15^0 M_2 phase shift completely to ocean tide loading, and came after correcting computed ocean tide gravitation and loading (using a very rough cotidal chart and a very rough method) to the conclusion that the gravimetric factor and phase for M_2 corrected for ocean tide loading is 1.20 ± 0.03 and $0.^0 \pm 2.^0$.

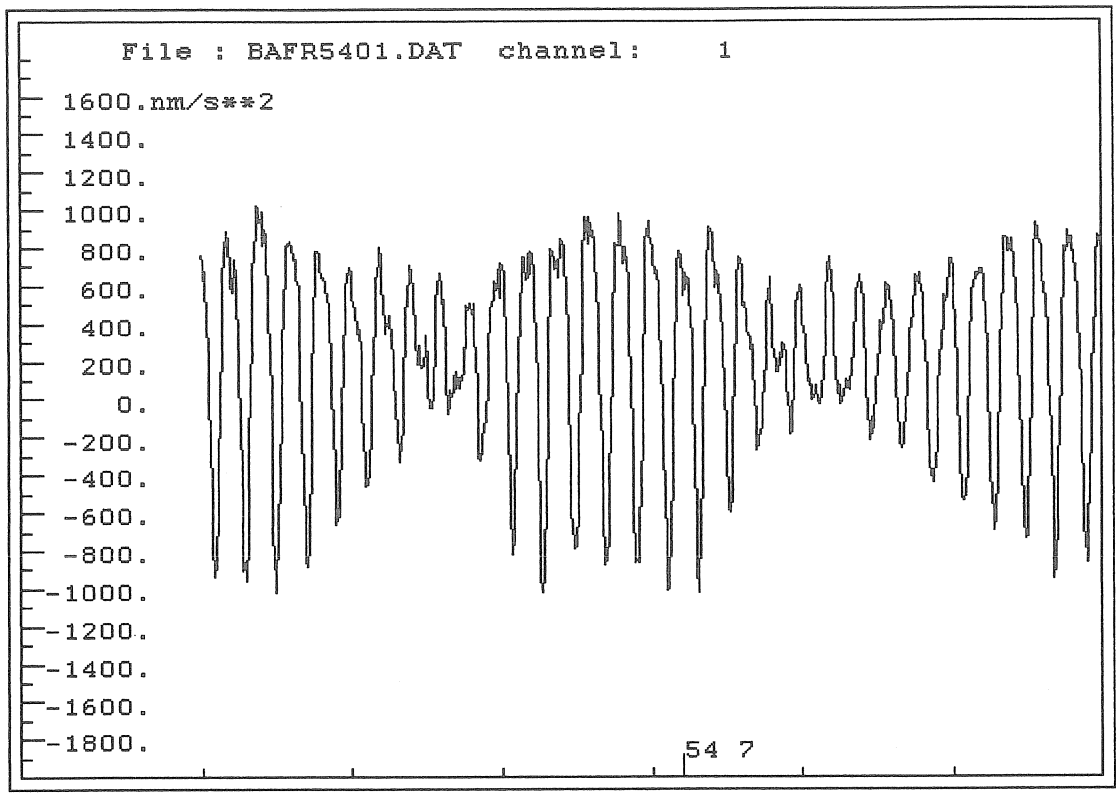

Figure 2: Hourly data set of gravity tides BAFR5401.DAT, recorded in 1954 with gravimeter Frost no. 54 with eyepiece readings.

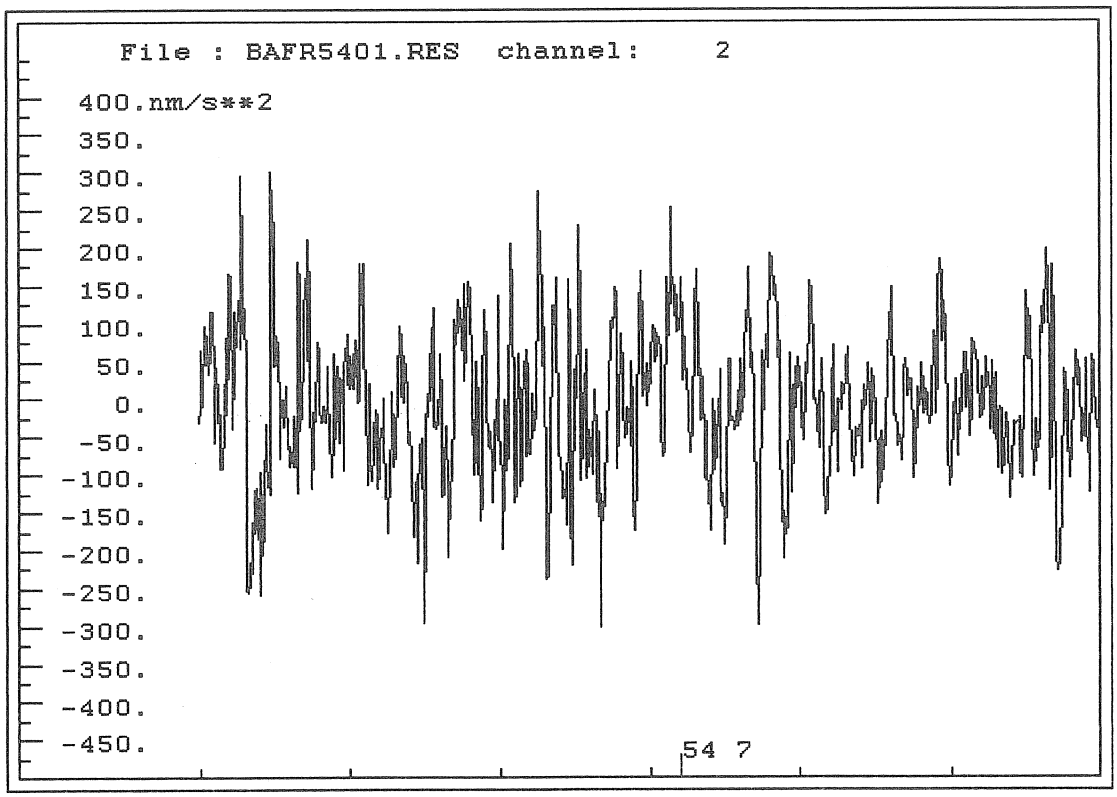

Figure 3: Residuals of hourly data set of gravity tides BAFR5401 after analysis with program ETERNA 3.22.

Tab. 1: ETERNA analysis of file BAFR5401 with drift modelling by a 2nd degree polynomial

```
 Program ETERNA, version 3.22 950320 Fortran 77,     file:   BAFR5401
#########################################################################
# Gravimetric Earth tide station Baltasound no.104 U.K.                 #
# 60.7625N   -0.8528E  H10M  P0M  D003KM    vertical component         #
# Gravimeter Frost no. 54 - half hourly ocular readings                 #
# Barn west of Halligarth near Baltasound on Unst                       #
# The observations were made to study the effect of the total           #
# eclipse of June 30, 1954 on gravity, see Nature, vol. 175,            #
# 937-939, 1955.                                                        #
# Observations: R.Brown, A.N.J. Hales,H.T. Rochelle,C.E. Saul,          #
#               and R. Tomaschek                                        #
#########################################################################

 Latitude: 60.7625 deg, longitude: -0.8528 deg, azimuth:  0.000 deg.
 Summary of observation data :
 19540615     0...19540714230000
 Initial epoch for tidal force     : 1954. 6. 1. 0
 Number of recorded days in total :    30.00
 TAMURA 1987   tidal potential used.
 WAHR-DEHANT-ZSCHAU inelastic Earth model used.
 UNITY window used for least squares adjustment.
 Numerical filter is NO FILTER    with   1 coefficients.

 Estimation of noise by FOURIER-spectrum of residuals
 0.1 cpd band   18.8049 nm/s**2       1.0 cpd band   20.5504 nm/s**2
 2.0 cpd band   13.9224 nm/s**2       3.0 cpd band    5.3861 nm/s**2
 4.0 cpd band    4.3468 nm/s**2       white  noise   11.6343 nm/s**2

 Adjusted tidal parameters, inertial correction not applied :
 from      to       wave   ampl. ampl.fac.    stdv. ph. lead    stdv.
 [cpd]     [cpd]     [nm/s**2 ]                        [deg]    [deg]

 0.721500 0.974188 O1   290.887   1.09743  0.03105   -4.574    1.775
 0.989049 1.216397 P1K1 427.634   1.14717  0.01843    7.175    1.057
 1.719381 1.976926 M2   213.903   1.19251  0.03364  -15.365    1.927
 1.991787 2.182843 S2    94.176   1.12848  0.09793    4.055    5.607
 2.753244 3.937897 M3     6.626   3.84029  1.33373  -59.675   76.424

 Adjusted TSCHEBYSCHEFF polynomial bias parameters :
 block    degree        bias                 stdv.

    1         0  1380.878377 nm/s**2      4.077717 nm/s**2
    1         1     3.056340 nm/s**2      6.172759 nm/s**2
    1         2    -0.555997 nm/s**2      5.964476 nm/s**2

 Standard deviation of weight unit:    95.691
 degree of freedom:                      707
 Standard deviation:                   95.691  nm/s**2
```

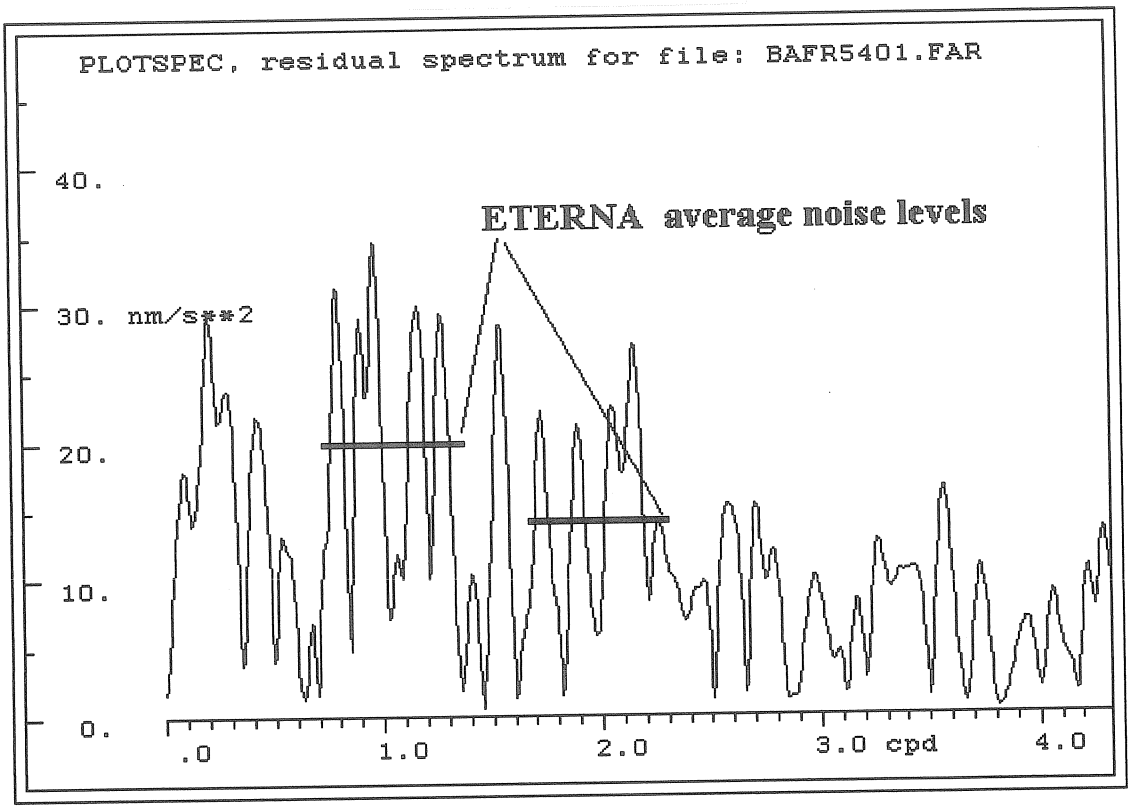

Figure 4: Fourier amplitude spectrum of residuals of hourly data set of gravity tides BAFR5401 after analysis with program ETERNA 3.22.

The Baltasound data have been re-analyzed by Melchior (1995) and in this investigation. Both analyses gave numerically almost the same results. Melchior (1995) proposes to correct the data set for half an hour "because nowhere in the world we have ever observed such a phase for M_2". My argument against such a correction is that Tomaschek knew already that the data gave a strong phase lag at M_2 and he derived almost the same phase lag from the data set recorded at integer hours (14.2^0, see Tab. II of Tomaschek 1957) and from the data set recorded at half hours (14.9^0). The modern analyses of the data set **assuming that the data were recorded at integer hours** give almost the sam phase lag as those reported by Tomaschek. The strong phase lags are most probably produced by the strong observational noise (the standard deviation is half the amplitude of wave M_2). My final conclusion is therefore to keep the data unchanged as they are and to put them into the historical section of the ICET data base.

Acknowledgements

This investigation was stimulated by P. Melchior, International Center for Earth Tides, Bruxelles, who also supplied the data sets and additional material. His support of this investigation is gratefully acknowledged.

References

Melchior, P. (1995): About "Data Rescue". Bulletin d'Informations Marées Terrestres, 123, 9365-9366

Tamura, Y. (1987): A harmonic development of the tide-generating potential. Bulletin d'Informations Marées Terrestres, 99, 6813-6855, Bruxelles 1987.

Tomaschek, R. (1955): Tidal gravity measurements in the Shetlands. Nature, **4465**, 937-939, 1955.

Tomaschek, R. (1957): Measurement of tidal gravity and load deformations on Unst (Shetlands). Geofisica pura e applicata, **37**, 55-78, 1957.

Wenzel, H.-G. (1976): Zur Genauigkeit von gravimetrischen Erdgezeitenbeobachtungen. Wissenschaftliche Arbeiten der Lehrstühle für Geodäsie, Photogrammetrie und Kartographie an der Technischen Universität Hannover Nr. 67 (Diss.), Hannover 1976.

Wenzel, H.-G. (1977): Estimation of accuracy for the earth tide analysis results. Bulletin d'Informations Marées Terrestres, **76**, 4427-4445, Bruxelles 1977.

Wenzel, H.-G. (1994): Earth tide data processing package ETERNA 3.20. Bulletin d'Informations Marées Terrestres, **120**, 9019-9022, Bruxelles 1994.

THE RELATION BETWEEN TIDAL DEFORMATIONS AND THE VELOCITIES OF RECENT TECTONIC MOVEMENTS.

L.A. Latynina
Institute of Physics of the Earth
Moscow, Russia

Abstract

The relationship between the local tidal strains and secular strain velocities, normalized by regional values, are considered on the basis of the geodetic and extensometric measurements data in Carpathian and Tadjikistan regions.

Introduction

Earth tides are a significant source of information about the structure and development of the Earth. During the last two decades great attention was drawn to the studies of tidal anomalies in the context of other geophysical fields. It was shown that global distribution of the parameters of gravitational tides is correlated to mobile regions of the Earth (Yanshin et al., 1985; Melchior et al., 1986, 1991; Jeligovskii et al., 1988). A high sensitivity of tidal strain and tilt to local inhomogeneities of the Earth's crust, to the faults primarily, is established theoretically and experimentally (Harrison, 1976; Berger et al/; 1976; Latynina et al., 1978, 1978a; Takemoto, 1981; Molodenski, 1988; Ostrovski et al., 1988; Zürn et al., 1991).

Relations between tidal strain and tectonic, meteorological and other deformation fields can appear as a result of influence of the Earth's crust inhomogeneity. The decrease of elastic modulus can produce the increase of tidal and tectonic deformations. Search of these relations is a main goal of geodynamic studies. The aim of this paper is the research of interrelations between the tidal parameters and the velocities of recent tectonic movements on the basis of extensometer's data.

Local tectonic strain velocities, denoted in this paper by V_{ii}, are measured with the help of extensometers on profiles several ten meters long, and are normalized to the values, which characterize regional structures. Comparison of local and regional movement velocities presuppose that these movements are stimulated by common tectonic reasons, but not local processes, such as landslide or ground sink. The choice of regional structures for local strain normalization is ambiguous, because recent movements of the Earth's crust are ranked in a complex order. The selection region must exist within the influence zone of a single tectonic mechanism and include areas differing in relief and structure. It extends for more than dozens of kilometres. Regional velocities of tectonic strains v_{ii} are determined according to geodetic data. Here we do not discuss the problem, where the measured secular movements really have tectonic origin. Local parameters of tidal strain measured by extensometers should be normalized according to regional tide parameters, which are defined as stations network average, or calculated numerically for the given geological model of the region. In the present paper we use the elastic Earth strain tide e_{ii} on the basis of the Molodenski earth model to normalize local tide strain E_{ii}. The most reliably estimated waves M_2 and O_1 are considered.

It is necessary to use multi-station data in order to decrease the influence of observation errors and obtain representative relations between the tidal and tectonic strain anomalies. Data sets from two test areas were considered on which geodetic measurements were carried out: the Carpathian and the Garm site located in the jointing area of the Pamirs and Tien Shan. In future experimental research the data set will be enlarged with extensometric and tilt measurements of other national and foreign stations.

Experimental data; Carpathian site

Local velocities of the Earth's crust secular movements in the zone of Transcarpathian inner through are evaluated according to data of two stations, Beregovo 1 and Beregovo 2 (Figure 1) regional velocities are estimated according repeated geodetic measurements. Data of the Matjashegi station from the Budapest region are also presented. All these stations are equipped with horizontal quartz extensometers with bases from 6 to 30 meters and optical, photoelectric or capacitive transducers.

Let us consider the velocities of tectonic movements in the Transcarpathian inner through. Geodetic networks in Carpathian - Balkan area were established by the Vienna Military Geographical Institute in the middle of the last century. In 1950s, Ukrainian geodesists carried out repeated measurements of horizontal crustal movements and a reasonably fair picture of recent crustal movements, which are inherited in this region, was obtained (Jurkevich et al., 1969; Magnitsky et al., 1985; Somov et al., 1992). Tectonic analysis of geodetic data demonstrate that the distribution of displacements corresponds to the expansion of the crust in the meridional direction and to compression in the latitudinal direction (Somov et al., 1983). The total deformation during 75 years in the direction of the principal axes is 65.10^{-6} and $- 52.10^{-6}$ respectively and deformation rates are $+ 0.9.10^{-7}$ and $- 0.7.10^{-7}$ a year. From geodimeters measurements carried out by the Lvov Polytechnic Institute in 1972 - 1992 the deformation velocity in the Southwest area of Transcarpathian through is of the order of 10.10^{-7} a year (Ostrovsky et al., 1994). Combining triangulation measurements data of 75 years with recent results it can be assumed that regional deformation velocity at the present stage is $+ 13.10^{-7}$ a year in NS direction and $- 10.10^{-7}$ a year in EW direction.

The stations Berogovo 1 and Beregovo 2 are located within the same structure of Beregovos hills at a distance of 10 km from each other. By extensometer data, the minor compression of rocks takes place in near-meridional direction (azimuth 37°) with rate 5.10^{-7} a year and the compression takes place in near-latitudinal direction (azimuth 73°) with rate 25 to 30.10^{-7} a year in Beregovo 1: the velocity of compression is 5.10^{-7} a year in NW direction (azimuth 140°) and the velocity of expansion is (1-2) 10^{-7} a year in NE (azimuth 52°) in Beregovo 2. Similar structures of the deformation fields obtained from geodetic data for long time and from extensometer data for some years suggest that the movement recorded by extensometer is related to regional sources (Latynina et al., 1994, Latynina et al., 1995).

Matjashegi station (Hungary) is situated in the suburbs of Budapest in the Northern part of the Pannonian basin. According to triangulation data the average rate of the horizontal crustal movements in the town is 4.0-14.5 millimetre a year during 75 years (Bendefy, 1965). Measurements at the station are carried out in the direction of low rate of movements. Thus we assume the regional deformation velocity to be equal to 4.10^{-7} a year. Secular movements, recorded by horizontal extensometer in the direction N24°W, evolve with the average velocity of 2.10^{-7} a year (Latynina et al, 1984; Varga et al., 1993).

Table 1 presents the station coordinates within the region under study, direction of horizontal deformation measurements, absolute magnitudes of local and regional tectonic strain rates according to extensometer's and geodetic data and their ratio. If tectonic strain velocities are small and lie within the error, local rate to regional rate ration is assumed to be equal to unity.

The analysis of tide records is conducted by Pertsev method for Beregovo stations and Venedikov method for station Matjashegi. Table 2 presents the amplitudes of the M_2 and O_1 tides determined over a observation series of six months and theoretical elastic Earth tide strains by the given azimuths. In the last two columns of the table the relations between local tide and Earth solid tide strains E_{ii}/e_{ii} are given.

The relation between V_{ii}/v_{ii} and E_{ii}/e_{ii} is shown in Figure 2. Points 1 to 10 belong to data from the Carpathian stations : eight points correspond to Beregovo stations, points 9, 10 to Budapest station, a pair of points for each measurement azimuth respectively. Even numbers correspond to wave M_2, odd numbers correspond to wave O_1. Points 3 to 10 are situated compactly. In case of uniform amplifying effect of inhomogeneities on tidal and tectonic deformations and if the local component E_{ii} depends primarily of the global strain component of same name e_{ii} the relationship between the values $y = E_{ii}/e_{ii}$ and $x = V_{ii}/v_{ii}$ would be represented by a straight line $y = x$. Points 1 and 2 /station Beregovo 1, azimuth 73°/belong to the area of anomalous high local strain velocities. The station is situated in the marginal zone of the deep Pannonian fault, and measurements are carried out along the segment normal to the strike of the fault; however there is no evident sign of tectonic dislocations at the station site. Additional geological exploration is required.

Garm site

A great amount of geophysical, geological and geodetic researches was conducted in Garm site. A network of deformation-measuring stations operated in this site during 10 years and geodetic measurements of recent crustal movements were conducted for more than 20 years in the whole area of the site. Garm site, therefore, is convenient for the studies of deformation processes. The site is crossed by two mobile belts South Tien Shan belt and Pamir belt. These belts are divided by deep-seated Surchob fault being part of Gissaro-Kokshaalsky faults (Fig. 3). Recent horizontal movements of the crust are determined by linear-angular and geodimeter measurements in the area of 50 km x 70 km [Guseva, 1986]. The maximal distance between geodetic stations located at mountain peaks is 30 km. Some local constructions were made in the Tadjik depression, in deep fault zones and foothills, showing in detail temporal and spatial developments of deformation process. As the features of recent crustal movements differ in various structures the mean regional velocities of deformation in this site were estimated by the formula :

$$\Sigma (L_i * V_i) / \Sigma (L_i)$$

where L_i is the length of the route and V_i is rate of movements along the route in a prescribed direction. The following values of compression rate were obtained; $-17\ 10^{-7}$ a year in North South direction and $-15\ 10^{-7}$ a year in West East direction. The principal axis of strain state in the region are parallel to the geographic axes.

The deformation stations Garm and Chusal are located in the area of Tien Shan, the station Childara is located in the central area of the Tadjik depression and the station Sari Pul is located in the zone of the deep fault. The location of the stations is shown in Fig. 3 [Latynina et al., 1978]. In addition, data of Djerino station of Dushanbe site located in the same

tectonic zone were considered [Starkov et al., 1988].

Data of tectonic deformation are presented in Table 1, data on local and theoretical tidal strains are given in Table 2 [Zharinov, 1976; Latynina et al., 1978a, 1980, 1981]. Extensometer data are relevant to 1971 - 1975 while data of Childara stations cover 1975 - 1982. No geodetic data of the horizontal movements in the area of Djerino station are available. Detailed measurements are conducted in Faizabad site located 20 - 60 km East from Dushanbe [Ustinov et al., 1986]. There the shortening of lines in the direction SE - NW with velocity of (15 - 20) 10^{-7} a year and extension with velocity of 5.10^{-7} a year in perpendicular direction was recorded. The velocity of compression is less than 10.10^{-7} in the profiles which do not intersect the deep-seated faults. We assume that strain rates are equal to $-(6 - 8)10^{-7}$ and $+(0 - 2)10^{-7}$ a year in the directions of extensometers.

Data from Garm stations are represented in Tables 1 and 2 and shown in Figure 2 by points 11 to 28. Points with coordinates $y = E_{ii}/e_{ii}$, $x = V_{ii}/v_{ii}$ concentrate in the area $y \leq 1$, $x \leq 1$. Data from two stations, Sari-Pul and Djerino make an exception.

Experimental points with coordinates $y = E_{ii}/e_{ii}$, $x = V_{ii}/v_{ii}$ are situated compactly enough. Exceptions correspond to station Sari-Pul (points 27, 28) and Djerino station in the azimuth 15°.

Extensometric measurements at the station Sari-Pul are carried out across the strike of the deep tectonic fault separating Pamir and Tien Shan mountain systems. According to Djerino station data increase of tidal and tectonic parameters occurs across the Kondarinskii fault which is well-pronounced in the relief.

One can deduce some relationship between the tidal wave local parameters and intensity of the Earth's crust secular movements. The correlation coefficient K between the relative values of tidal wave amplitude and the tectonic movement velocity is equal to 0.63 ± 0.12 for all observation points except Sari-Pul and Beregovo 1 at azimuth 73°. It is not clear what kind of relation between these parameters we can expect for the Earth's crust. Therefore in the next section we consider the problem of connection between local and regional strain in elastic media within the framework of inhomogeneous inclusion.

Estimation of local inhomogeneity influence on tidal and tectonic strain fields

In elastic media with frequency independent parameters one can evaluate inhomogeneity influence with the help of tidal data and apply these estimations to assessment of tectonic movements local velocities according to their regional values. A number of papers show, that surficial local strain can be represented by a linear combination of three independent tidal components of the radial symmetric Earth model [King et al., 1976; Berger et al., 1976; Agnew, 1986; Zürn et al., 1991]. Local (E_{ii}) and global (e_{ii}) tidal strains near the surface have three independent components which are connected by a relation [Beavan et al., 1979] :

$$\begin{pmatrix} E_{11} \\ E_{12} \\ E_{22} \end{pmatrix} = B \begin{pmatrix} e_{11} \\ e_{12} \\ e_{22} \end{pmatrix} \qquad (1)$$

Here B is the third-order matrix. We select the system of coordinates with the first axis (axis 1) in the direction of measurements. Then the measured linear deformation E_{11} can be represented as :

$$(E_{11}) = a_{11}\, e_{11} + a_{12}\, e_{12} + a_{22}\, e_{22} \qquad (2)$$

Coefficients a_{ij} are called the site coefficients, or strain-strain coupling coefficients. Three unknown coupling coefficients for direction 1 can be calculated from three equation of the type (2), using in three independent strain measurements. The fields M_2 and O_1 in phase with the potential and one of the quadrature waves M_2 and O_1, can be selected. The second quadrature wave, not involved in calculations, can be used for verification of representativity of a_{ij} coefficients. We evaluate the coupling coefficients a_{ij} for future tectonic strain calculations. It is assumed that the coupling coefficients reflect that the perturbation effects of inhomogeneities are equal for tidal and tectonic strain.

Coupling coefficients are calculated according to the data on tidal strain from all the observation points. Simultaneous equations, connecting the tide observed in direction "1" with the elastic Earth tide strains in the given coordinate system, are set up for each strain component :

$$E_{11}\,(Mp) = a_{11}\, e_{11}\,(Mp) + a_{12}\, e_{12}\,(Mp) + a_{22}\, e_{22}\,(Mp) \qquad (3)$$

$$E_{11}\,(Op) = a_{11}\, e_{11}\,(Op) + a_{12}\, e_{12}\,(Op) + a_{22}\, e_{22}\,(Op) \qquad (4)$$

$$E_{11}\,(Mc) = a_{11}\, e_{11}\,(Mc) + a_{12}\, e_{12}\,(Mc) + a_{22}\, e_{22}\,(Mc) \qquad (5)$$

$$E_{11}\,(Oc) = a_{11}\, e_{11}\,(Oc) + a_{12}\, e_{12}\,(Oc) + a_{22}\, e_{22}\,(Oc) \qquad (6)$$

here E_{11} (Mp), e_{ij} (Mp) and E_{11} (Op), e_{ij} (Op) are M_2 and O_1 strains, in phase with the potential, E_{11} (Mc), e_{ij} (Mc) and E_{11} (Oc), e_{ij} (Oc) are the quadrature strains.

Table 3 gives the values of a_{ij} coefficients, resulting from simultaneous equations (3, 4, 5) - solution I, and from simultaneous equations (3, 4, 6) - solution II for all the observation points. The largest discrepancies in the solutions I and II correspond to the largest relative errors of amplitudes (Table 2). Orientation of extensometers close to meridional or latitudinal is not favourable for such estimates because of small amplitude of the quadrature wave. All the reliable estimations show, that the difference between the a_{ij} values in the solutions I and II do not exceed 20% of a_{ij} level; and the input of strain component e_{11} in strain E_{11} in most cases is from 5 to 10 times bigger than other components input. Large discrepancies in solutions I and II can presumably be due to low accuracy of experimental data.

We apply evaluated coupling coefficients to calculation of tectonic strain local velocity on the basis of regional velocity values and compare it to experimental value. Local strain velocity V_{11} (L) is :

$$V_{11}\,(L) = a_{11}\, v_{11} + a_{12}\, v_{12} + a_{22}\, v_{22} \qquad (7)$$

where v_{ij} are the components of regional tectonic strain velocity. In the cases, in which coefficients a_{12} and a_{22} of solutions I and II differ from each other, we use the following relation :

$$V_{11} = a_{11}\, v_{11} \qquad (8)$$

Experimental values V_{11}/v_{11} and calculated values V_{11} (L)$/v_{11}$ are given in the Table 3, the same relation is shown graphically in Figure 4. If the calculation accuracy for strain velocities is sufficiently high, and coefficients a_{ij} are frequency independent, then the sequence of points with coordinates $X = V_{11}/v_{11}$, $Y = V_{11}$ (L)$/v_{11}$ can be approximated by a straight line : $Y = X$. IN practice the scatter is large and it is reasonable to speak about the correlation between the observed and calculated values. Correlation coefficient between Y and X arrays is equal to 0.72 ± 0.02 if Sari-Pul station and Beregovo 1 station at azimuth 73° are excluded.

The results

To identify connections between tidal and tectonic strain fields we consider the relationship between the anomalies of local tide and secular strain velocities, recorded by extensometer. The former are normalized to the elastic earth tide level, the latter to strain velocities, characteristic for the regional structures. Data of geodetic measurements in Carpathian and Tadjikistan regions and extensometric measurements data from eight stations are used. The obtained results are preliminary. Mass analysis of high-accuracy observation data is required to draw a reliable geophysical conclusion.

The analysis has proved the existence of a significant correlation between the tidal strain anomalies and the local velocities of tectonic movements: higher intensity of the tidal variations corresponds to the more mobile media. Averaging straight line for experimental data lies lower than the straight line $Y = X$. It means that tectonic strain is more influenced by inhomogeneity that the tidal one. Presumably, the former contain the creep component.

For many observation points local velocities of tectonic strain are close to regional and local tidal strain is less or close to theoretical value. Exceptions belong to observation points situated in large tectonic fault zones, such as Kondarinskii fault, deep fault separating Northern Tjan-Shan and Pamir systems, and marginal zone of the deep Pannonian fault.

Anomalies in the fault zones are of different character. High velocity of the secular strain is detected at Beregovo 1 station in the direction normal to the deep fault strike. Taking into account the position of the station in the marginal part of the deep fault and the direction of anomalous strain, it can be accounted for non elastic rock displacement, that do not influence elastic stress field, and, therefore, the tidal strain. If this assumption is true, the creep takes over 90% of the total displacement. Local reasons for the movements are improbable.

Sari-Pul station is situated straight in the deep fault zone. Here 3 to 4 times intensification of the tidal strain is caused by redistribution of elastic stress in the fault zone. Fifteen times increase of tectonic movement velocity is connected with both elastic inhomogeneity effects and rock creep, moreover, about 80% of recorded strain is caused by creep.

At Djerino station in azimuth 15° the tidal amplitudes increase 1.64 times (M_2) and 2.13 times (O_1), tectonic strains increase 1.6 times. Anomalous effects of almost equal intensity are observed for both tidal and tectonic strains, which should be related to elastic processes. The contribution of creep is small.

Local tidal strain is related to global strain by linear relations. Coupling coefficients characterize the site of measurements. Note that the obtained coefficients are representative in all cases, for which accurate tidal parameters are used. Local strain component E_{11} depends primarily on the global strain component of the same name, e_{11}, even in an area of considerable

topography and in fault zones.

We assume that tectonic strain is of elastic character, and coupling coefficients, obtained from tide measurements, are frequency independent and calculate velocities of local tectonic strain on the basis of their regional values. Observed and calculated velocities are correlated, though not coincide each other. Data from stations in the fault zones, where slow movements are controlled by the rock creep, make an exception. Observed and calculated tectonic strain velocities are close for Djerino station, also situated in the fault zone, where slow movements probably are determined by elastic deformation.

The research is supported by the Russian Fund for Fundamental Investigations (RFFI).

Table 1

Regional v_{ii} and local V_{ii} rates of tectonic strains

NN	Region	Station	Location Lat. Long. (deg)	Azimuth (deg) α	Strain rates * 10^{-7} in the direction α V_{ii}	v_{ii}	V_{ii}/v_{ii}
1.	Transcarpatian trough	Beregovo1	48.22 22.70	73.	25	8	3.1
2.	-"-	-"-	-"-	37.	4	5	0.8
3.	-"-	Beregovo2	48.23 22.65	140.	4	3	1.3
4.	-"-	-"-	-"-	52.	1	1	1.0
5.	Pannonian basin	Matyashegy	48.50 19.00	114.	2	4	0.5
6.	South Tien Shan	Garm	39.33 70.32	2.5	8	17	0.5
7.	-"-	-"-	-"-	98.5	11	15	0.7
8.	-"-	Chusal	39.11 70.75	17.6	18	17	1.1
9.	-"-	-"-	-"-	111.1	12	15	0.8
10.	Tadjik depression	Childāra	38.80 70.32	82.	15	15	1.0
11.	-"-	-"-	-"-	171.	5	15	0.3
12.	South Tien Shan	Djerino	38.80 68.81	105.	2	2	1.0
13.	-"-	-"-	-"-	15.	13	8	1.6
14.	Surchob fault	Sary-Pul	39.33 70.33	177.3	260	17	15.3

Table 2

Amplitudes of M_2 and O_1 tidal strains

NN	Azimuth (deg)	Amplitudes * 10^{-9} M_2 Observed tide E_{ii}	M_2 earth tide e_{ii}	O_1 Observed tide E_{ii}	O_1 earth tide e_{ii}	Ratio of E_{ii} to e_{ii} M_2	O_1
1.	73.	1.8±0.2	3.3	2.7± 0.4	6.8	0.55	0.40
2.	37.	1.8±0.3	8.6	1.7± 0.4	5.6	0.21	0.30
3.	140.	7.4±0.4	8.4	3.0± 0.2	5.7	0.88	0.53
4.	52.	4.0±0.4	6.7	4.3± 0.8	6.3	0.60	0.68
5	114.	2.7±0.2	4.6	5.4± 0.4	6.7	0.59	0.81
6	2.5	7.7±0.4	12.7	3.2± 0.5	4.3	0.61	0.74
7.	98.5	0.8±0.1	4.2	1.9±0.1	6.9	0.19	0.27
8.	17.6	11.5±0.5	12.2	3.8±0.2	4.7	0.94	0.81
9.	111.1	1.4±0.03	5.7	2.0±0.1	6.7	0.25	0.30
10.	82.	2.6±0.1	4.4	4.5±0.1	6.9	0.59	0.65
11.	171.	5.6±0.2	12.7	2.0±0.1	4.4	0.44	0.45
12.	105.	3.2±0.1	5.0	6.3±0.2	6.8	0.64	0.93
13.	15.	20.4±0.2	12.4	9.8±0.1	4.6	1.64	2.13
14.	177.5	36.7±1.5	12.7	18.2±1.7	4.3	2.89	4.23

Table 3. Observed and calculated rates of local tectonic strains

NN	Azimuth (deg)	Site coefficients Solution I and II a_{11}	a_{12}	a_{22}	Ratio of local strain rate to regional rate V_{ii}/v_{ii} Observation	Calculation
1	73	0.39	-0.05	0.01 (I)	3.1	0.4-0.2 **
		0.24	0.16	0.16 (II)		
2.	37	0.23	0.04	0.08 (I)	0.8	0.2-0.1 **
		0.11	-0.02	0.03 (II)		
3.	140	0.69	0.22	-0.06 (I)	1.3	1.0
		0.60	0.24	0.03 (II)		
4.	52	0.58	-0.02	0.06 (I)	1.0	0.6-0.9 **
		0.92	-0.11	-0.29 (II)		
5.	24	0.71	-0.10	0.07 (I)	0.5	0.7-0.8 **
		0.83	0.01	- 0.05 (II)		
6.	2.5	0.56	-0.04	0.11 (I)	0.5	0.66
		0.56	-0.14	0.12 (II)		
7.	98.5	0.24	-0.13	- 0.01 (I)	0.7	0.2-0.3 **
		0.31	0.15	-0.07 (II)		
8.	17.6	0.94	0.10	0.06 (I)	1.1	0.9
		0.90	-0.15	-0.02 (II)		
9.	111.1	0.40	-0.03	-0.17 (I)	0.8	0.2
		0.39	-0.05	-0.16 (II)		
10.	82.	0.70	0.02	-0.04 (I)	1.0	0.7
		0.71	0.04	-0.04 (II)		
11.	171.	0.43	-0.01	0.01 (I)	0.3	0.4
		0.43	-0.01	0.01 (II)		
12.	105.	0.90	-0.20	-0.01 (I)	1.0	0.9 **
		0.88	-0.25	0.02 (II)		
13.	15.	1.50	0.13	0.40 (I)	1.6	1.5 **
		1.58	0.28	0.30 (II)		
14.	177.3	2.56	0.07	1.03 (I)	15.3	3.5
		2.55	0.15	1.03 (II)		

** Local strain rate is determined from (8).

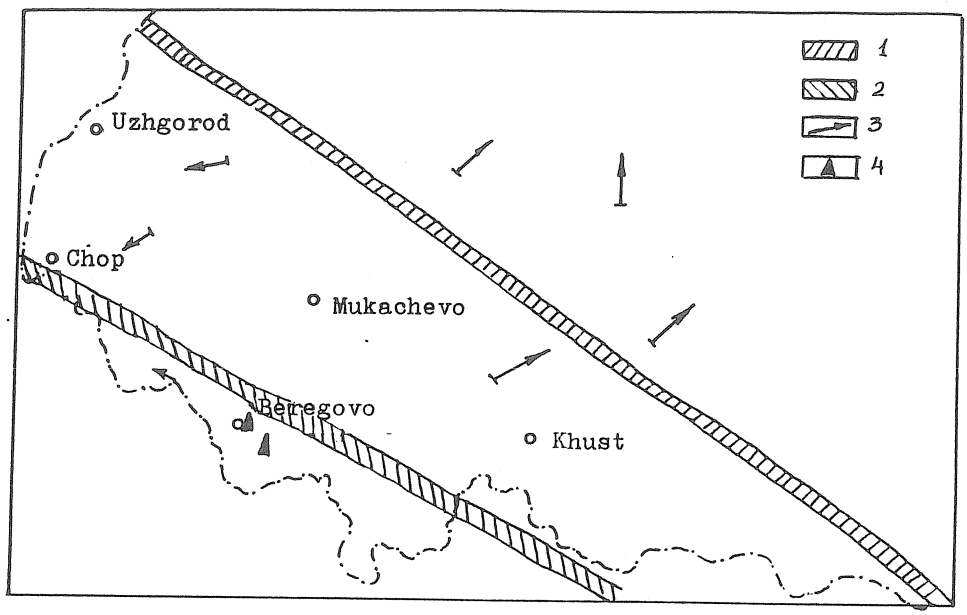

Figure 1. Tectonic scheme of Transcarpathian inner basin. 1-Transcarpathian (Pennin) deep fault, 2-Transpannonian deep fault, 3-recent crust horizontal movements (geodetic data), 4-extensometer stations Beregovo 1 and Beregovo 2.

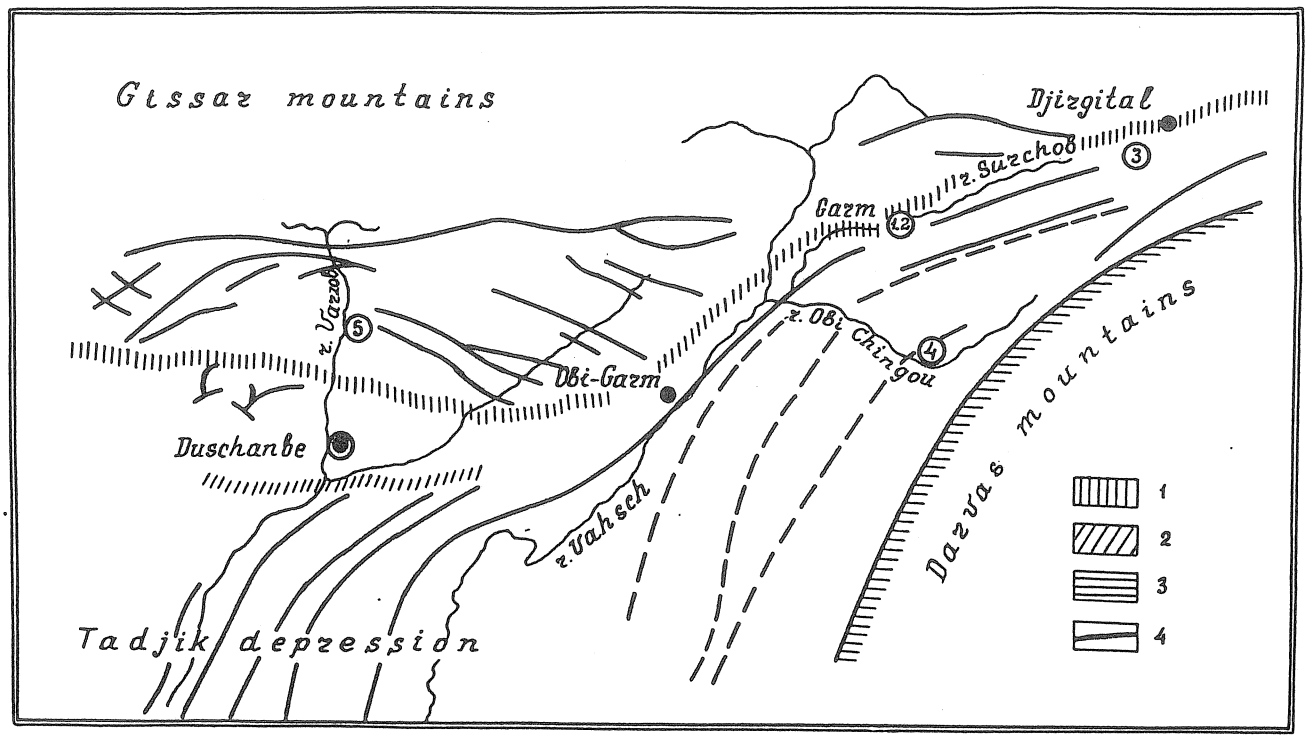

Figure 3. Tectonic scheme of Garm-Dushanbe site. Deep faults: 1. Gissaro-Kokshaalcky; 2. Ilyaksky; 3. Darvaz-Karakulsky; 4. regional faults. Extensometer stations (5): 1. Garm; 2. Sary-Pul; 3. Chusal; 4. Childora; 5. Djerino.

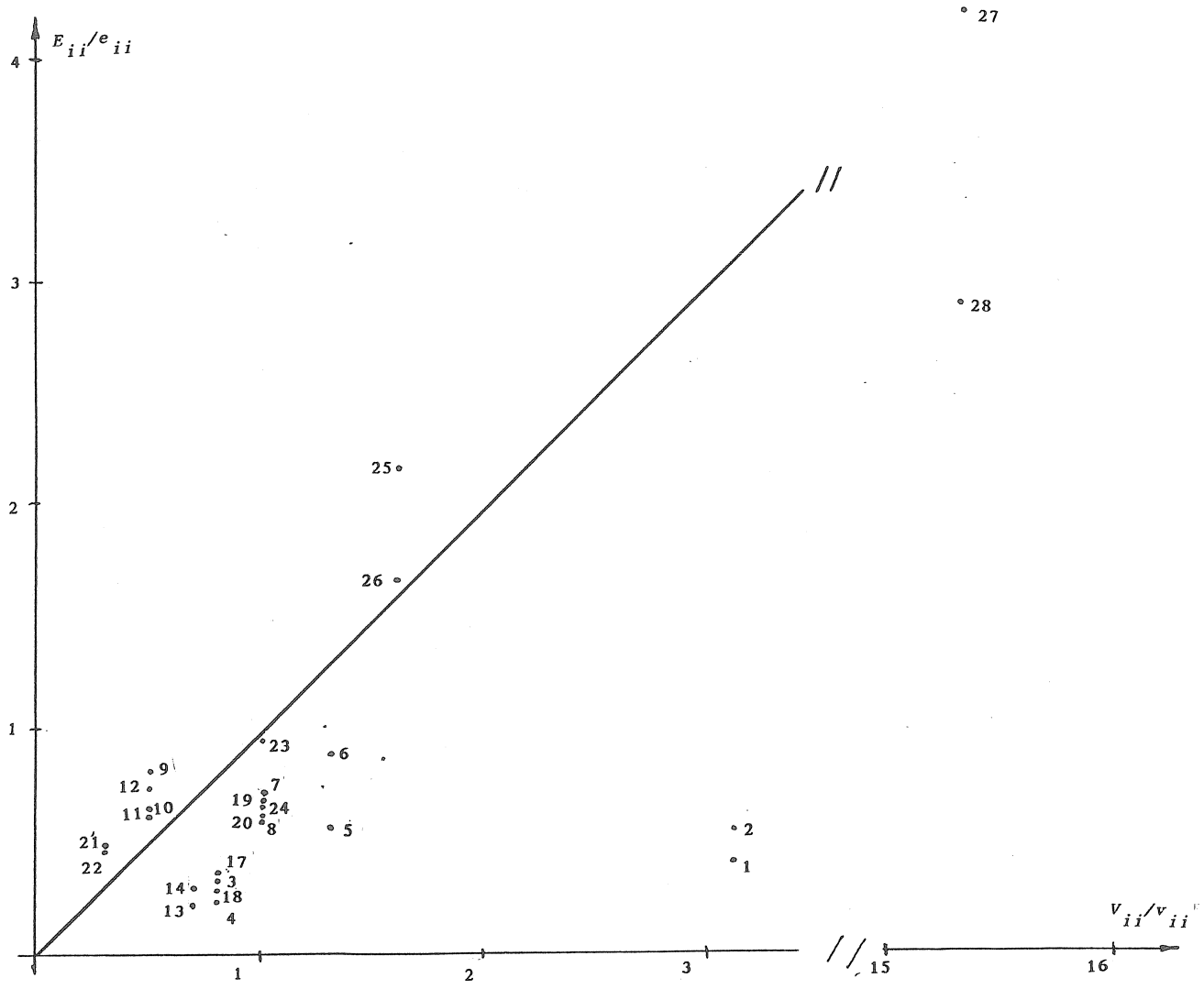

Figure 2. The relation between normalized values of tidal strains E_{ii}/e_{ii} and velocities of tectonic movements V_{ii}/v_{ii}. Points 1 ... 28 correspond: 1 ...8 to Beregovo stations, 9, 10 to Matyashegy station, 11 ...22 to stations Garm, Chusal, Childora, 23 .... 26 to station Djerino, 27, 28 to station Sary-Pul; Odd numbers are obtained by O_1, even numbers are obtained by M_2.

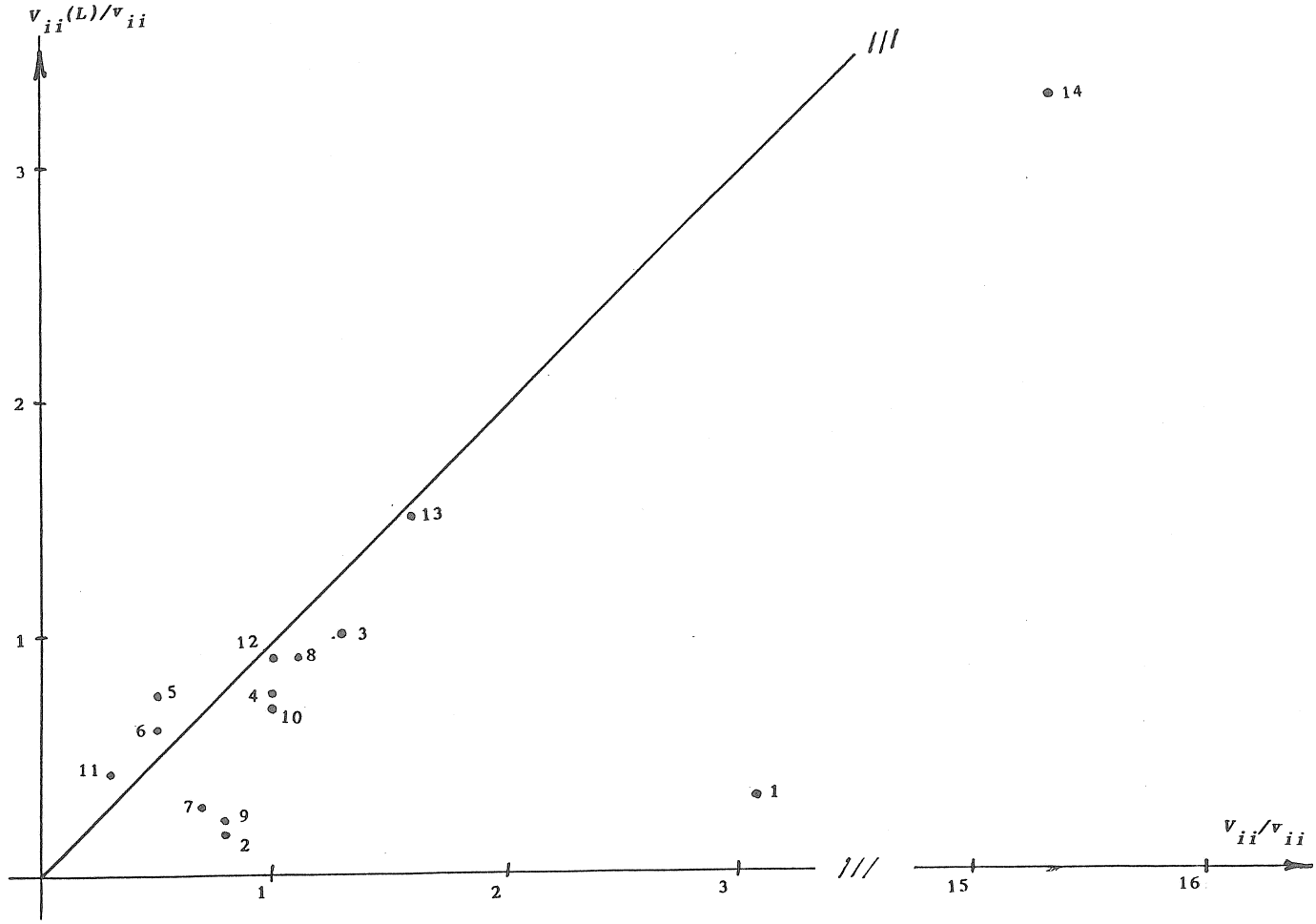

Figure 4. The relation between calculated rates V_{ii} (L) and observed rates v_{ii} of local tectonic strains. The straight line correspond to theoretical relationship. Observed values: points 1, 2- station Beregovo 1 (azimuth 73° and 37°); 3, 4- Beregovo 2; 5- Matyashegy; 6, 7- Garm; 8, 9- Chusal; 10, 11- Childora; 12, 13-Djerino; 14- Sari-Pul.

REFERENCES

Agnew D.C., 1986.
Strainmeters and tiltmeters.
Review of Geophysics, v. 24, N 3, 579-624.

Beavan J., Bilham R., Emter D., King G., 1979.
Observations of strain enhancement across a fissure.
Geophysics der Bundesrepublik Deutschland, Munchen, 1979, s. 47-58.

Bendefy L., 1965.
Grundlegende Probleme der Erforschung der rezenten Erdkrustenbewegung.
Gerlands Beitrage Geophys., 74, N 6, s. 484-495.

Berger J., Beaumont C., 1976.
An analysis of tidal strain observations from the United States of America. II. The inhomogeneous tide.
Bull. Seism. Soc. of America. v; 66, N 6, pp. 1821-1846.

Guseva T.V., 1986.
Recent crustal movements at the joint of the Pamir and Tien Shan.
Moscow, 171 p., (in russian).

Harrison J.C., 1976.
Cavity and topographic effects in tilt and strain measurement.
J. Geoph. Res., v. 81, N2, p 319-328.

Jeligovskii V.A., Melchior P., Sadovskii A.M., 1988.
Tidal anomalies, heat flow and seismicity.
Probl. Seismolog. Informatiki, Moscow, Nauka 21, 32-37, BIM 106, 7535-7545.

Jurkevich O.I., Volosezki B.I., Zabluk N.S. et al., 1969.
Repeated levellings of Beregovo earthquake 24.10.1965.
Seismicity of the Ukraine, Kiev, 103-106 (in russian).

King. G., Zürn W., Evans R., Emter D., 1976.
Site correction for long period seismometers, tiltmeters and strainmeters.
Geophys. J.R. Astr. Soc. v. 44, p. 405-411.

Latynina L.A., Karmaleeva R.M., 1978.
Extensometric measurements.
Moscow, Nauka, 154 p (in russian).

Latynina L.A., Shihkina T.P., 1978a.
Intensity of tidal and tectonic movements in the Surchob fault zone.
Izv. AN. USSR, Phyzika Zemli, N6, 87-92 (in russian).

Latynina L.A., 1980.
Tidal deformations at Chusal station in Tadjikistan.
The study of Earth tides, Moscow, pp. 207-214 (in russian).

Latynina L.A., Karmaleeva R.M., (1981.
Tidal deformations at Garm station in Tadjikistan.
Izv. AN, Physika Zemli, N12, pp 84-87 (in russian).

Latynina L.A., Szabo Gy., Varga P., 1984.
Observations of the deformation of the Earth's crust in the Matyashegy-cave near Budapest.
Acta Geod., Geoph. et Montanist. Hung. v. 19 (3-4), pp. 197-205.

Latynina L.A., Baisarovich I.M., Brimich L., Varga P., Jurkevich O.I., 1993.
Variation of deformations in the Carpatho-Balkan region.
Phyzika Zemli, RAN, N1, 3-6 (in russian).

Latynina L.A., Verbizki T.S., Ignatishin V.V., 1995.
Deformation processes in North-East zone of Carpatho-Balkan region.
Physika Zemli, RAN, N4, 3-16 (in russian).

Magnitsky V.A., Grachev A.F., Kalashnikoval I.V., Bronguleev V.V., 1985.
Recent vertical crustal movements of the Carpathian-Balkan region and their relationship with neotectonic movements and geophysical fields.
5th Intern. Symposium Geodesy and Physics of the Earth, Magdeburg, 1984, s. 113-123.

Melchior P., Sadovsky A.M., 1986.
Tidal anomalies and heat flow in West and Central Europe.
Dokladi AN USSR, v. 286, N6, pp 1351-1354 (in russian).

Melchior P., Ducarme B., 1991.
Tidal gravity anomalies and tectonics.
Proc. of the XIth Intern. Symposium on Earth tides, Stuttgart, pp. 445-454.

Molodenski S.M., 1988.
Plain areas relief effect on Earth crust tidal inclinations and deformations.
Prediction of the Earthquakes, Moscow-Dushanbe, N8, 61-64 (in russian), BIM 112.

Ostrovski A.E., Starkov V.I., Starkova E.Ya., 1988.
Anomalies in amplitudes and phases of tidal tilts observed at Djerino station.
Prediction of the Earthquakes, Moscow-Dushanbe, N8, 78-103 (in russian), BIM 112.

Ostrovski A.L., Sabolozki Ph.D., Tretjak K.R. et al., 1994.
Recent stress-strain state of Ukraine Carpathians lithosphere.
The 1st Intern. Symposium of the stresses in lithosphere, 19-23 september 1994, Moscow, Abstracts, p. 134-136.

Somov V.I., Rachimova I.Sh., 1983.
Recent crustal movements of the Carpatho-Balkan region and contacting structures.
Kiev, Naukova Dumka, 144p (in russian).

Somov V.I., Djun I.V., Rachimova I.Sh. et al., 1992.
Statistic methods for recent geodynamics of the Carpatho-Dinar region.
Kiev, Naukova Dumka, 251p (in russian).

Starkov V.I., Latynina L.A. Karmaleeva R.M. et al., 1988.
Tidal deformation parameters in Djerino according 19 years observations. Prediction of the Earthquakes, Dushanbe-Moscow, N8, 65-77 (in russian), BIM 112.

Takemoto S., 1981.
Effects of local inhomogeneities on tidal strain measurements. Bull. of the Disaster Prevention Institute, Kyoto University, v. 31, pp. 211-237.

Ustinov S.N., Teitelbaum Ju. M., 1986.
Strain variations of free surface according geodetic data. Seismic monitoring of Earth crust. M., pp 192-199.

Varga T., Latynina L.A., Brimich L., Mentes Gy., Katona Gy., Varga P., 1993.
Study of the Extensometric records of the Pannonian Basin in the non-tidal frequency domain.
BIM 116, pp. 8537-8545.

Yanshin A.L., Melchior P., Keilis-Borok V.I., De Becker M., Ducarme B., Sadovsky A.M., 1985.
Global distribution of tidal anomalies and an attempt of its geotectonic interpretation.
Proc. 10th Intern. Symp. on Earth tide, Madrid, pp. 731-755.

Zharinov N.A., 1976.
Deformations of the Earth surface at Childora station.
Recent crustal movements, Novosibirsk, pp. 142-153 (in russian).

Zürn W., Emter D., Otto H., 1991.
Ultra-short strainmeters: tides are in the smallest cracks.
BIM 109, pp. 7912-7921.